Special Report on the Wirdum Earthquake 8th October 2022 with Magnitude M_L = 3.1

Datum October 2022

Editors [redacted]

Contents

Summary and Conclusions

Seismological Comparison

On the 8th October 2022 an earthquake with a magnitude 3.1 occurred near the village of Wirdum located some 1.5 km to the south-east of Loppersum. Just over 3 hours later this earthquake was followed by an earthquake at the same location with a magnitude 1.2.

In the last year a number of earthquakes have in a period of weeks to months occurred in a small area of the field. Examples of these are the earthquake swarm near Zeerijp starting 4th October 2021 and the earthquakes near Uithuizen in August, September and October 2022. This might indicate a more intense clustering of recent earthquakes in space and time. However, this might also be associated with a lower event rate and a shrinking seismically active area. As part of the studieplan into the seismicity during the pressure equilibration phase NAM is performing a systematic study into the Groningen earthquake catalogue for after-shock sequences.

Ground Motion Comparison

The M_L 1.2 - 3.1 Wirdum earthquakes of 8 October 2022 have generated a large number of ground-motion recordings. The largest component of PGA recorded is 0.06 *g* and the largest value of PGV—which is generally considered a better indicator of the damage potential of the motion—recorded in the M_L3.1 event is 2.46 cm/s. This is smaller than the largest value of the Groningen ground-motion database (the 3.46 cm/s recorded in the larger 2012 M_L3.6 Huizinge earthquake) but now the fifth largest value recorded in Groningen.

An important observation is that, although the amplitudes of motion recorded in the M_L3.1 Wirdum earthquake are within the range of predictions of the empirical PGV GMPEs as well as the SA_{AVG} predictions of the V6 and V7 GMM, they are, on average, 10-15% larger than the median predictions of the models and appear to be also larger than the average amplitudes recorded during previous events of similar magnitude.

Empirical Green's Function Analysis

The empirical Green's Function analysis for the earthquake pair Wirdum en Garrelsweer on the 8th October 2022 showed a rupture propagation direction for the Wirdum earthquake coinciding very well with the underlying faults.

1 Introduction

1.1 Reason for this Special Report

When larger earthquakes have occurred or other remarkable events have happened (like a swarm of smaller earthquakes or an earthquake with a larger magnitude), NAM publishes a report within two weeks after the event. To date thirteen of these reports have been published. These reports are listed in table 1.1.

Title	Date
Rapportage recente aardbevingen Wirdum en Garsthuizen 2016/2017	Mar 2017
Ground Motions from the M_L 2.6 Slochteren Earthquake of 27th May 2017	June 2017
Special Report on the earthquake density and activity rate following the earthquakes in Appingedam (M_L=1.8) and Scharmer (M_L=1.5) in August 2017	Sept 2017
Special Report on the Loppersum Earthquakes – December 2017	Dec 2017
Special Report on the Zeerijp Earthquake	Jan 2018
Short special report Exceedance Activity Rate - February 2018	Feb 2018
Special Report - Westerwijtwerd Earthquake - 22nd May 2019	May 2019
Analyse overschrijding MRP-grenswaarde Aardbevingsdichtheid 9 september 2019	Sept 2019
Analyse overschrijding aardbevingsdichtheid - 3 december 2019	Dec 2019
Special Report on the Zijldijk M_L = 2.5 Earthquake of 2nd May 2020	May 2020
Special Report on the Loppersum M_L=2.7 Earthquake of 14th June 2020	Aug 2020
Special Report on the Zeerijp Earthquake Swarm starting 4th October 2021 (with a separate supplement)	Nov 2021
Special Report on the Garrelsweer Earthquake 16th November 2021 with Magnitude ML = 3.2	Nov 2021
Special Report on the Earthquakes near Uithuizen in August, September and October 2022	Oct 2022

Table 1.1 Reports analysing remarkable events in the earthquake record, like larger events or earthquake swarms.

The earthquake near Wirdum on the 8th October 2022 had a magnitude of 3.1 on the Richter-scale. As a result the 'signaalwaarde' for magnitude was exceeded. This exceedance requires NAM to submit a Special Report. This special report has been prepared and shared with both SodM and the ministry of Economic Affairs and Climate Policy.

Title	Date
Analyse seismiciteit	Nov 2016
Rapportage Seismiciteit Groningen - November 2017	Nov 2017
Rapportage Seismiciteit Groningen - Juni 2018	July 2018
Rapportage Seismiciteit Groningen - November 2018	Nov 2018
Rapportage Seismiciteit Groningen - Mei 2019	May 2019
Rapportage Seismiciteit Groningen - November 2019	Nov 2019
Rapportage Seismiciteit Groningen - Mei 2020	Apr 2020
Rapportage Seismiciteit Groningen - November 2020	Nov 2021
Rapportage Seismiciteit Groningen - Mei 2021	June 2021
Rapportage Seismiciteit Groningen - November 2021	Nov 2021
Rapportage Seismiciteit Groningen - Mei 2021	June 2022

Table 1.2 Half-yearly surveillance reports issued by NAM to SodM and published on the NAM onderzoeksrapporten-webpage.

1.2 Content of this Special Report

In this report a seismological analysis of the Wirdum earthquake on 11th October 2022 and the after-shock near Garrelsweer also on the 11th October 2022 are presented in chapter 2. In chapter 3, the records obtained during the Wirdum earthquake are discussed.

The automated FWI analyses of the Wirdum earthquake and the Garrelsweer earthquake both of 11th October 2022 have been included in this report as Appendices A and B.

2 Analysis of recent earthquakes near Wirdum

2.1 Introduction

On Saturday 8th October 2022, two earthquakes occurred near the villages of Wirdum and Garrelsweer in Groningen. The first event, with a magnitude of M_L3.1, occurred at 02:17 UTC (04:17 local time), while the second, of M_L1.2, followed at 05:35 UTC (07:35 local time).

2.2 Epicentres

The two events have been found by the geophysicists of the Induced Seismicity Taskforce at Shell to have the same hypocentre with RD coordinates (in metres) of 247250 (X) and 593550 (Y), and a depth of 2900 metres. Five days later on the 13th October 2022, a third earthquake occurred with an epicentre 300 m to the north of these two earthquakes on the 8th October 2022 (Table 2.1).

No	Date	Time	Location	Northing	Easting	Depth	Magnitude
43	13-Oct-22	16:08:49	Wirdum	593350	247550	3000	1.4
41	8-Oct-22	05:35:37	Garrelsweer	593550	247250	2900	1.2
40	8-Oct-22	02:17:17	Wirdum	593550	247250	2900	3.1

Table 2.1 Timing, location and magnitude of earthquakes in October 2022 near the village of Wirdum.

Map with the location of the earthquakes near Wirdum on the 8th October 2022 is provided in figures 2.1 and 2.2.

The highest observed earthquake density is currently located near Uithuizen, where in the last two months some eight earthquakes occurred. As Wirdum is located some 10 km to the south of Uithuizen, the highest earthquake density is not affected by these earthquakes near Wirdum (Fig. 2.3).

2.3 Source mechanism

Despite the two earthquakes on the 8th October having the same epicentre, the orientation of their source mechanism is quite different, indicating these earthquake did not originate from the same fault (Table 2.2).

No	Date	Time	Location	Strike	Dip	Rake	Magnitude
43	13-Oct-22	16:08:49	Wirdum	129.12	64.65	-104.59	1.4
41	8-Oct-22	05:35:37	Garrelsweer	312.24	69.15	-115.10	1.2
40	8-Oct-22	02:17:17	Wirdum	153.39	307.89	-69.04	3.1

Table 2.2 Source mechanism of earthquakes in October 2022 near the village of Wirdum.

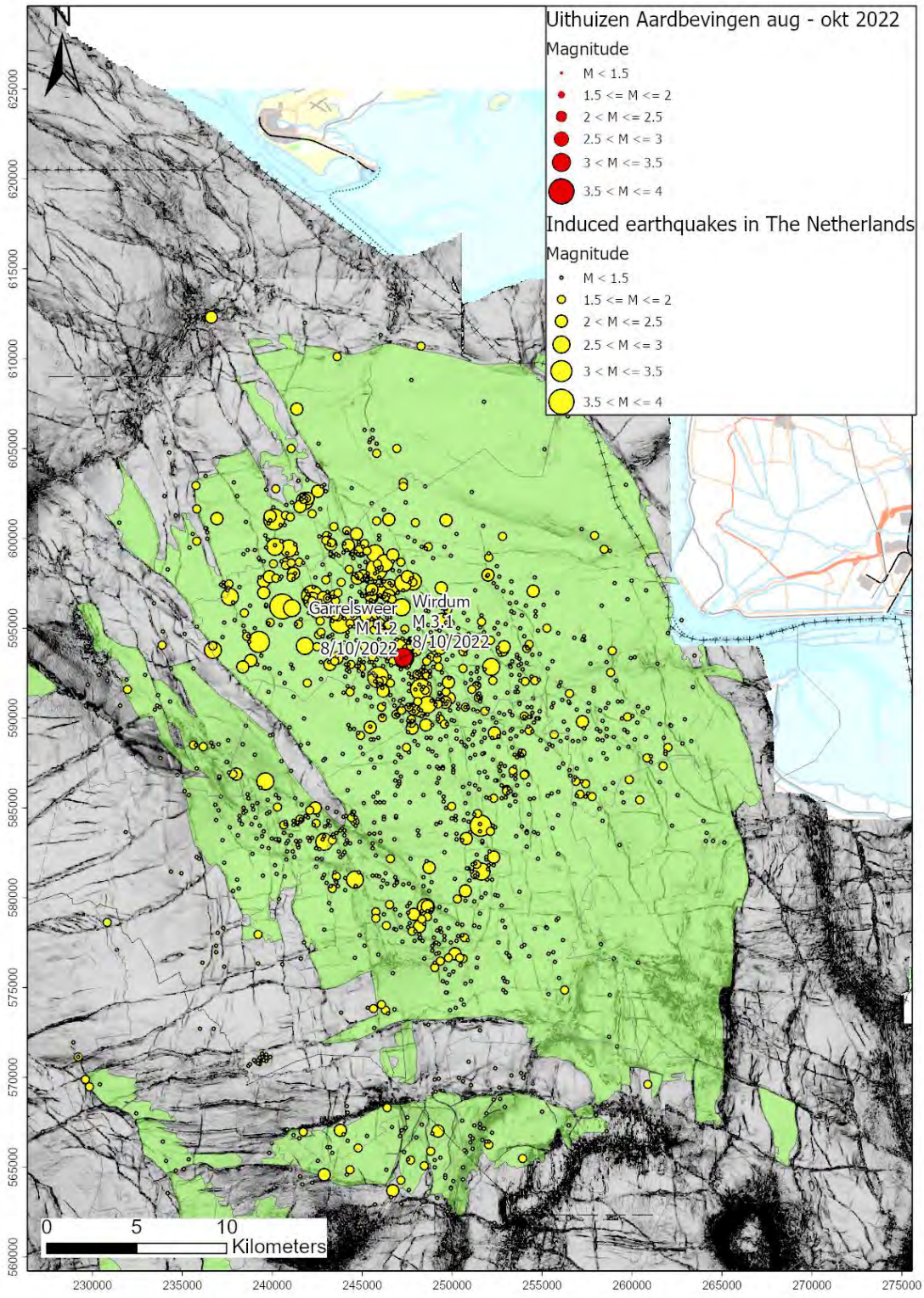

Figure 2.1 Map of the deep subsurface with in green the Groningen gas field and surrounding gas fields. The red dot shows the location of the earthquake near Wirdum on 8th October 2022. All other earthquakes before 1st October 2022 have been indicated as yellow dots. The size of the dot is an indication of the magnitude of the earthquake.

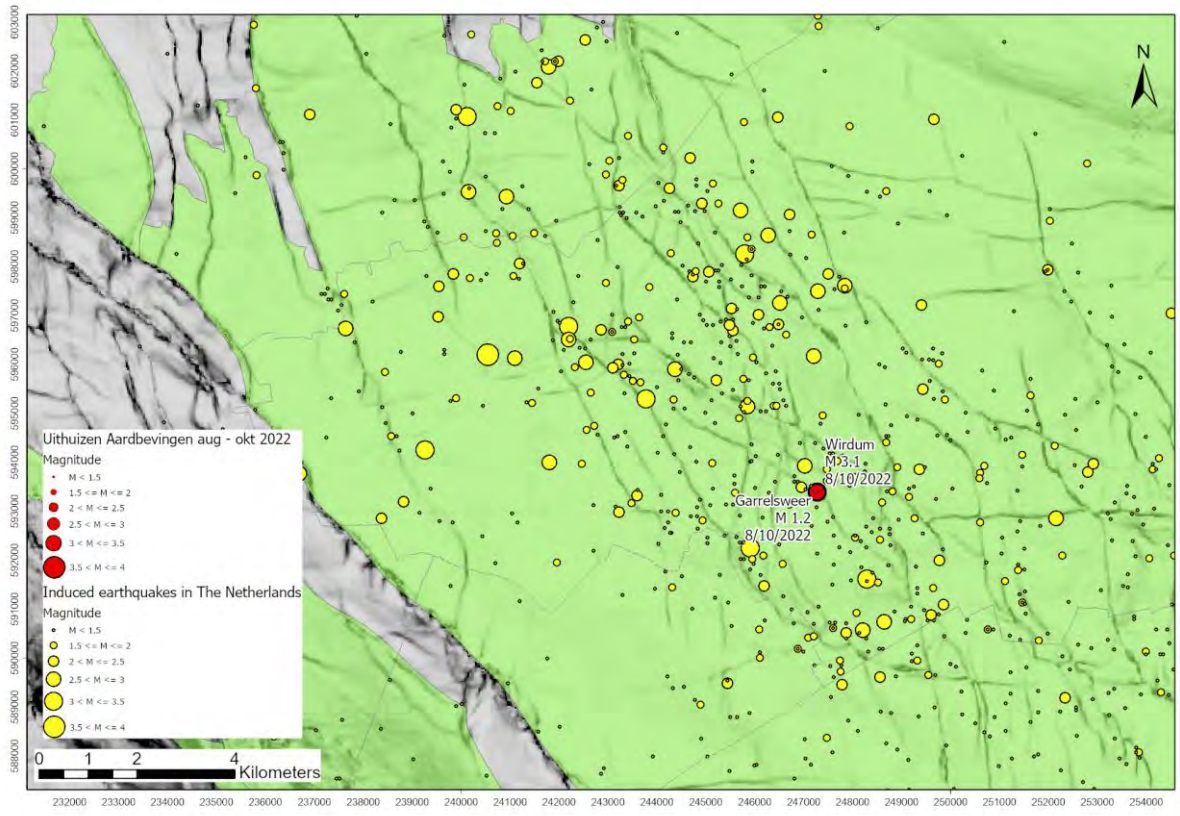

Figure 2.2 Enlargement of figure 2.1 showing the location of the earthquakes on the 8th October 2022 near Wirdum.

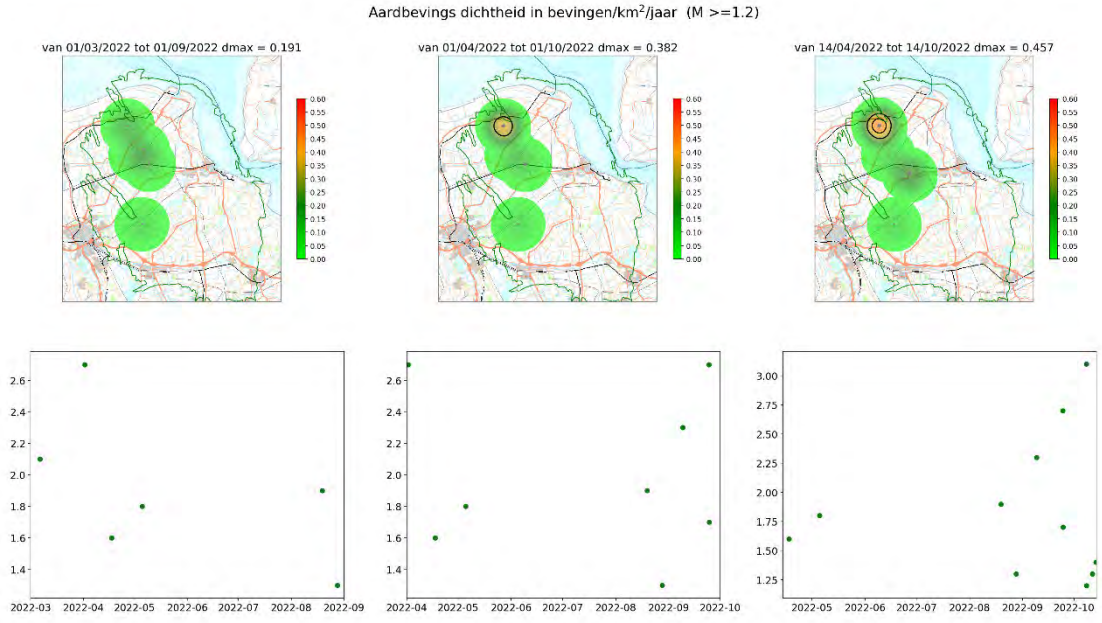

Figure 2.3 Top: Earthquake density maps for earthquakes with a magnitude larger ML ≥ 1.2 during the previous six months. The earthquake density is shown as an annual density. Bottom: Graphs of earthquake magnitude versus date. Left map shows the earthquake density at 1st September 2022. The middle map shows earthquake density at 1st October 2022 and the right map at 14th October 2022.

3 Analysis of the recorded surface ground-motions Recorded During the ML 1.2 and 3.1 Wirdum Earthquakes of 8th October 2022

3.1 Introduction

The locations of the epicentres with respect to the B-network and G-network, the two strong-motion networks operated by the KNMI in the Groningen field (Ref. 44 and 46), as well as with respect to the earthquakes of the database of Ntinalexis *et al*. (Ref. 47), are as shown in Figure 3.1.

The magnitude of first and larger of the two events (M_L3.1) falls within the range considered in the Groningen Hazard and Risk Assessment, where the lower limit is M_L2.5, and therefore within the range of applicability of the Groningen V6 and V7 Ground-Motion Models (GMMs; Ref. 39, 41 and 43). It also falls within the range of applicability of the current empirical Ground-Motion Prediction Equations (GMPEs) used to estimate values of peak ground velocity (PGV) due to earthquakes in the Groningen field (GMPE: Ref. 42 and 43), where the lowest magnitude considered is M_L1.8. The most recent event with a magnitude greater than 1.8 and 2.5 prior to this latest earthquake was the M_L2.7 Uithuizen earthquake of 24th September 2022. The purpose of this chapter is to provide an overview of the ground-motions recorded in the two Wirdum events on the 8th October 2022 in terms of their amplitudes and durations and compare the amplitudes of motion recorded during the M_L3.1 event with predictions from the empirical PGV GMPEs as well as the V6 and V7 Groningen Ground-Motion Models.

In order to carry out this analysis, a total of 83 records from each of the two events were accessed from the online portal of the KNMI (KNMI, 1993; http://rdsa.knmi.nl/dataportal/), corresponding to 74 records from the surface accelerographs of the G-network and 9 records from the accelerographs of the B-network. The records were processed as described by Edwards & Ntinalexis (Ref. 45); there are 75 usable records from the M_L3.1 event, obtained at distances ranging from 1.00 to 27.94 km, and four usable records from the M_L1.2 event, obtained at distances ranging from 1.25 to 14.43 km. Figure 3.2 shows the usable recordings in the magnitude-distance occupied by the database of Ntinalexis *et al*. (Ref. 47).

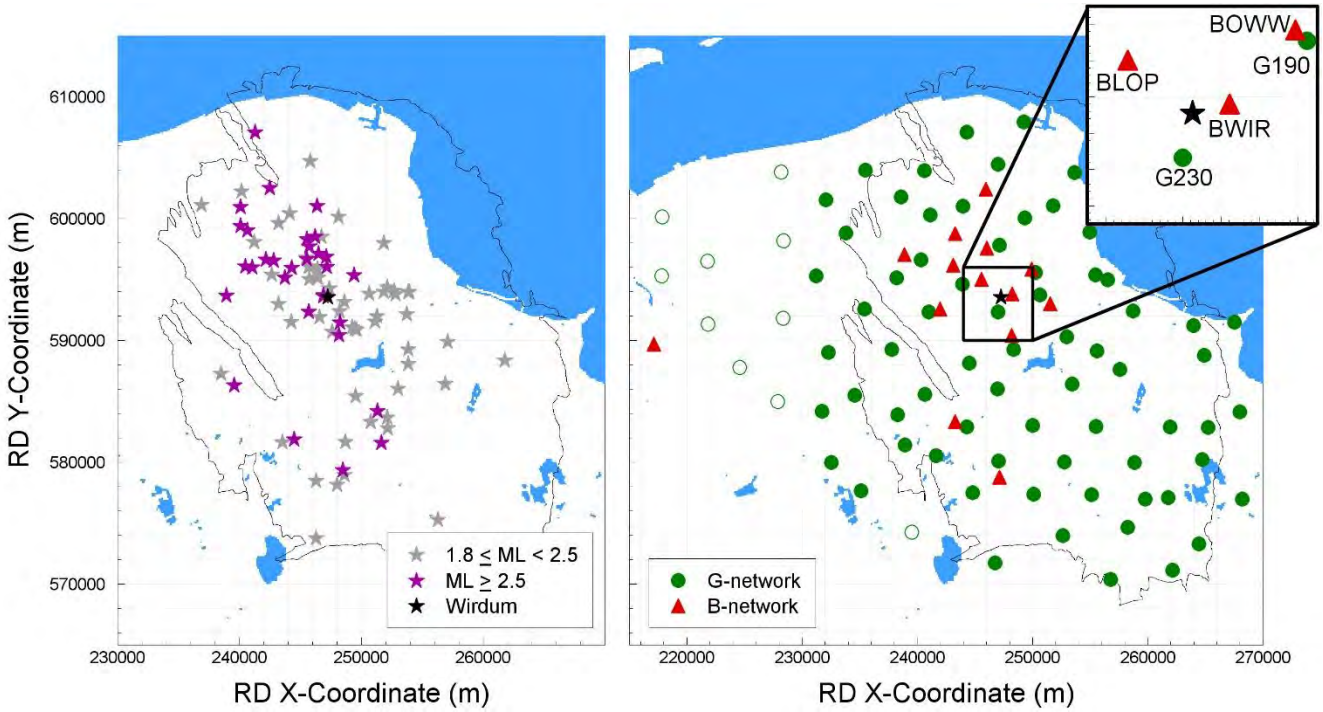

Figure 3.1 *Left: Epicentres of the two earthquakes (black stars) together with epicentres of previous earthquakes of $M_L \geq 2.5$ (magenta stars) and of M_L 1.8-2.4 (grey stars). Right: G-network (green) and B-network (red) stations; open circles indicate G-stations without borehole geophones.*

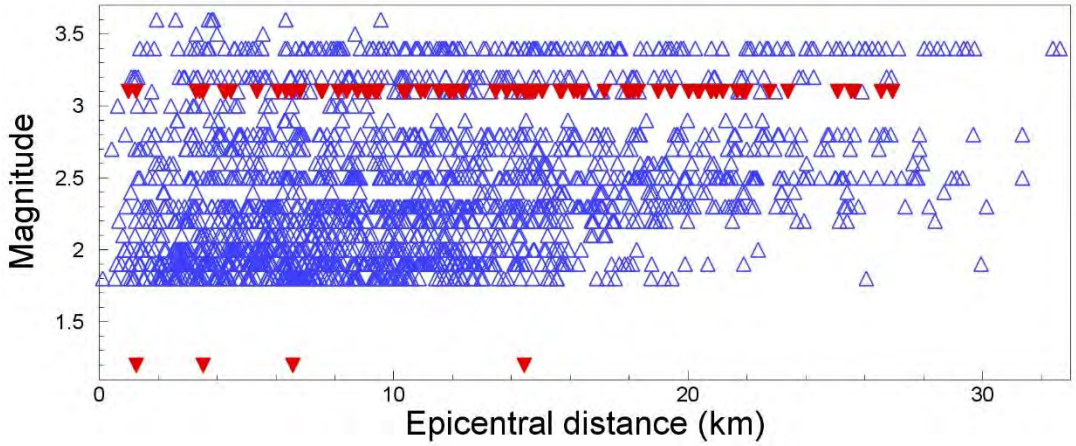

Figure 3.2 Magnitude-distance distribution of the recordings (red) compared with the database of Ntinalexis et al. (Ref. 47; blue)

3.2 Peak Ground Accelerations and Velocities

Figure 3.3 shows the geometric mean horizontal components of PGA and PGV plotted against magnitude together with the corresponding values from the complete database of Ntinalexis *et al*. (Ref. 47). Overall, the motions appear to have a similar amplitude range to those observed in previous earthquakes. At the same time, the largest PGA and PGV values recorded during the M_L3.1 event are now the largest values recorded for an event of that magnitude in Groningen. Figures 3.4 and 3.5 show the horizontal values of PGA and PGV of three component definitions from each recording obtained during the Wirdum earthquakes plotted against the distance of the recording site from the epicentre. The definitions shown are a) the geometric mean component (GM), which is the geometric-mean of

the values corresponding to each as-recorded horizontal component, b) the larger component, which corresponds to the larger of the two values recorded by the horizontal components and c) maximum-rotated component (MaxRot) or vector component, which is the largest value that can be obtained by rotating the two horizontal components through all angles.

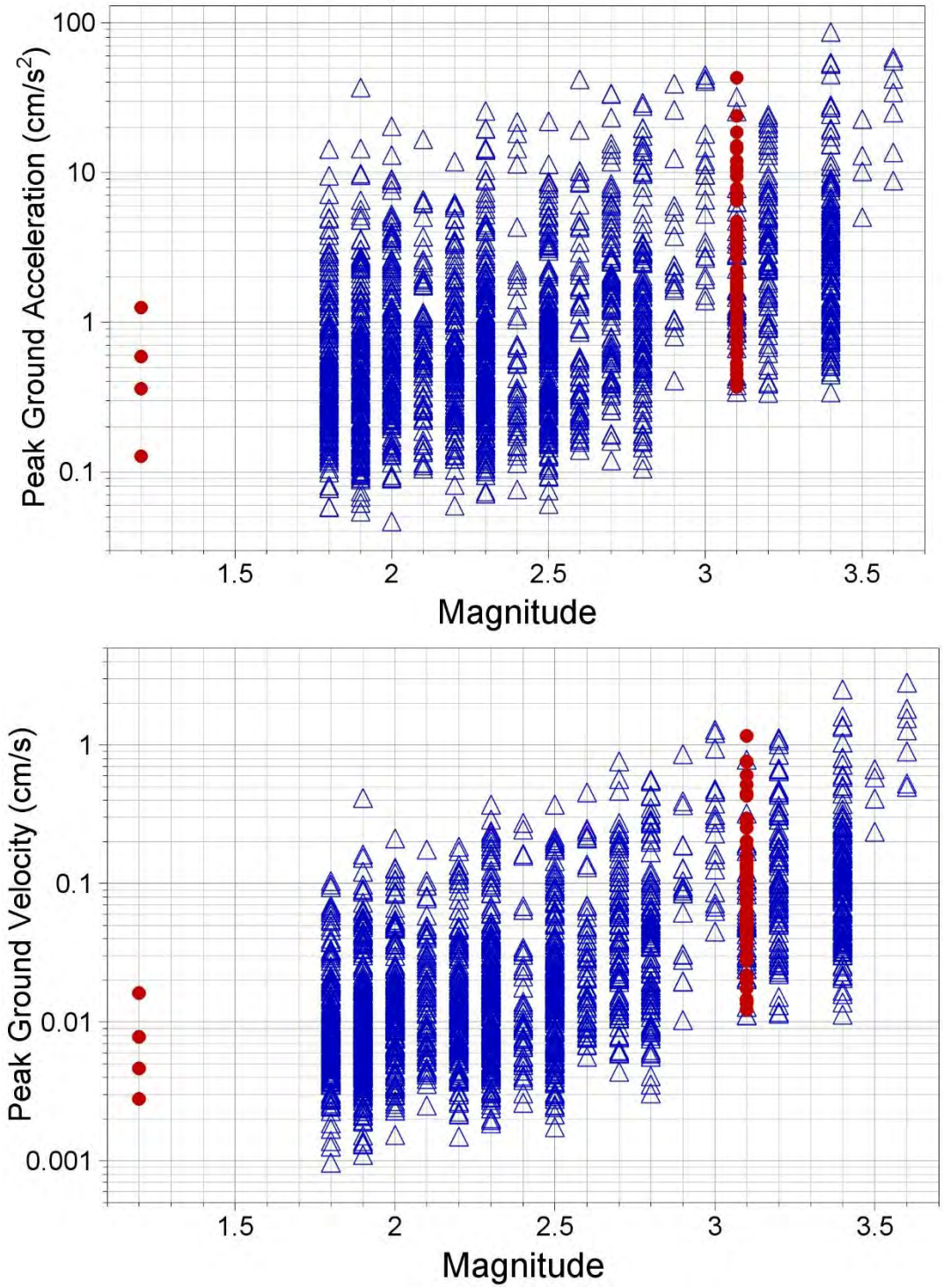

Figure 3.3 Geometric mean horizontal components of PGA (upper) and PGV (lower) recorded during the two Wirdum earthquakes (red) and in previous earthquakes (blue) plotted against local magnitude.

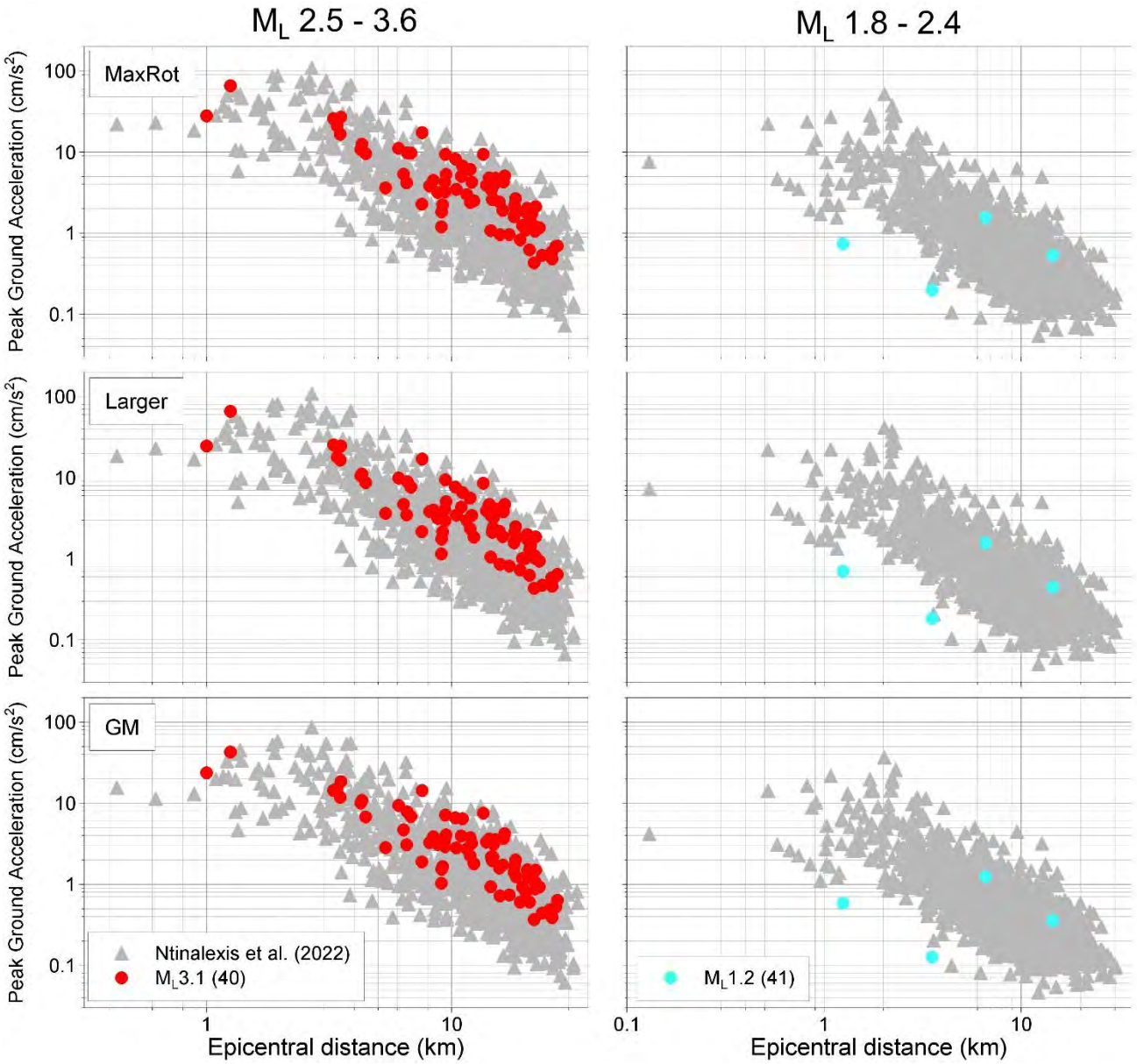

Figure 3.4 Horizontal components of PGA recorded during the Wirdum earthquakes and previous earthquakes plotted against epicentral distance

The PGA and PGV values from the M_L3.1 event appear on Figures 3.4 and 3.5 to be, on average, larger than those of the other events, although it must be noted that the majority of the values plotted on the frames of the left side originate from events of M_L2.5-2.9, as can be seen in Figure 3.2.

The largest recorded PGA and PGV values of the M_L3.1 event were at station G230 located 1.25 km from the epicentre, on the H1 (NS) component. The largest PGA was 65.78 cm/s^2, which is now the ninth-largest value that has been recorded by the KNMI networks in Groningen since 2006, but appreciably smaller than the largest PGA which was recorded at the EW component of the BGAR station during the 8 January 2018 M_L3.4 Zeerijp earthquake with a value of 108.68 cm/s^2. The largest PGV was 2.46 cm/s, the fifth largest recorded since 2006; the largest PGV recorded to date was a 3.46 cm/s on the NS component of the MID1 station during the 16 August 2012 M_L3.6 Huizinge earthquake. The largest PGA and PGV values of the M_L1.2 event were 1.56 cm/s^2 and 0.02 cm/s and were recorded at station G240, 6.58 km from the epicentre, on the H1 (NS) component. The horizontal and vertical components of both acceleration and velocity from these recordings are shown in Figures 3.6 and 3.7.

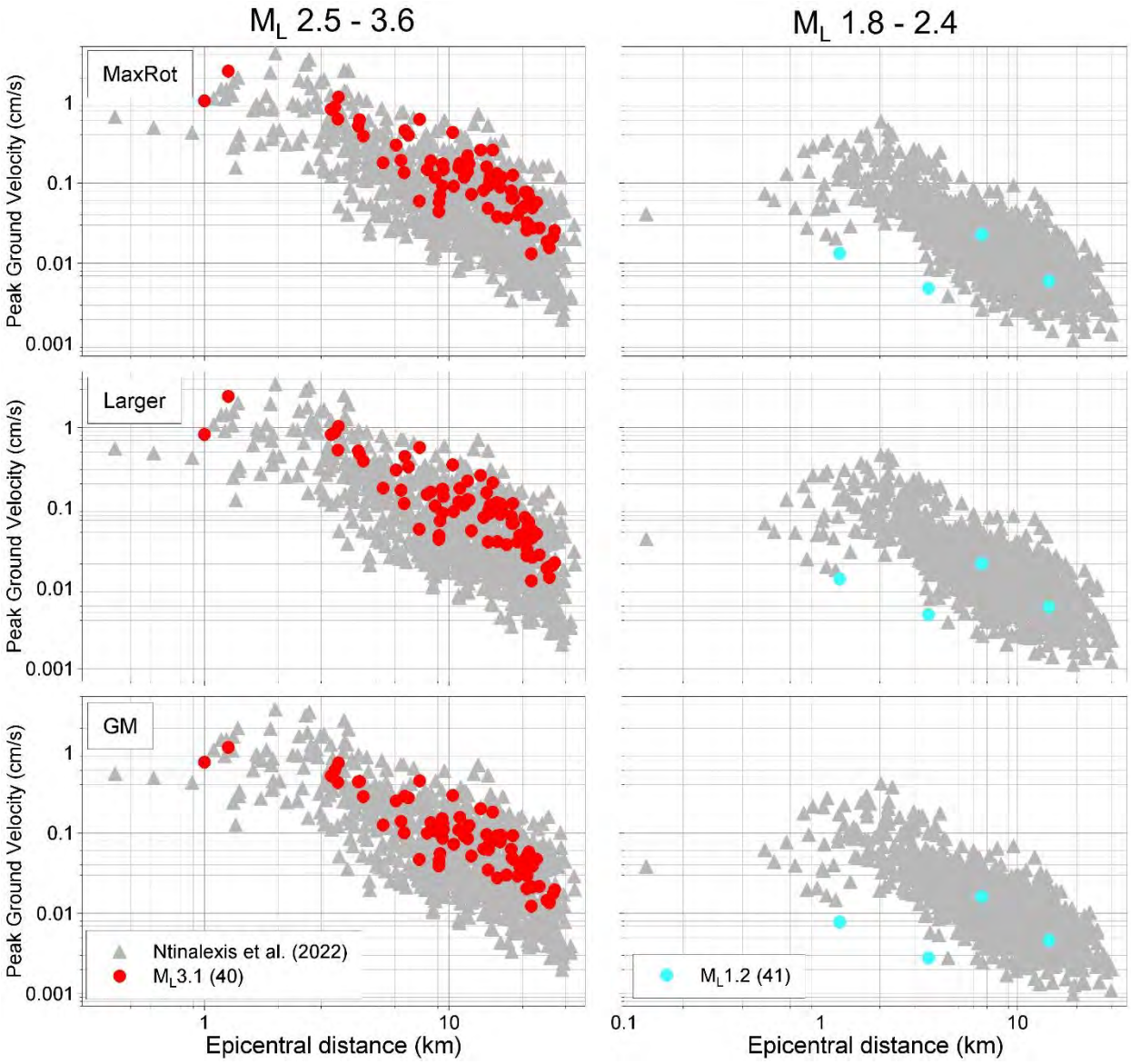

Figure 3.5 Horizontal components of PGV recorded during the Wirdum earthquakes and previous earthquakes plotted against epicentral distance

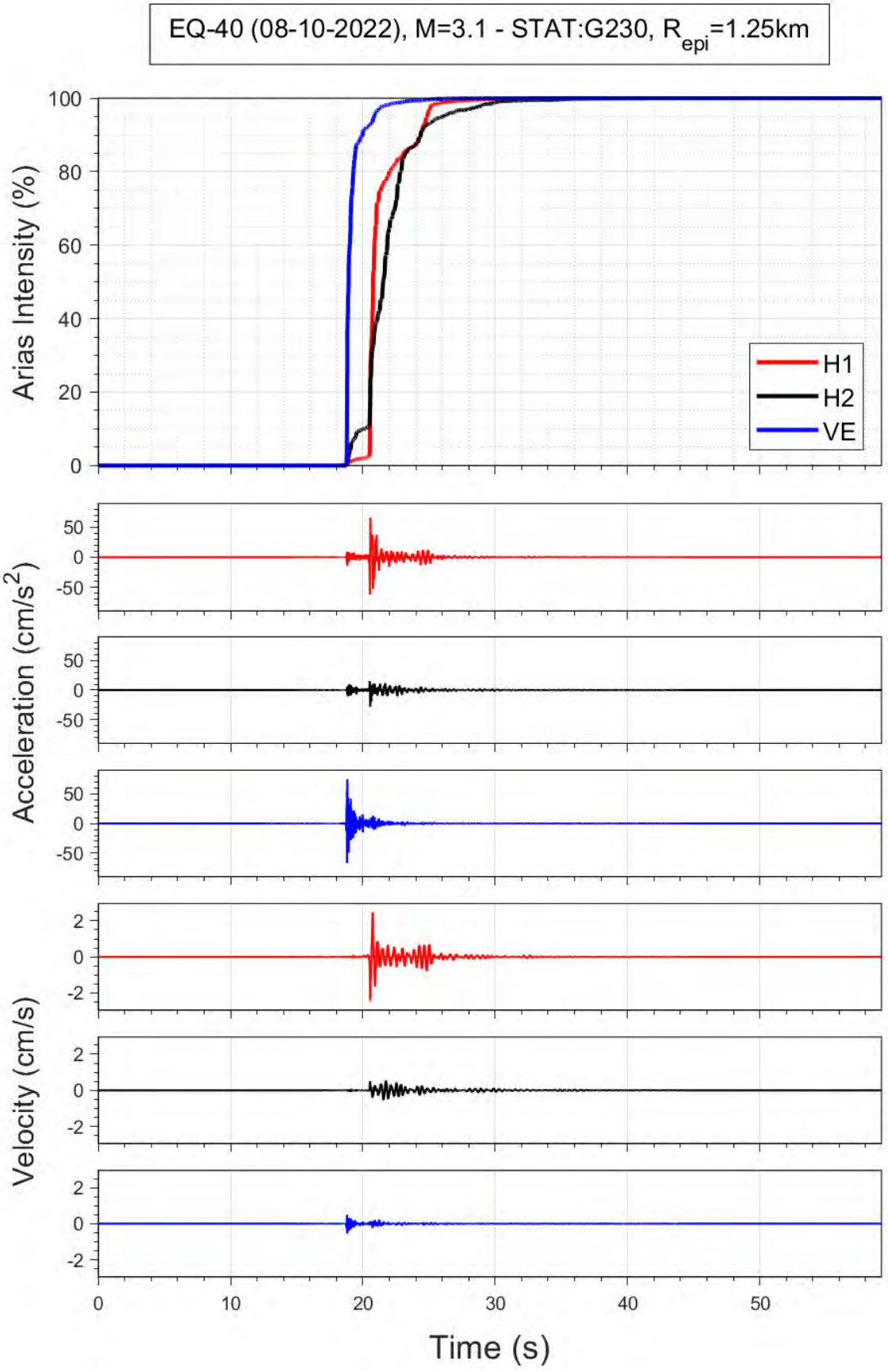

Figure 2.6 Horizontal components of acceleration and velocity recorded at the G230 station during event 40 (M_L3.1); the upper frame shows the accumulation of Arias intensity (energy) over time.

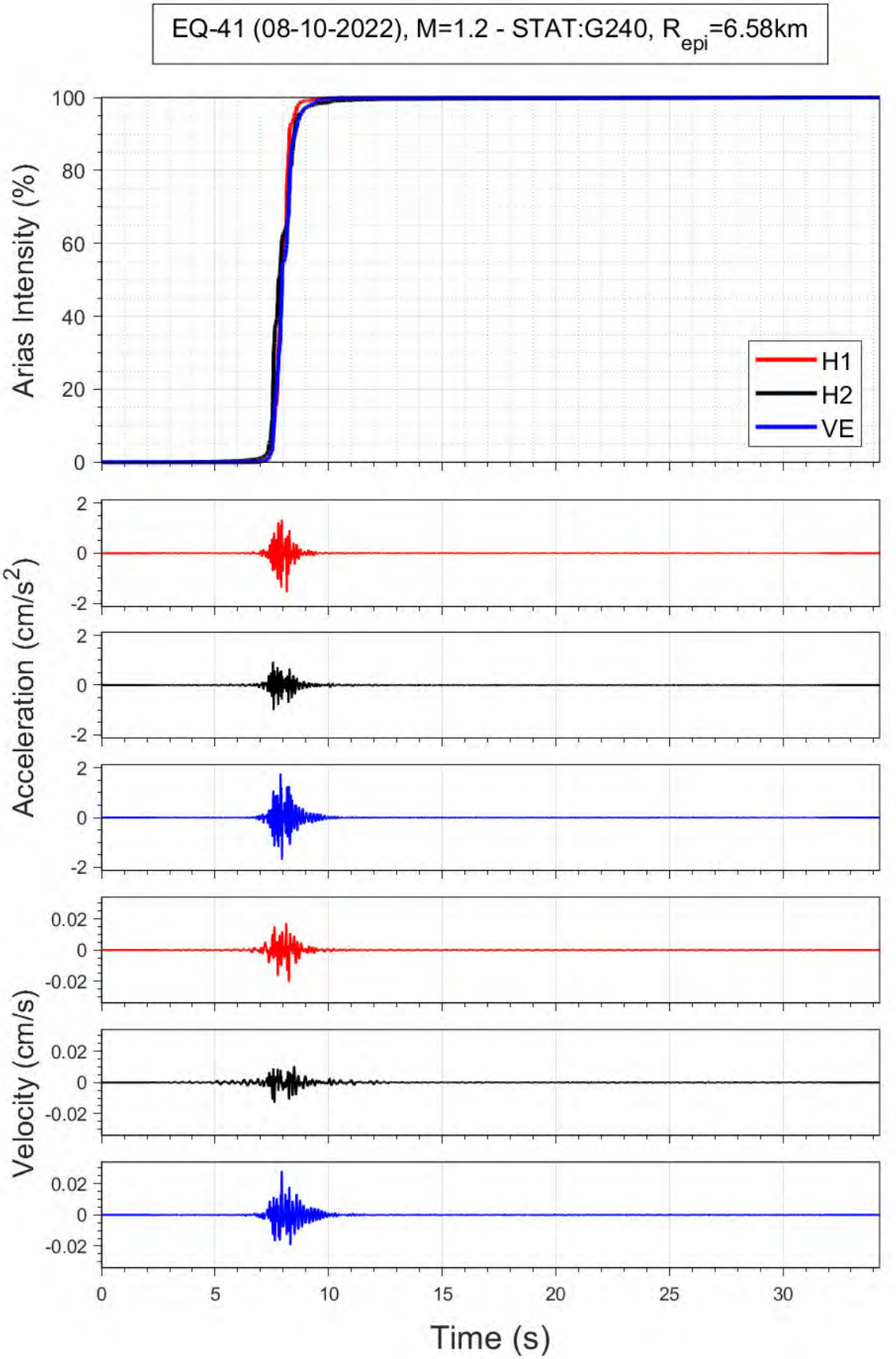

Figure 2.7 Horizontal components of acceleration and velocity recorded at the G240 station during event 41 (M_L1.2); the upper frame shows the accumulation of Arias intensity (energy) over time.

Figures 3.8 and 3.9 show the horizontal components of PGA and PGV obtained within 4 km of the epicentre, from which a number of observations can be made. First of all, it can be appreciated that the very strong polarisation often observed in Groningen recordings due to the distinct radiation pattern of small-magnitude events (Ref. 40 and 49) is also significantly prominent in the records of these events, especially during the M_L3.1 event at stations G180, G230, BOWW, and BHKS. At BHKS particularly, the component-to-component ratio exceeded a value of 3; the time-histories of this record are shown in Figure 3.10.

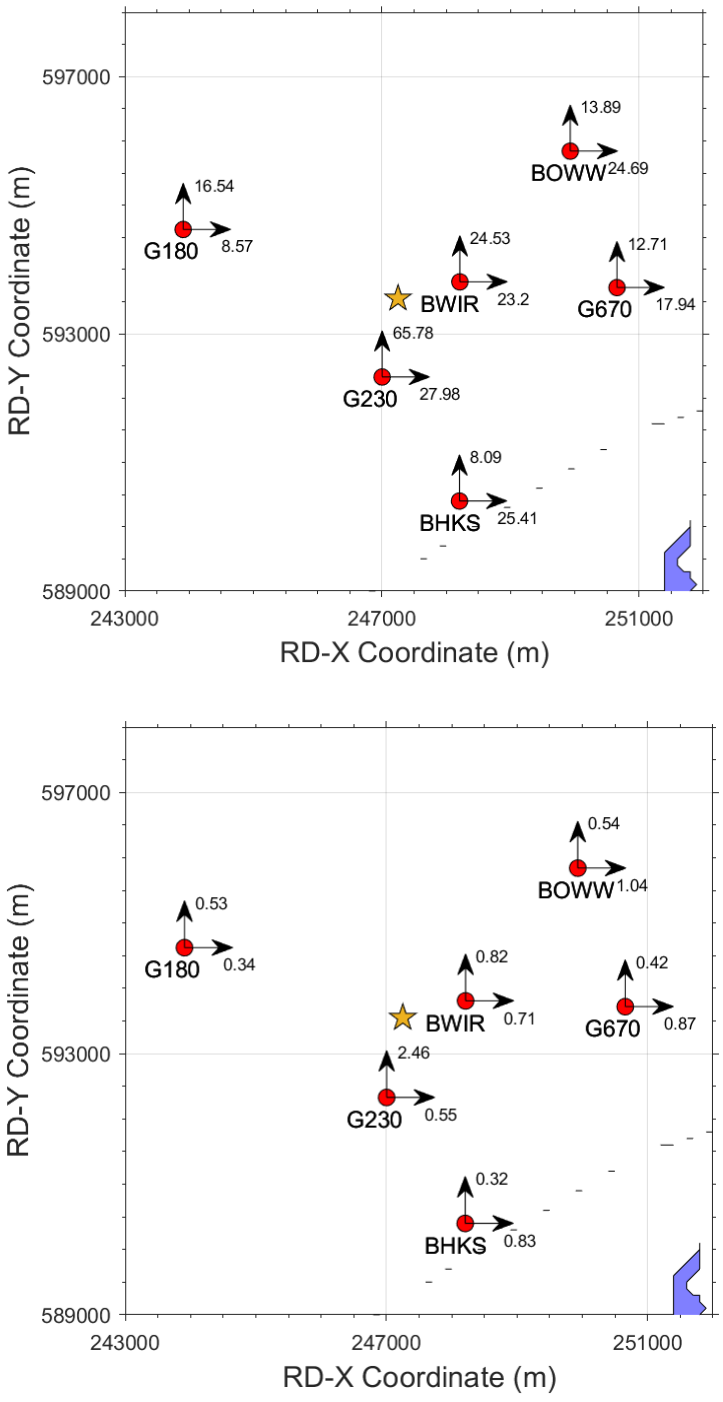

Figure 2.8 Horizontal components of PGA (upper) and PGV (lower) recorded during event 40 (M_L3.1) at epicentral distances of less than 4 km; units are cm/s^2 and cm/s, respectively.

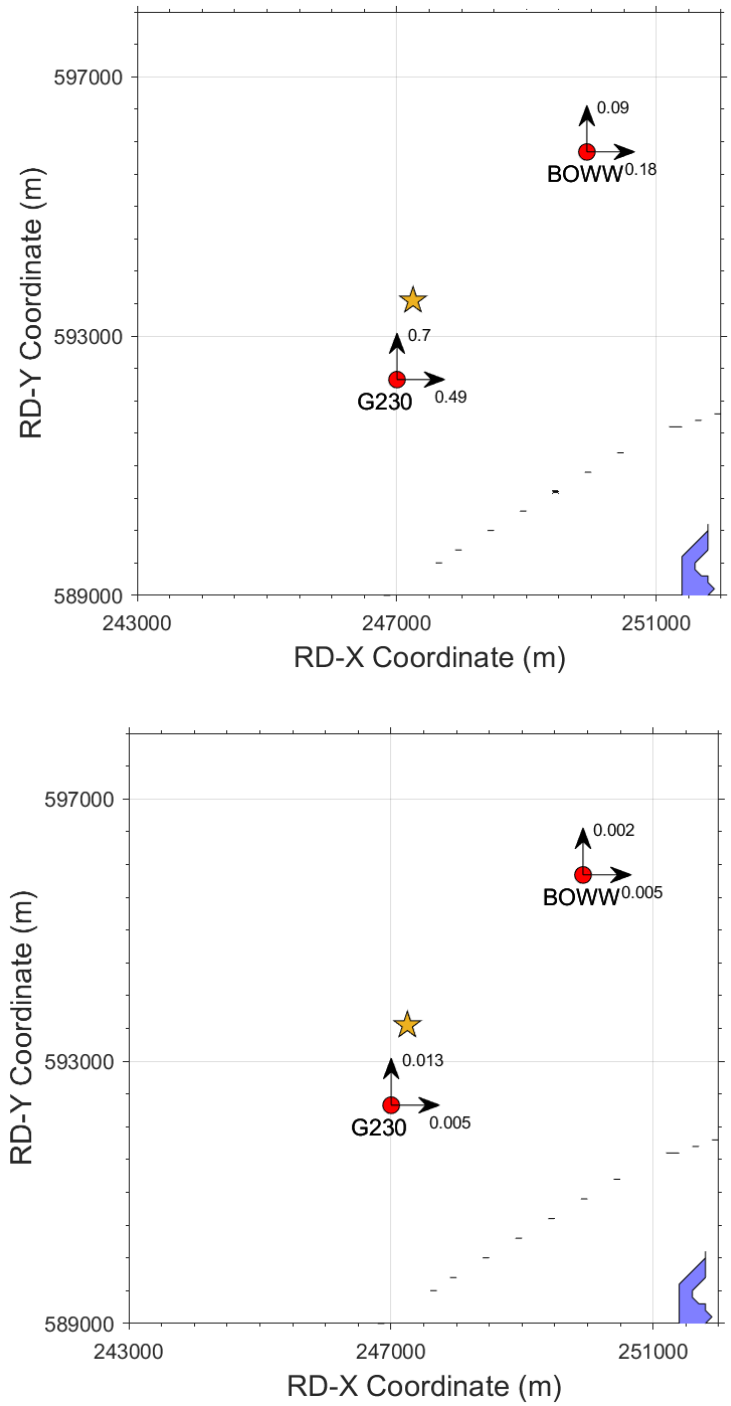

Figure 2.9 Horizontal components of PGA (upper) and PGV (lower) recorded during event 41 (ML1.2) at epicentral distances of less than 4 km; units are cm/s2 and cm/s, respectively.

The effects of the radiation pattern are also apparent when comparing the amplitudes of the recordings, with significantly larger amplitudes recorded to the southwest and northeast of the epicentre. Another observation that can be made in Figure 3.9 is also related to the radiation pattern: the absence of usable records from a number of stations near the epicentre. This is a combination of the reduction in amplitudes due to the small magnitude of the event, as well as the location of most of those stations outside the southwest-northeast azimuth of the radiation pattern, as well as the strong polarization of the recordings, which resulted in some records having one usable horizontal

component and one unusable, with a much smaller amplitude. An example of this is shown in Figures 3.11 and 3.12.

As already shown in Figures 3.4 and 3.5, the amplitudes decay rapidly with distance although the effect of simultaneous arrivals of direct and critically refracted/reflected waves leads to an increase in amplitudes at some locations between 12 and 20 km from the epicentre. However, these effects do not lead to significant absolute amplitudes at those distances, and it is clear that, outside the epicentral area, the motions are of very low amplitude: < 0.01*g* for PGA and < 0.1 cm/s for PGV.

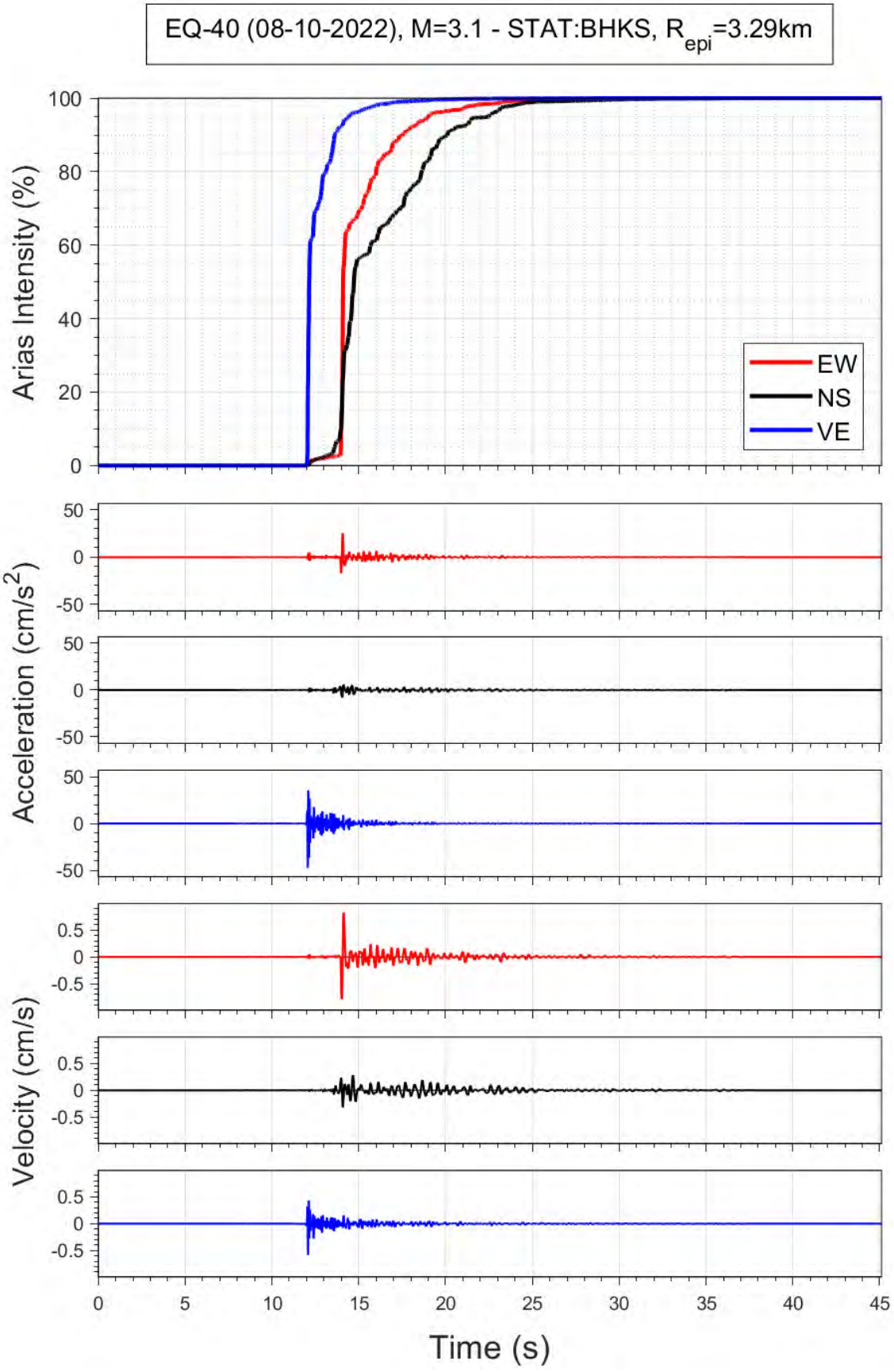

Figure 3.10 Horizontal components of acceleration and velocity recorded at the BHKS station during event 40 (M_L3.1); the upper frame shows the accumulation of Arias intensity (energy) over time.

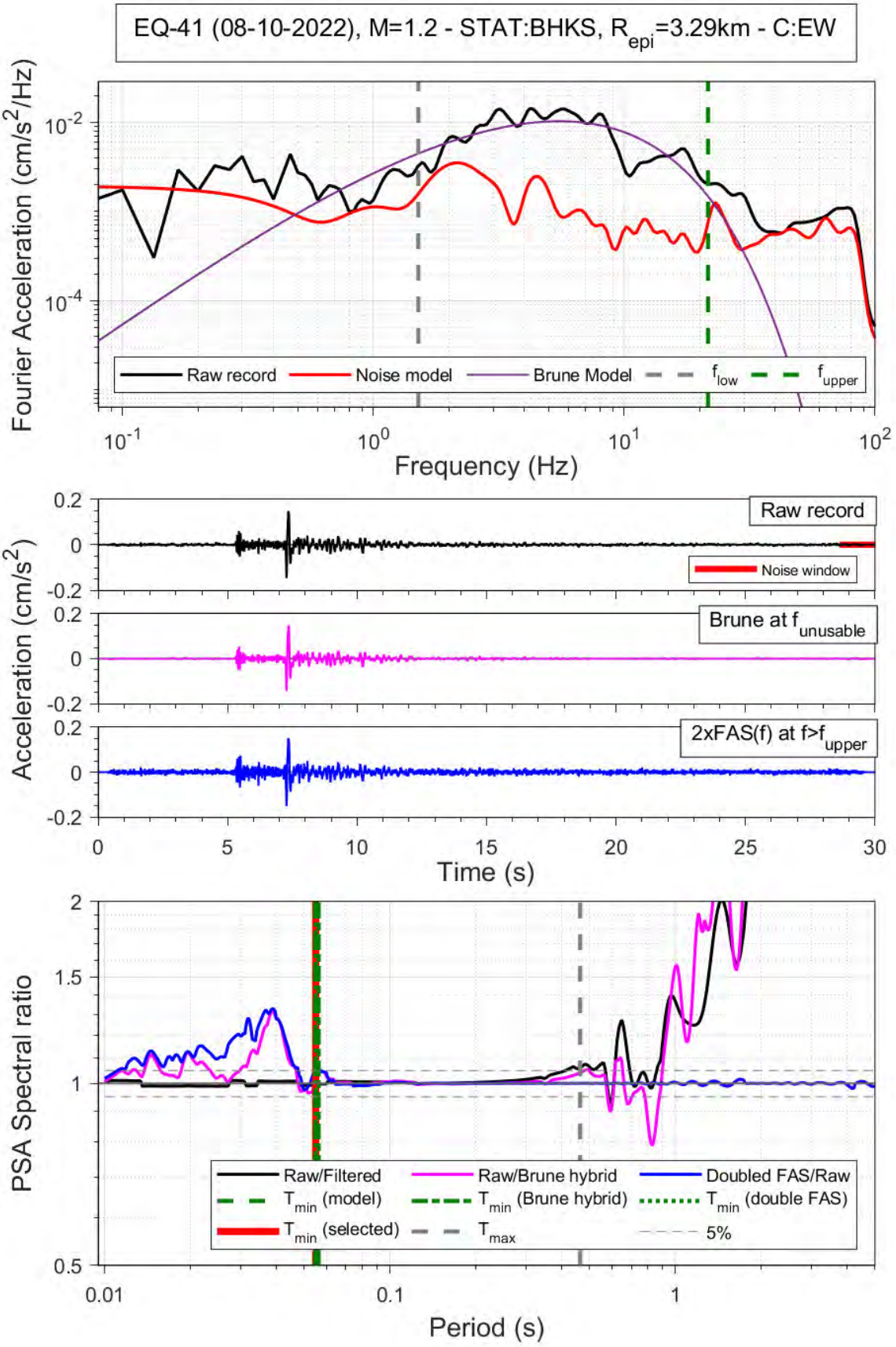

Figure 3.11 Usability assessment of the EW component of the BHKS station during event 41 (M_L1.2); for a detailed discussion of what is shown, the reader is referred to Edwards & Ntinalexis (Ref. 45)

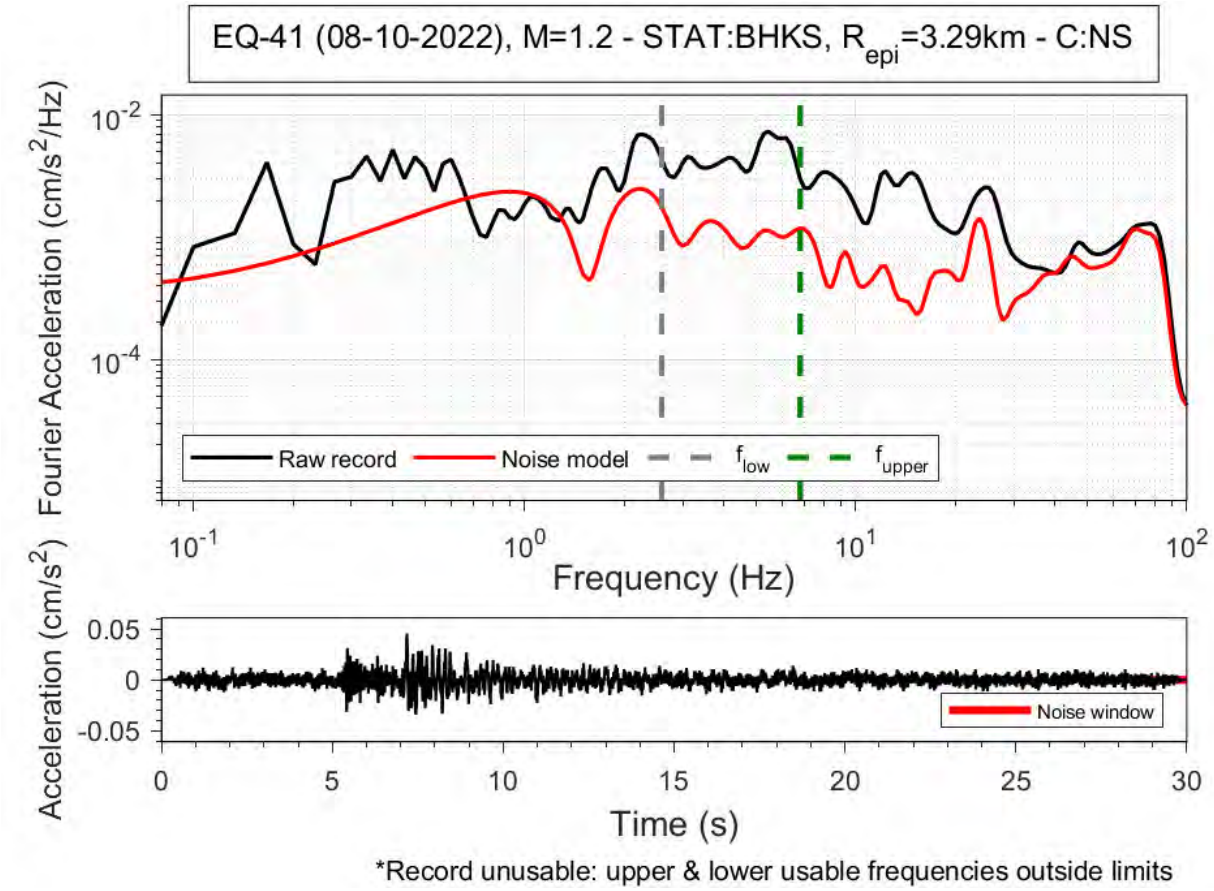

Figure 3.12 Usability assessment of the NS component of the BHKS station during event 41 (M_L1.2); for a detailed discussion of what is shown, the reader is referred to Edwards & Ntinalexis (Ref. 45). The amplitude of this recording is very small due to the strong polarization observed at this station; hence, the amplitude of the earthquake signal is not large enough for the signal to be clearly distinguishable from the noise that is also recorded. This is not true for the other horizontal component (EW), where the signal amplitude was sufficient.

3.3 Ground-Motion Durations

The maximum amplitude of ground shaking, whether represented by PGA or PGV, provides a simple indication of the strength of the motion but the potential for adverse effects—such as damage to masonry buildings or triggering of liquefaction—also depends on the duration or number of cycles of the motion.

A feature that has been consistently observed in the Groningen ground motions is a very pronounced negative correlation between PGA and duration, with high amplitude motions consistently associated with shaking of very short duration (Ref. 38). The same pattern is observed in the recordings of the Wirdum earthquakes, as shown in Figure 3.13. The two shortest durations recorded during the Wirdum events were only 0.63 and 0.64 seconds; the first is associated with a PGA of 1.56 cm/s^2 and belongs to the H1 component of station G240 from the M_L1.2 event, while the latter is associated with a PGA of 24.69 cm/s^2 and belongs to the EW component of station BOWW from the M_L3.1 event. The acceleration and velocity time-histories from these recordings are shown in Figures 3.7 and 3.14, which also show the build-up of Arias intensity (which is a measure of the energy in the motion) over time. The strong concentration of the energy in a single pulse of motion in both cases is immediately apparent. Durations of the signals recorded in the H1 component of station G230, where the largest

PGA and PGV values of the M_L3.1 event were recorded, are also small at 0.845 seconds. The time-histories of that record are shown in Figure 3.6.

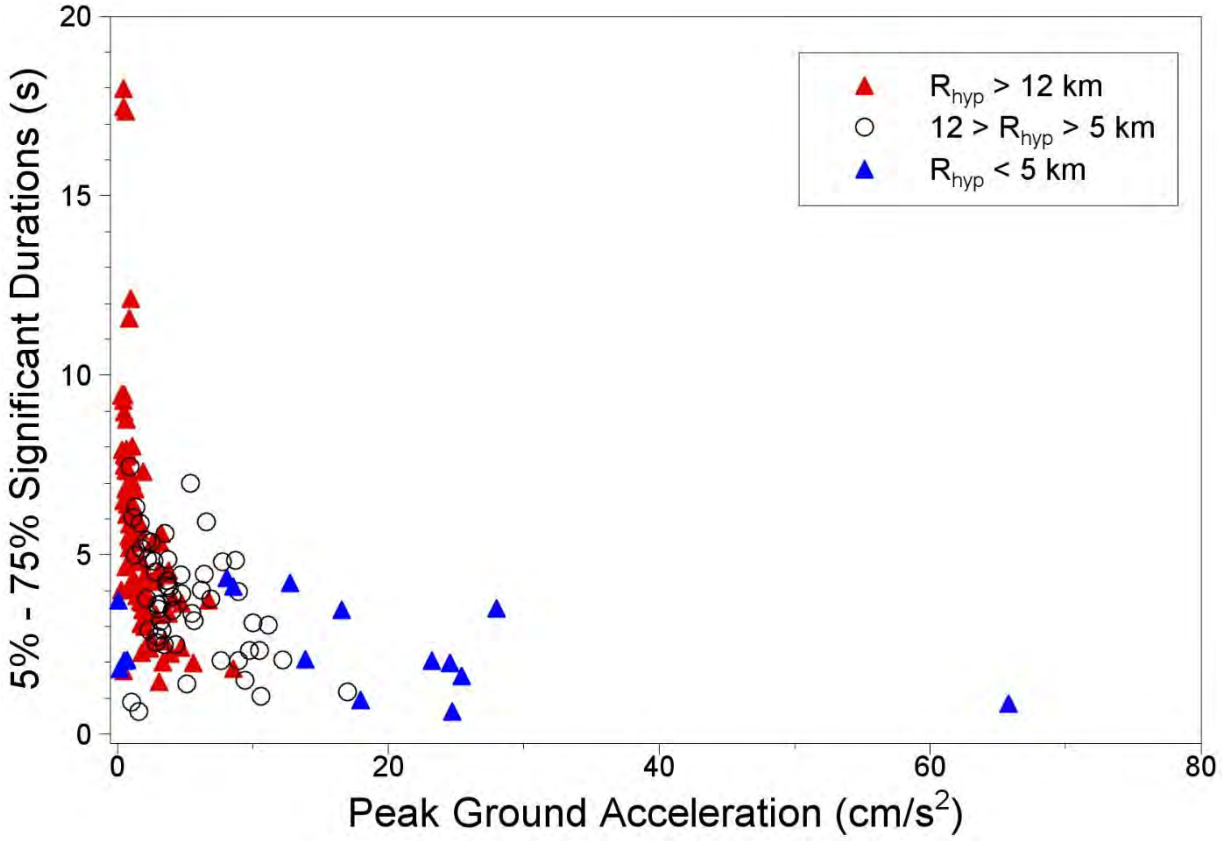

Figure 3.13 Pairs of PGA and significant duration for individual components of the Wirdum records, with symbols indicating the hypocentral distance of the recording.

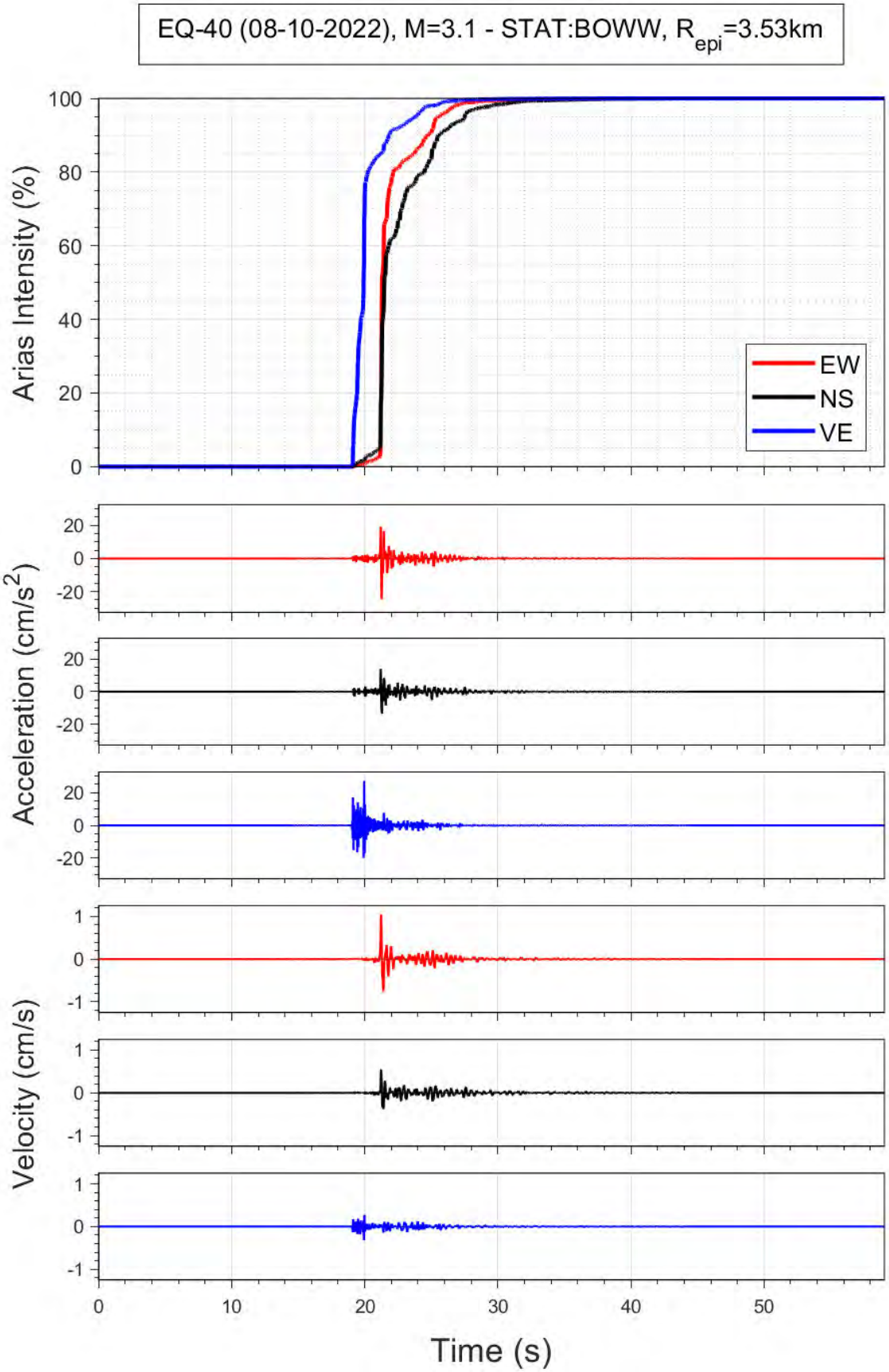

Figure 3.14 Horizontal components of acceleration and velocity recorded at the BOWW station during event 40 (M_L3.1); the upper frame shows the accumulation of Arias intensity (energy) over time.

3.4 Spectral Accelerations and Comparison with Ground-Motion Models

Additional insight into the nature of the ground motions can be obtained from the 5%-damped acceleration response spectra and Fourier spectra. The spectra from the recordings discussed above are shown in Figures 3.15 – 3.18. The spectral shapes are consistent with previous observations in the field. The divergence between the red and black curves in both frames shows that the horizontal polarisation of the recordings seen previously for PGA and PGV (Figures 3.8 and 3.9) persists across the entire range of usable response periods. As observed before in Groningen, and can also be seen in Figures 3.6, 3.7, 3.10 and 3.13, the spectral accelerations recorded on the vertical components are large relatively to the horizontal components.

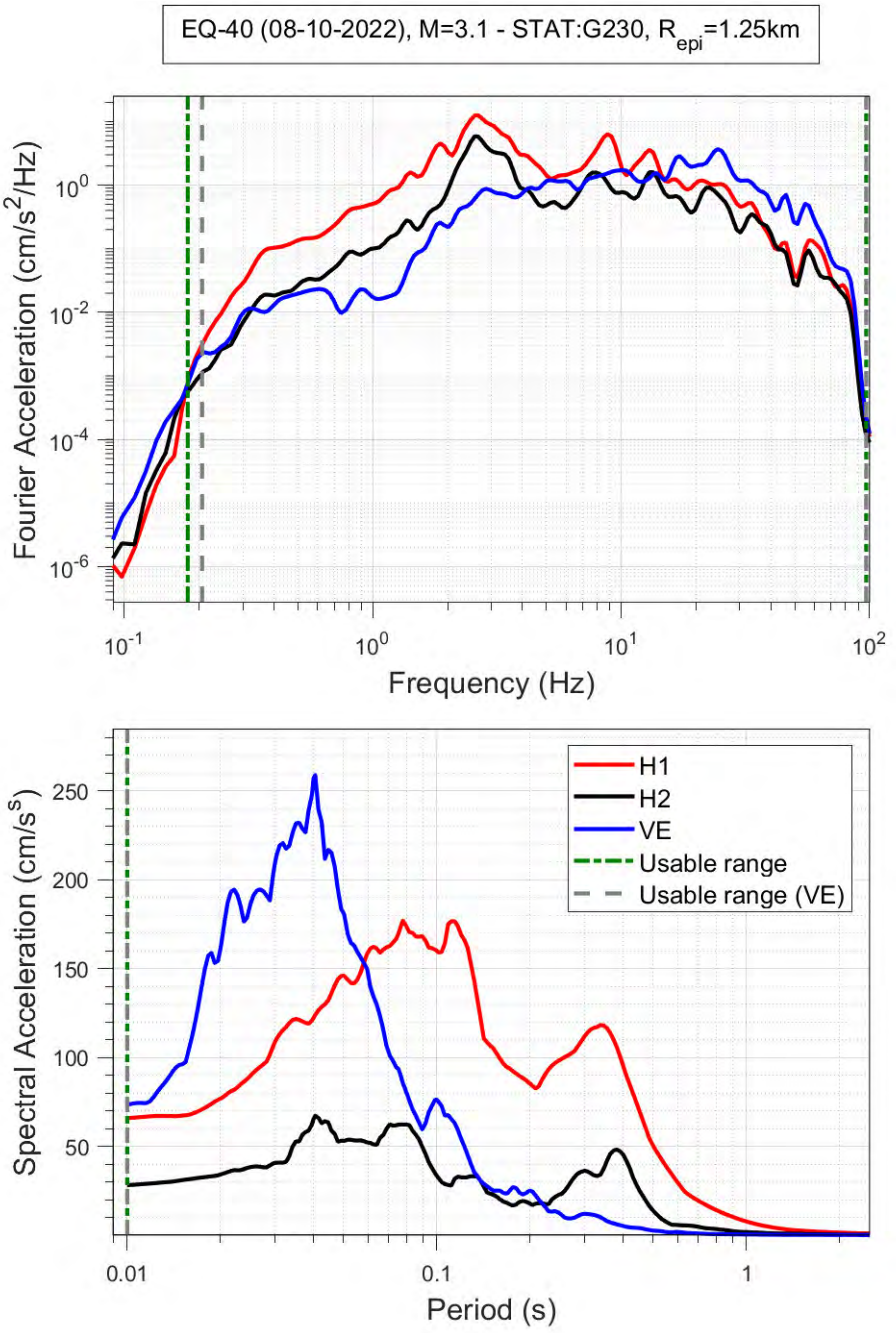

Figure 3.15 Fourier and response spectra from the G230 record of event 40 (M_L3.1).

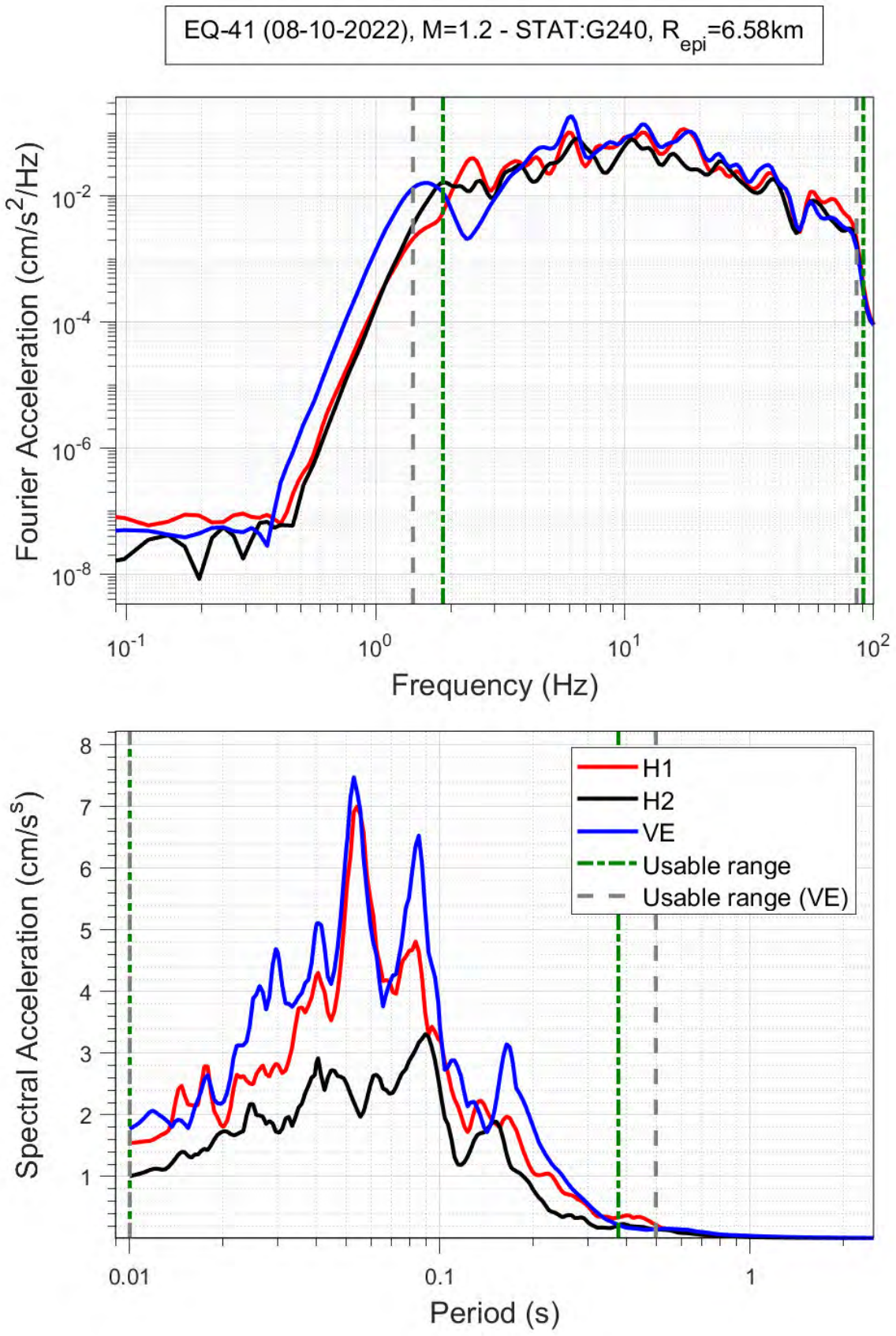

Figure 3.16 Fourier and response spectra from the G240 record of event 41 (M_L1.2).

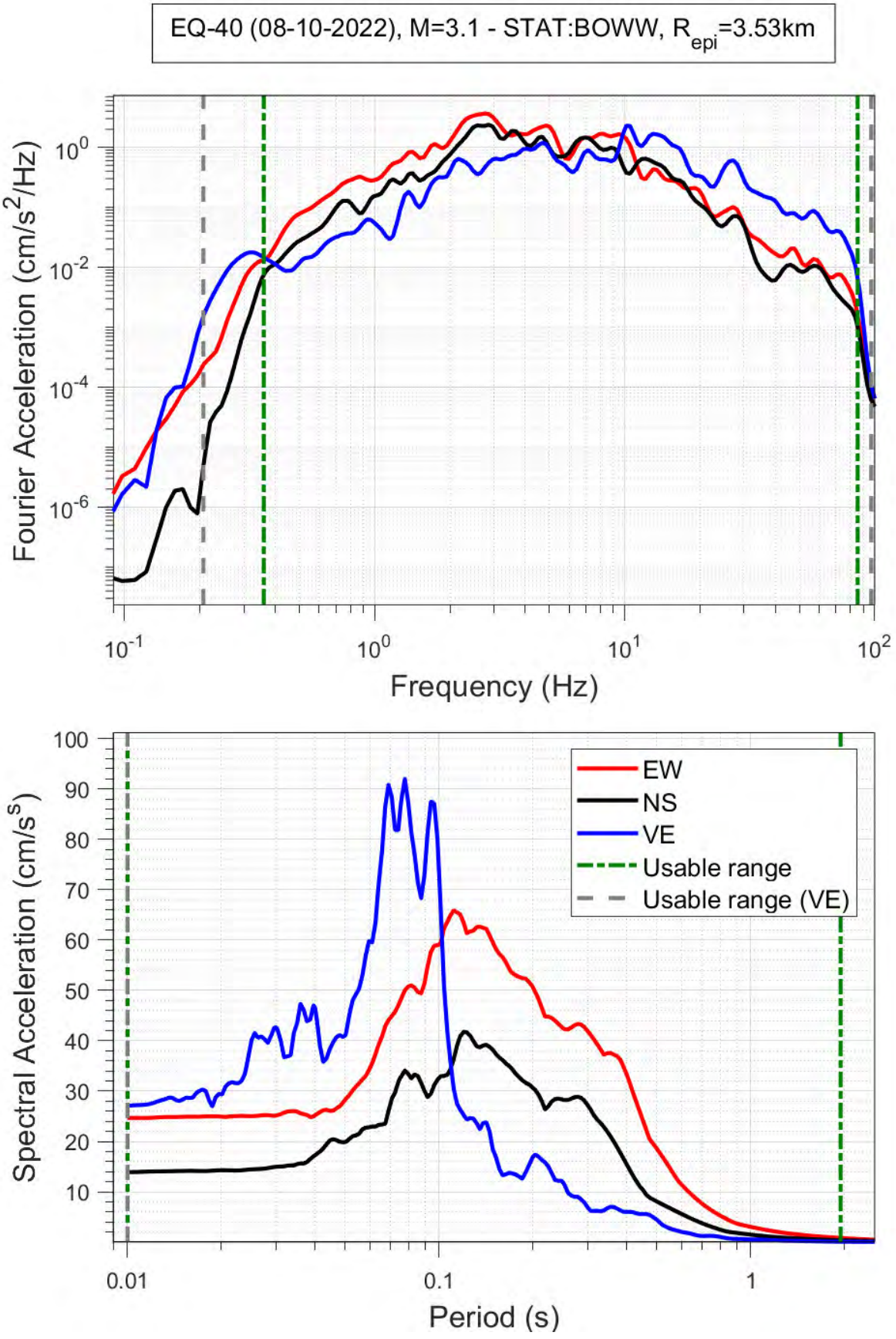

Figure 3.17 Fourier and response spectra from the BOWW record of event 40 (M_L3.1).

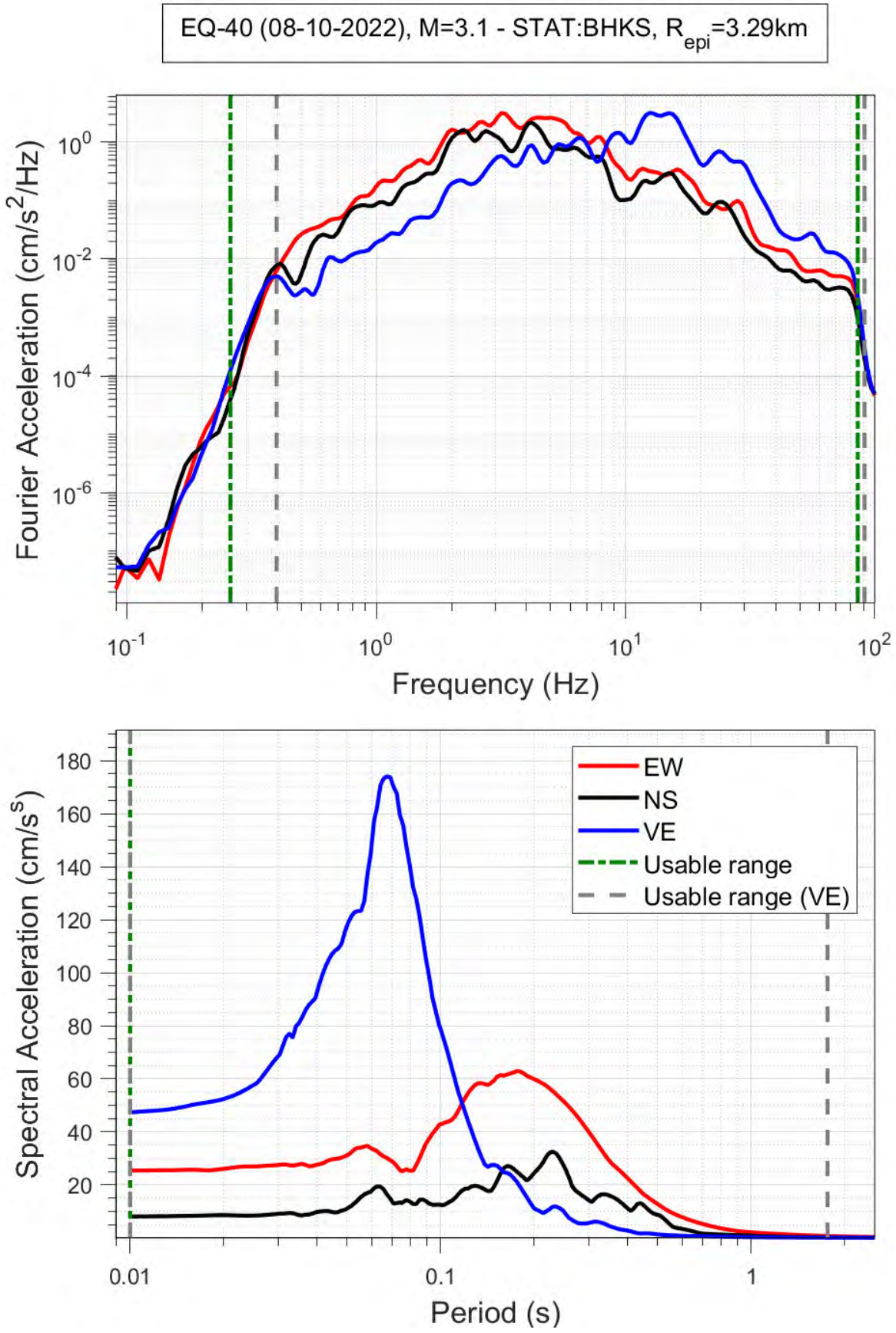

Figure 3.18 Fourier and response spectra from the BHKS record of event 40 (M_L3.1).

3.5 Comparisons with Groningen-specific GMM and GMPE predictions

For this preliminary analysis, the key question of interest is whether the motions recorded in the M_L3.1 earthquake are consistent with the current GMM and empirical PGV GMPEs being used in the Groningen field. The current GMM is the V7 GMM (Ref. 39 and 43) and event 40 is within its range of applicability (2.5-7.25). It is important to note that the V7 GMM is calibrated to match the average spectral accelerations over the periods between 0.01 and 1 seconds, and not spectral accelerations at individual periods. The residuals with respect to the average spectral acceleration are shown in Figure 3.19. In each case, the residual is the natural logarithm of the ratio of the observed (recorded) to the median predicted value, so a residual of 0.7 indicates that the recorded value was underestimated by a factor of 2 by the model and a residual of -0.7 would indicate over-prediction by a factor of 2. The residuals were separated in six bins with respect to the logarithm of their distance and the means and 95% confidence intervals of each mean are shown. Here, it can be observed that the means of the Wirdum records are larger, to a small degree, than those of the database used to develop the V7 GMM, indicating that the ground-motions of the Wirdum earthquake were slightly stronger-than-average. The average of the means is approximately 0.1, indicating a 10% underestimation of the ground-motions by the median predictions of the model. In all cases the V7 database means are within the confidence intervals of the Wirdum event means.

Figures 3.20 – 3.24 show the residuals of the Wirdum ground-motions to the periods of 0.01, 0.1, 0.2, 0.5 and 1.0 seconds, which the V7 GMM predicts (although, as explained earlier, it is not calibrated to). The pattern is similar: the bin means of the Wirdum data are similar, and in some cases slightly larger than the means of the V7 database, indicating that the ground-motions are also similar albeit slightly stronger-than-average.

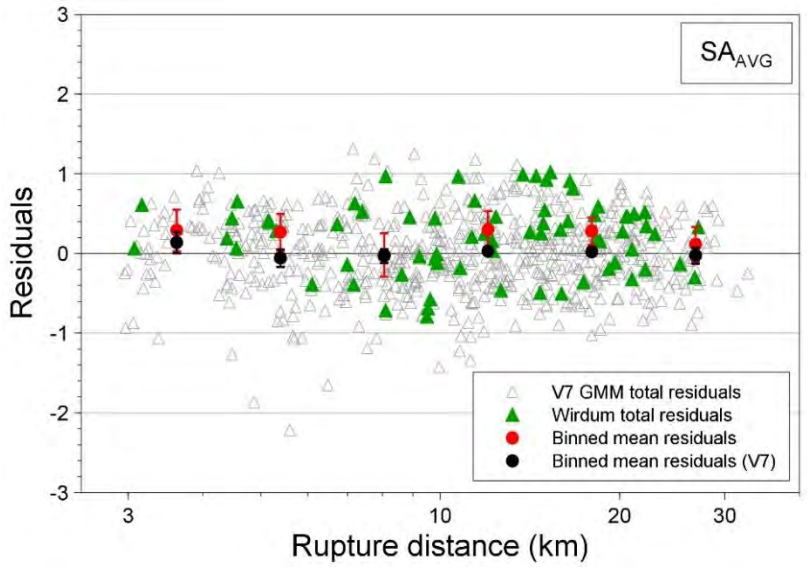

Figure 3.19 Residuals of period-averaged Sa with respect to the central branch of the V7 GMM.

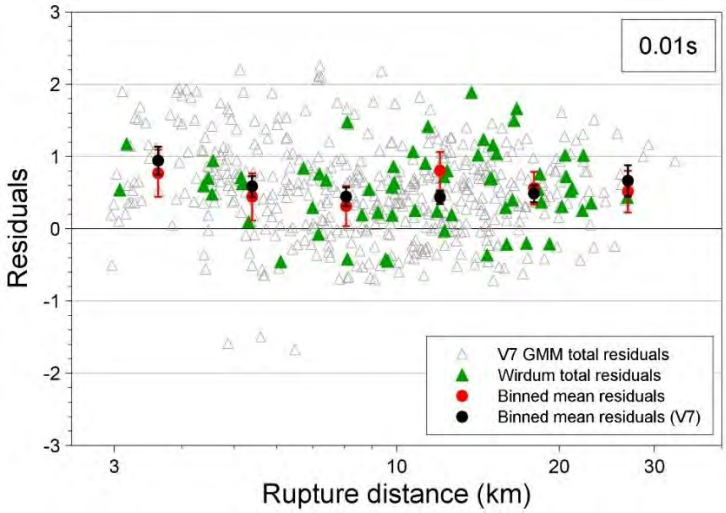

Figure 3.20 Residuals of Sa(T) with respect to the central branch of the V7 GMM at 0.01 seconds

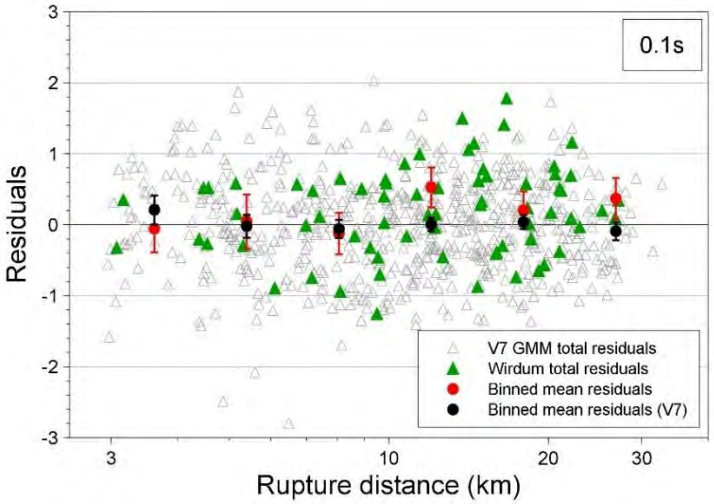

Figure 3.21 Residuals of Sa(T) with respect to the central branch of the V7 GMM at 0.1 seconds

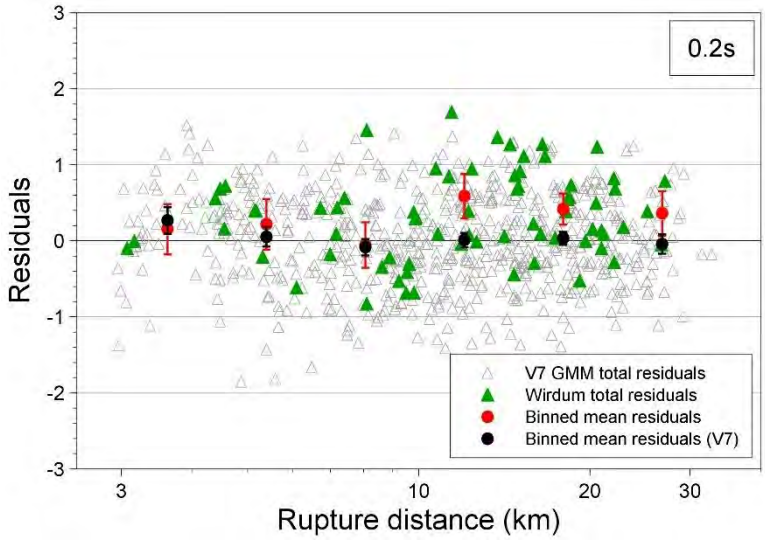

Figure 3.22 Residuals of Sa(T) with respect to the central branch of the V7 GMM at 0.2 seconds

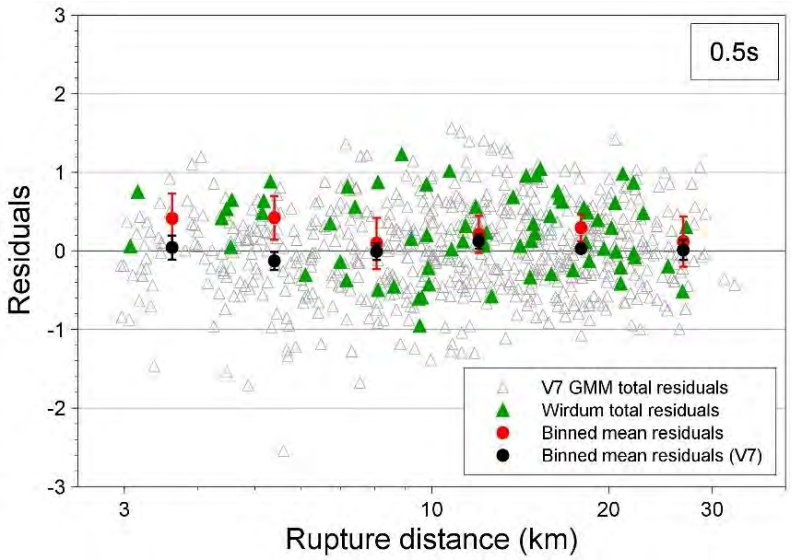

Figure 3.23 Residuals of Sa(T) with respect to the central branch of the V7 GMM at 0.5 seconds.

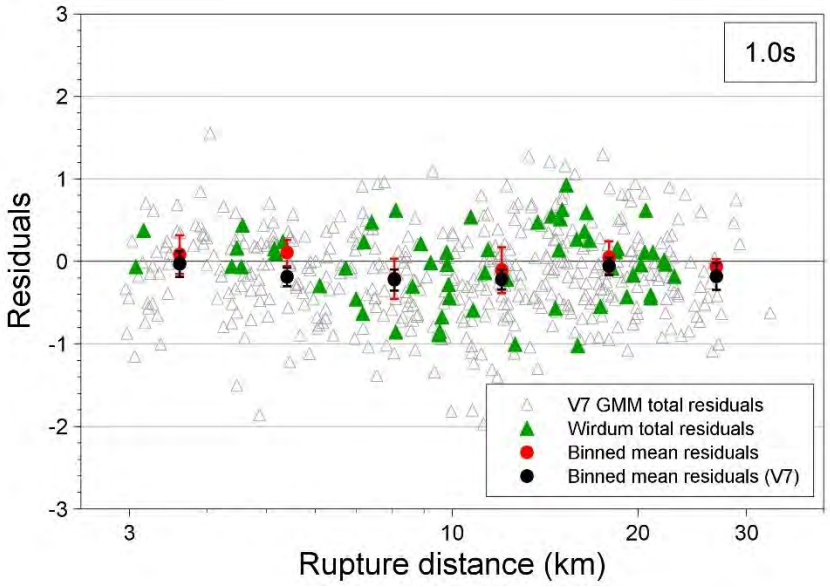

Figure 3.24 Residuals of Sa(T) with respect to the central branch of the V7 GMM at 1 second.

The V7 GMM superseded and replaced the V6 GMM (Ref. 41); the extensive additions, improvements and changes that the V7 GMM has in comparison to V6 are described in detail in Bommer *et al*. (Ref. 39). However, for completeness, and because the V6 GMM was used in the TNO-SDRA on which the current operational strategy for the Groningen field is based, we repeat the comparisons of Figures 3.19 – 3.24 for the V6 GMM in Figures 3.25 – 3.30 below. Figure 3.25 shows the residuals of SA_{AVG} of the Wirdum ground-motions with respect to the V6 GMM predictions. At distances longer than 6 km, the model appears to predict the ground-motions well, while at short distances the means are positive which indicates underprediction. This distance trend is not apparent in Figures 3.26 – 3.28, which show the residuals at 0.01, 0.1 and 0.2 seconds; in those cases, the means are similar at all distance bins and positive, indicating under-prediction. It is, however, apparent at longer periods (Figures 3.29 – 3.30), where there is a clear separation between positive means at short distances and negative means at distances longer than 6 km. The V6 database was not included in Figures 3.25 – 3.30 for comparison, as it was processed and compiled following different methods than the records of this event.

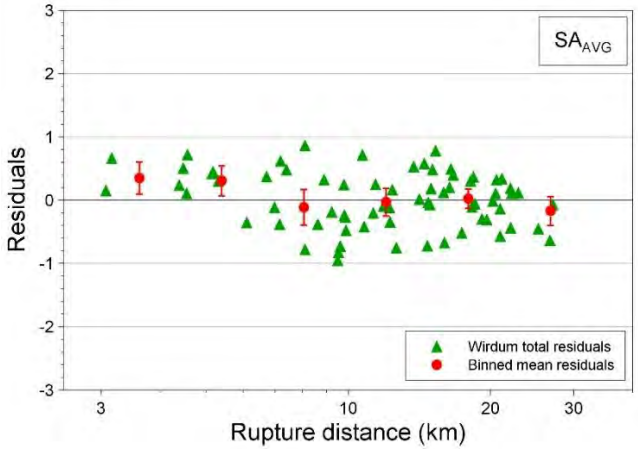

Figure 3.25 Residuals of period-averaged Sa with respect to the central branch of the V6 GMM

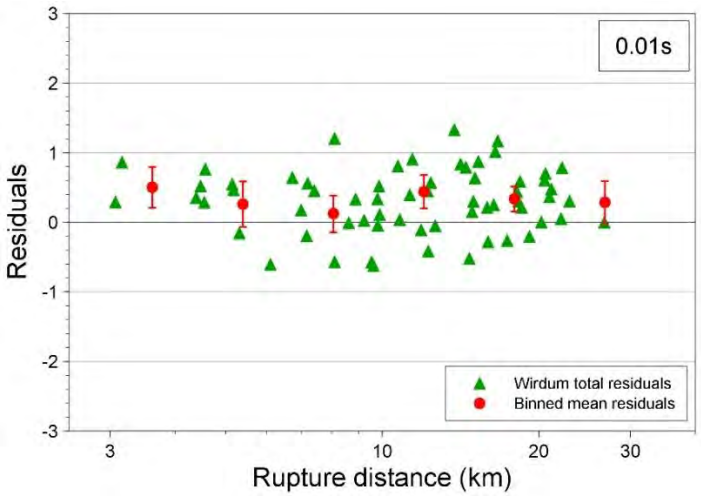

Figure 3.26 Residuals of Sa(T) with respect to the central branch of the V6 GMM at 0.01 seconds

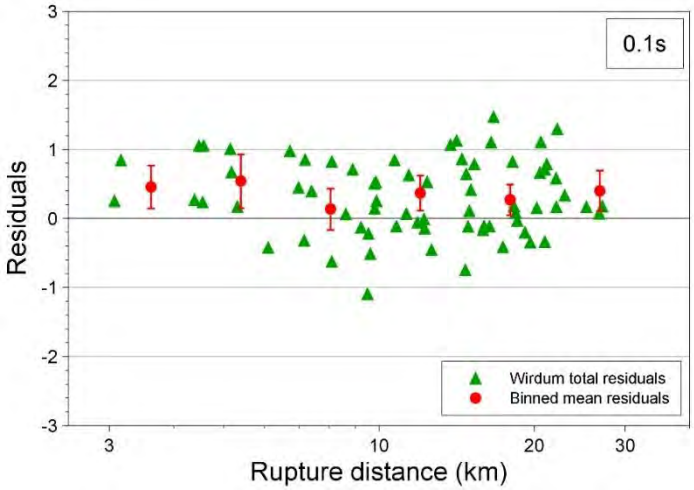

Figure 3.27 Residuals of Sa(T) with respect to the central branch of the V6 GMM at 0.1 seconds

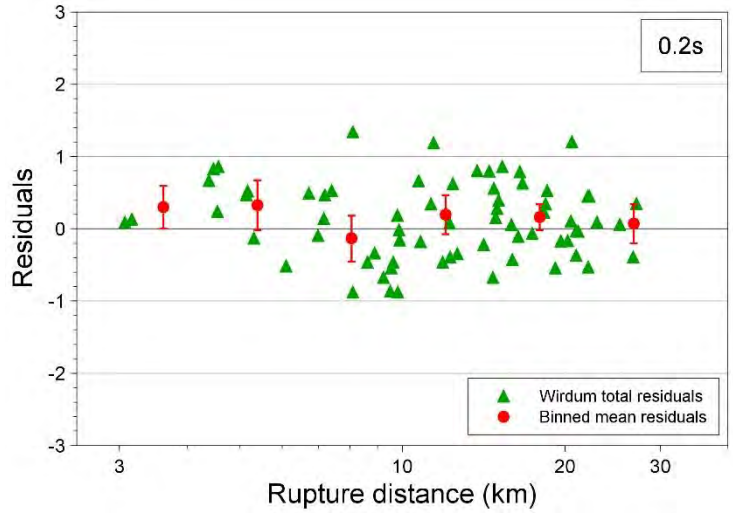

Figure 3.28 Residuals of Sa(T) with respect to the central branch of the V6 GMM at 0.2 seconds

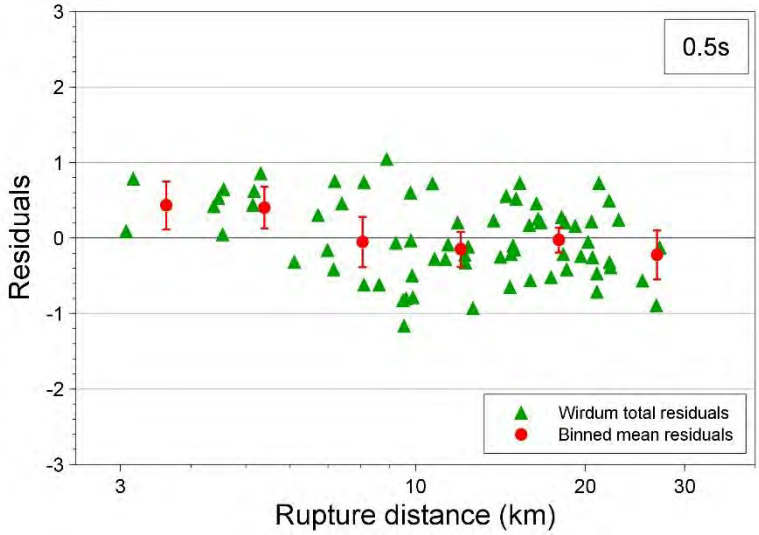

Figure 3.29 Residuals of Sa(T) with respect to the central branch of the V6 GMM at 0.5 seconds

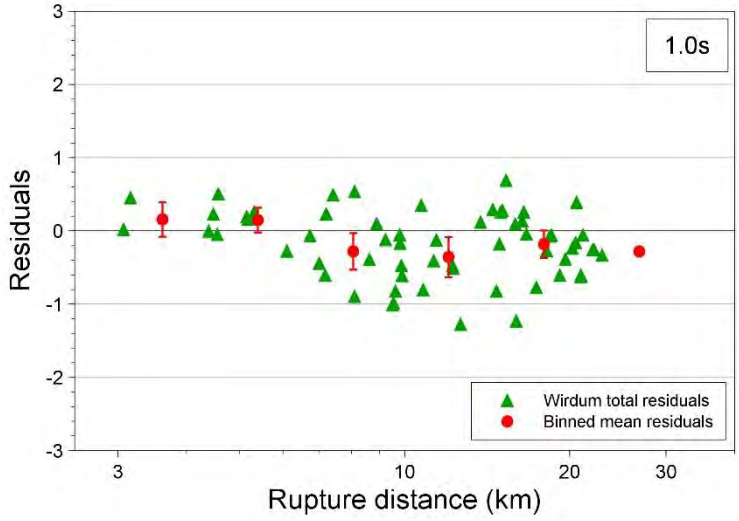

Figure 3.30 Residuals of Sa(T) with respect to the central branch of the V6 GMM at 1 second

The current empirical PGV model used to assess structural damage in the Groningen field was developed in 2021 (Ref. 42). Event 40 is within the applicability range of the GMPEs (M_L1.8-3.6);

therefore, we have calculated the total, inter- and intra- event residuals for the PGV values recorded during this event. Figure 3.31 show the within-event model residuals of the three component definitions of PGV predicted by the GMPEs, plotted against hypocentral distance. In all cases, nearly all residuals of the Wirdum earthquake recordings are within two within-event standard deviations of the zero line, which suggests that the model captures well the variability of the data.

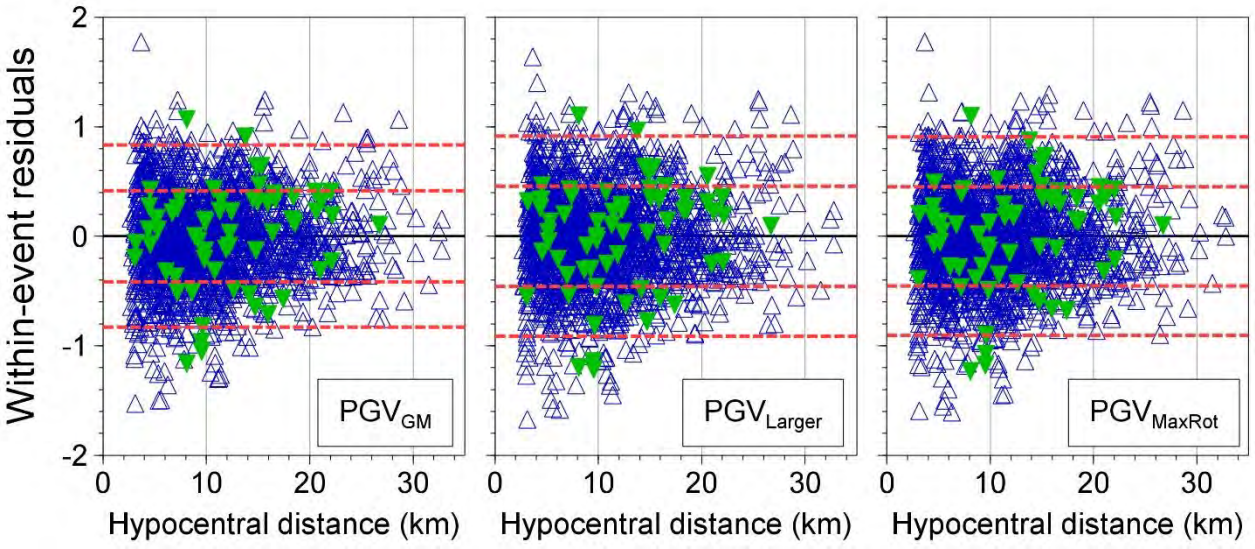

Figure 3.31 Event- and station-corrected within-event residuals of three component definitions of PGV with respect to the equations of the empirical PGV GMPE (Bommer et al., 2021) for event 40. Residuals of the Wirdum earthquake recordings are shown in green and of other events in blue. The within-event standard deviation (φ_{SS}) is shown in red dashed lines.

Figure 3.32 compares the inter-event residuals (event-terms) of the M_L3.1 earthquake to those of the previous events of the database. These event terms effectively represent the average offset of the recorded motions from each earthquake compared to the median prediction from the empirical model for the event magnitude, with a positive event-term indicating a stronger-than-average earthquake, a negative value a somewhat weaker-than-average earthquake. At magnitudes larger than 2.8, the event-terms appear to be concentrated in two clusters, one with positive event-terms and one with negative event-terms. The clusters appear centred at plus and minus one inter-event standard deviation. The event-terms of the Wirdum earthquake are part of the positive cluster; hence, the ground-motions of the event are stronger-than-average. More specifically, their values are in all three cases approximately 0.16, indicating a 15% average underestimation of the observed ground-motions by the median predictions of the model. However, they are smaller than other positive event-terms of the cluster and also lie all within one standard deviation of the expected mean, indicating that the PGV values recorded are within the prediction range of the model.

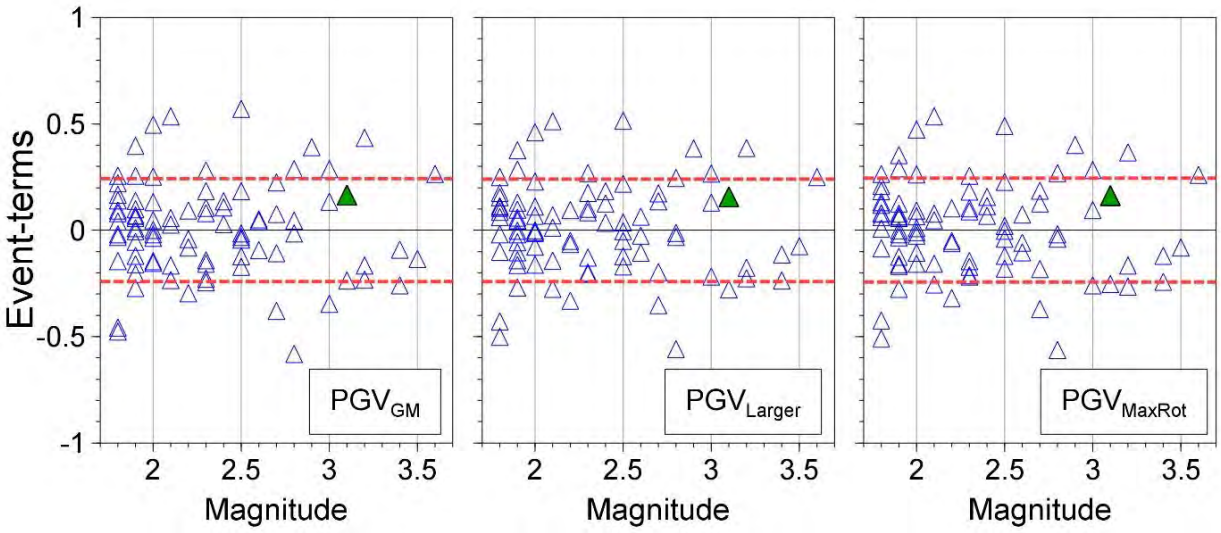

Figure 3.32 Inter-event residuals of three component definitions of PGV with respect to the equations of the empirical PGV GMPE (Bommer et al., 2021b). Residuals of the Wirdum earthquake recordings are shown in green and of older events in blue. The inter-event standard deviation is shown in red dashed lines.

4 Empirical Greens function Analysis for the Wirdum earthquake and After-shock

We have applied the Empirical Green's Function (EGF) method to the recent pair of earthquakes which occurred near Wirdum on 8th October 2022 (events 22040 and 22041, shown in figure 4.1). Analysis of the waveforms shows that these events have strongly correlated seismograms. The full waveform inversion locations show these events to be collocated and with very similar normal faulting mechanisms. The aim of the EGF analysis is to estimate the horizontal rupture propagation direction and distance for comparison with mapped reservoir-level faulting.

The EGF method takes pairs of nearby events with similar mechanisms but usually significantly different magnitudes and, by deconvolution of the larger event with the smaller, removes the effects of propagation through the subsurface from the larger event's seismogram. The aim is to give a clean representation of the earthquake source time function which is suitable for further quantitative analysis. If the smaller event in the EGF data analysis – the so-called empirical Green's Function – is small enough to be considered a point source, then the output from the deconvolution is an approximation of the larger event's source time function. More generally, the output from the EGF deconvolution process is referred to as the Relative Source Time Function (RSTF). It can be shown that the horizontal component of rupture propagation leads to a sinusoidal azimuthal variation of the duration of the source time function, with amplitude proportional to the rupture propagation distance. This variation of the source duration due to rupture propagation can be understood as an example of Doppler broadening of a signal, exactly analogous to the shift in pitch as a source of sound, such as a car siren, approaches and then recedes. The EGF process can also be applied to pairs of events which are both large enough to be considered as propagating ruptures. If the rupture propagation directions of the two events are parallel or opposite to each other, the azimuthal variation of the duration is proportional to respectively the sum or difference of the rupture propagation distances of the two events. Our EGF workflow involves deconvolution, trace scaling and then picking of the zero crossings at the start and end of the source time function traces. This gives a dataset of measurements of the duration as a function of the source-receiver azimuth angle which is then fitted with a sinusoidal Doppler broadening expression to generate estimates of the rupture propagation direction and distance. A quality measure, ξ, for the parameter inversion is calculated from the residuals for the best fit Doppler model: this quality measure varies between 0 (the Doppler model fit is no better than the azimuth-independent average) and 1 (the data points fall exactly on the sinusoidal model curve).

Further explanation of the technical details of the EGF method and its application to the Groningen earthquake data up to mid-2019 can be found in the NAM report by Oates et al (Ref. 50).

In the earlier EGF analysis of event pairs up to mid-2019, it was found that rupture propagation directions for the best quality results ($\xi \geq 0.5$) correlated very well with the mapped fault traces at Top Rotliegend level; for smaller values of ξ this visual correlation degrades. The EGF analysis of the event pair 22040/22041 gives $\xi = 0.32$. Plotting all results with $\xi \geq 0.3$ from the current and previous EGF analyses gives the plot of rupture propagation vectors in figure 4.2. Note how the rupture propagation direction found for event 22040 coincides very well with the underlying faults, showing that the horizontal component of the rupture propagation is along strike. In figures 4.3 and 4.4 the azimuthally varying EGF trace output and picked source time function duration are shown for the 22040/22041 event pair.

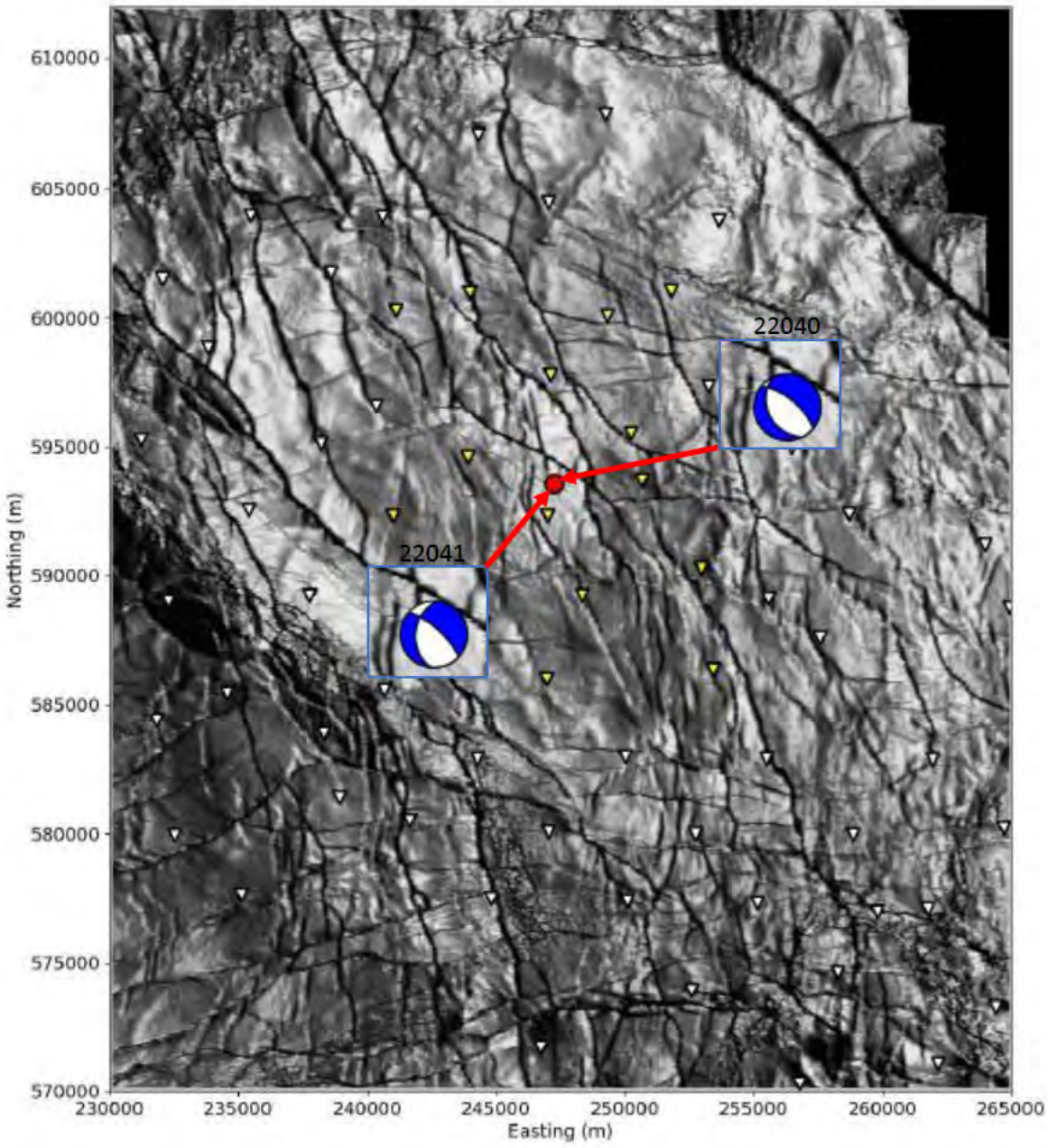

Figure 4.1 Location and focal mechanism plots for the event pair 22040/22041.

Child Event ID	Parent Event ID	Child Magnitude	Parent Magnitude	Child Easting	Child Northing	Child Depth	Parent Easting	Parent Northing	Parent Depth	Azimuth (° from N)	L (m)	ξ
22041	22040	1 2	3.1	593550	247250	2900	593550	247250	2900	113.07	56	0.32

Table 4.1. Summary of EGF results for the event pair 22040/22041.

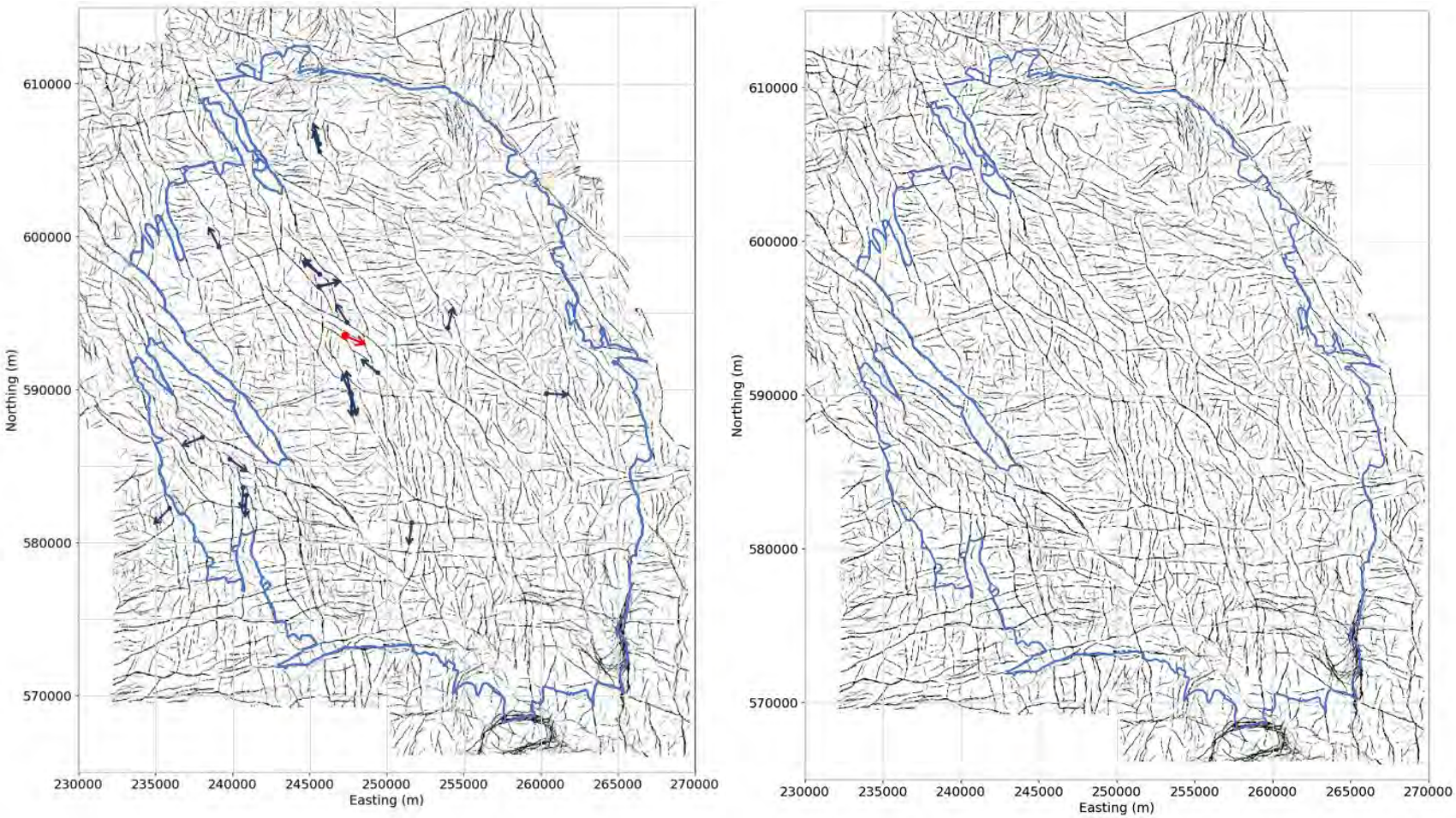

Figure 4.2 *Scaled horizontal rupture vectors overlain on the top reservoir fault map. In each of these plots the base map shows the detailed fault interpretation generated by Kortekaas & Jaarsma (2017). The outline of the gas field is shown as a blue contour. The vectors give only the horizontal rupture propagation direction (vectors are drawn with a constant length), obtained from the inversion of the picked durations. The plot on the left shows the highest quality EGF analysis (event pairs for which $\xi \geq 0.3$); the red vector is the result for event pair 22040/22041; the blue vectors are for event pairs from the previous EGF analysis. The plot on the right is the base fault map and field outline without propagation vectors overlain (this is to expose fault lineaments overlain by vectors in the left plot).*

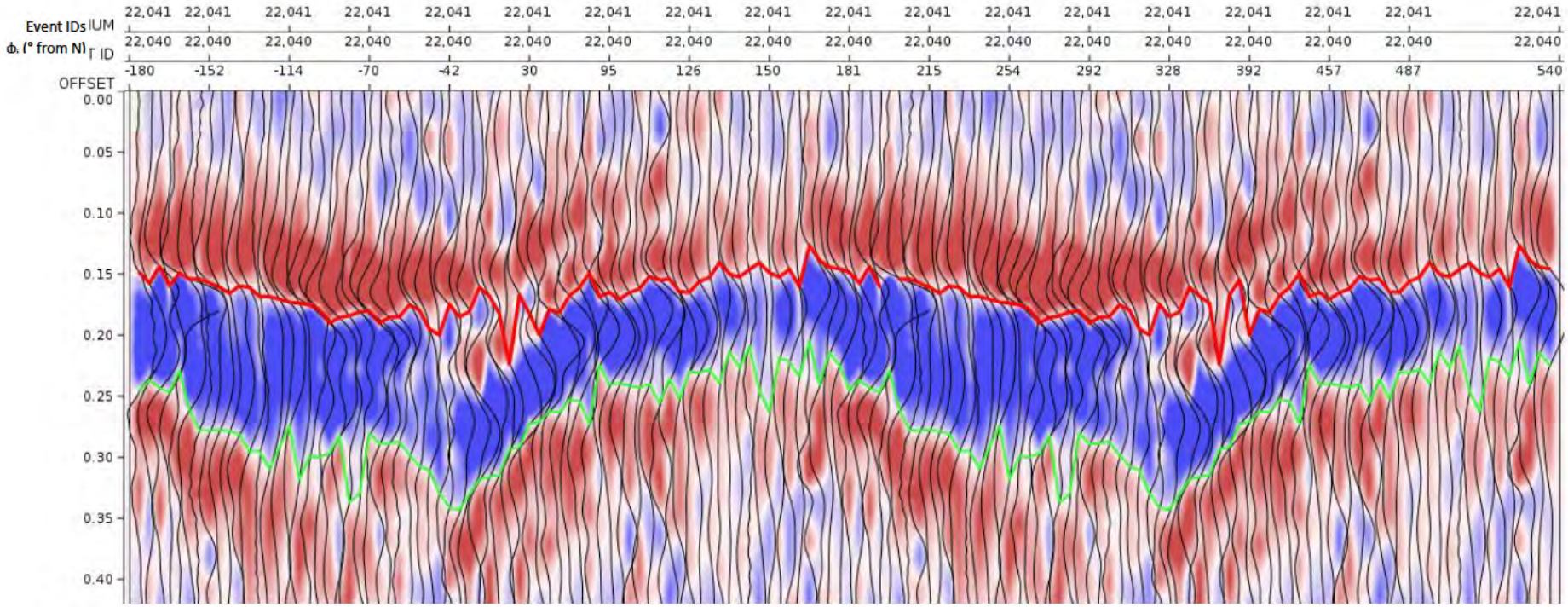

Figure 4.3 *EGF trace output for event pair 22040/22041 as a function of azimuth with respect to North. The traces have been duplicated and displayed on the interval* $[-180°, 540°]$ *to ensure that periodic effects are not obscured at the ends of the plot. Duration is the difference between picked start and end times of the source function (the red and green arrival picks shown).*

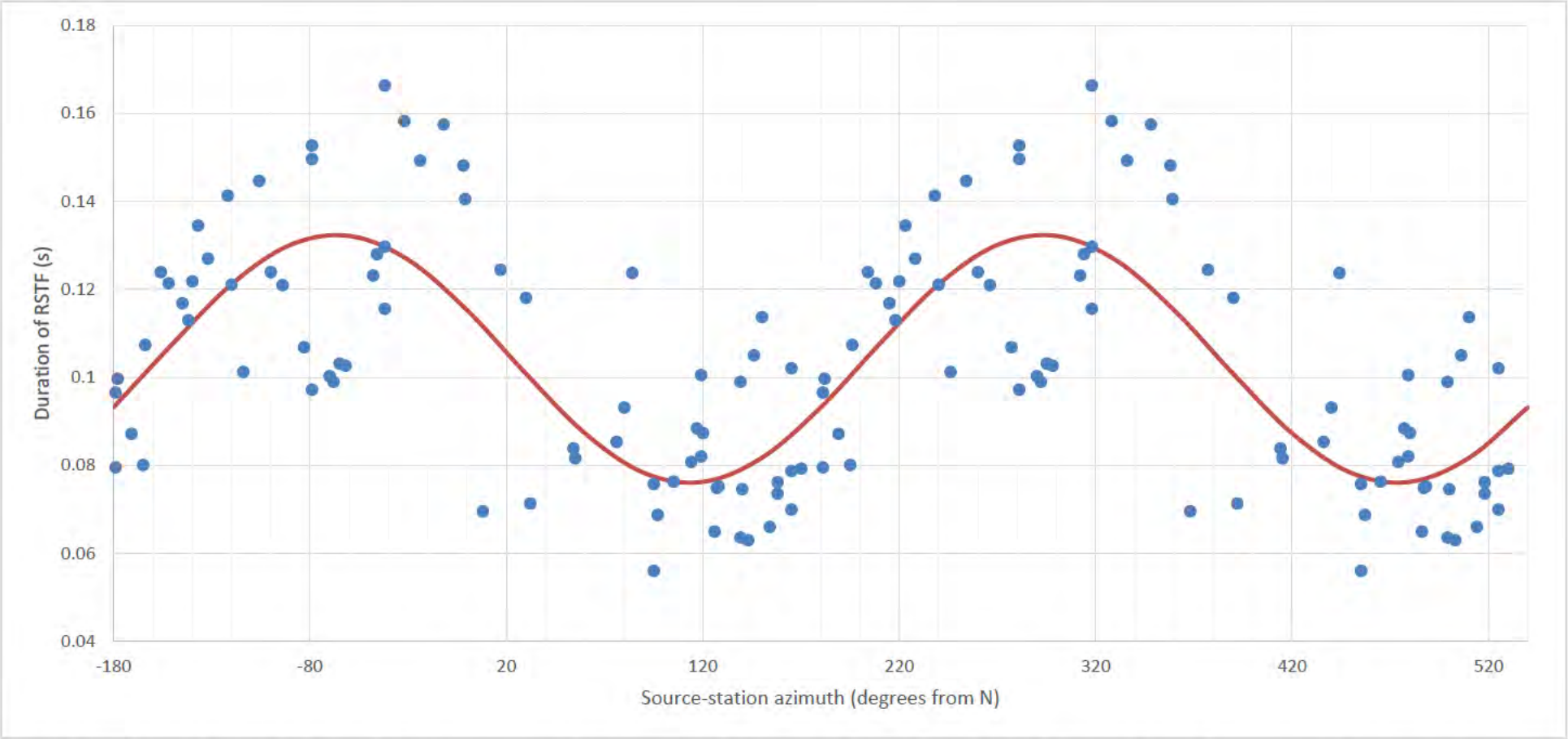

Figure 4.4 Picked duration between the zero crossings of the RSTF traces for event pair 22040/22041 (blue data points) with Doppler model fit (orange curve), shown on the interval $[-180°, 540°]$ *as for the seismogram display.*

5 Conclusions

5.1 Event rate, epicentres and source mechanism

On the 8th October 2022 an earthquake with a magnitude 3.1 occurred near the village of Wirdum located some 1.5 km to the south-east of Loppersum. Just over 3 hours later this earthquake was followed by an earthquake at the same location, with a magnitude M_L 1.2. A third earthquake with a magnitude ML=1.4 occurred 5 days later 300 m to the north of these two earthquakes.

In the last year a number of earthquakes have in a period of weeks to months occurred in small area of the field. Examples of these are the earthquake swarm near Zeerijp starting 4th October 2021 and the earthquakes near Uithuizen in August, September and October 2022. This might indicate a more intense clustering of recent earthquakes in space and time. However, this might also be associated with a lower event rate and a shrinking seismically active area. As part of the studieplan into the seismicity during the pressure equilibration phase NAM is performing a systematic study into the Groningen earthquake catalogue for after-shock sequences.

5.2 Ground Motions

The M_L 1.2-3.1 Wirdum earthquakes of 8 October 2022 have generated a large number of ground-motion recordings. The largest component of PGA recorded is 0.06 *g* and the largest value of PGV—which is generally considered a better indicator of the damage potential of the motion—recorded in the M_L3.1 event is 2.46 cm/s. This is smaller than the largest value of the Groningen ground-motion database (the 3.46 cm/s recorded in the larger 2012 M_L3.6 Huizinge earthquake) but now the fifth largest value recorded in Groningen.

An important observation is that, although the amplitudes of motion recorded in the M_L3.1 Wirdum earthquake are within the range of predictions of the empirical PGV GMPEs as well as the SA_{AVG} predictions of the V6 and V7 GMM, they are, on average, 10-15% larger than the median predictions of the models and appear to be also larger than the average amplitudes recorded during previous events of similar magnitude.

5.3 Empirical Green's Function Analysis

The EGF analysis was carried out for the Wirdum earthquake and the Garrelsweer earthquake pair of 11th October 2022, which gave $\xi = 0.32$. The rupture propagation direction found for the Wirdum earthquake coincides very well with the underlying faults, showing that the horizontal component of the rupture propagation is along strike.

References

1. Analyse seismiciteit, Nov 2016.
2. Rapportage recente aardbevingen Wirdum en Garsthuizen 2016/2017, NAM, Mar 2017.
3. Gaswinning Groningen Periodieke rapportage ontwikkeling seismiciteit - Volgens artikel 5, lid 3 van het Instemmingsbesluit winningsplan Groningenveld Rapportage 1 mei 2017, NAM, May 2017.
4. Ground Motions from the ML 2.6 Slochteren Earthquake of 27th May 2017, June 2017.
5. Special Report on the earthquake density and activity rate following the earthquakes in Appingedam (ML=1.8) and Scharmer (ML=1.5) in August 2017, NAM, Sept 2017.
6. Rapportage Seismiciteit Groningen - 1 Nov 2017, NAM, Nov 2017.
7. Special Report on the Loppersum earthquakes – December 2017, Taco den Bezemer and Jan van Elk, NAM, Dec 2017.
8. Special Report on the Zeerijp Earthquake, Taco den Bezemer and Jan van Elk, NAM, Jan 2018.
9. Short special report Exceedance Activity Rate February 2018, NAM, Feb 2018.
10. Rapportage Seismiciteit Groningen - 1 Juni 2018, NAM, July 2018.
11. Rapportage Seismiciteit Groningen - 1 November 2018, NAM, Nov 2018.
12. Periodieke rapportage Seismiciteit Groningen - Mei 2019, Jan van Elk and Dirk Doorkhof, NAM, May 2019.
13. Special Report - Westerwijtwerd Earthquake - 22nd May 2019, Jan van Elk and Dirk Doorkhof, NAM, May 2019.
14. Analyse overschrijding MRP-grenswaarde Aardbevingsdichtheid 9 september 2019, NAM, NAM, Sept 2019.
15. Rapportage seismiciteit Groningen - November 2019, NAM, NAM, Nov 2019.
16. Rapportage artikel 6, tweede lid, Vaststellingsbesluit Groningen gas veld 2019 - 2020, NAM, NAM, Dec 2019.
17. Analyse overschrijding aardbevingsdichtheid - 3 december 2019, NAM, NAM, Dec 2019.
18. Rapportage Seismiciteit Groningen - mei 2020, NAM, NAM, Apr 2020.
19. Special Report on the Zijldijk ML 2.5 Earthquake of 2nd May 2020, Jan van Elk, NAM, May 2020.
20. Special Report on the Loppersum ML 2.7 Earthquake of 14th June 2020, Jan van Elk, Dirk Doornhof and Jeroen Uilenreef, NAM, Aug 2020.
21. Rapportage Groningen gasveld Artikel 52H Mijnbouwwet Gasjaar 2019/2020, NAM, Nov 2020.
22. Periodieke rapportage seismiciteit Groningen - 1 november 2020, NAM, NAM, Nov 2020.
23. Rapportage Seismiciteit Groningen - mei 2021, NAM, NAM, May 2021.
24. Periodieke rapportage seismiciteit Groningen - 1 november 2021, NAM, NAM, Oct 2021.
25. Special Report on the Zeerijp Earthquake Swarm starting 4th October 2021, Jan van Elk and Jeroen Uilenreef, NAM, Oct 2021.
26. Rapportage Groningengasveld artikel 52h Mijnbouwwet gasjaar 2020-2021, NAM, NAM, Oct 2021.
27. 48-uur brief voor de Garrelsweer aardbeving aan SodM, NAM, NAM, Nov 2021.
28. 48-uur brief voor de Garrelsweer aardbeving aan ministerie EZK, NAM, NAM, Nov 2021.
29. Special Report on the Garrelsweer Earthquake 16th November 2021 with Magnitude ML = 3.2, Jan van Elk and Jeroen Uilenreef, NAM, Nov 2021.
30. Supplement to Special Report on the Zeerijp Earthquake Swarm starting 4th October 2021, Jan van Elk and Jeroen Uilenreef, NAM, Nov 2021.
31. Periodieke rapportage seismiciteit Groningen - 1 mei 2022, Jan van Elk and Jeroen Uilenreef, NAM, May 2022.
32. Appendix bij het Meet- en Regelprotocol Groningen – Cases, NAM, June 2017, NAM, June 2017.
33. Appendix bij het Meet- en Regelprotocol Groningen – Cases, NAM, June 2017, NAM, June 2017.
34. Meet- en Regelprotocol Groningen, NAM, June 2017.
35. Meet- en Regelprotocol Groningen, NAM, June 2017.
36. Technisch Addendum bij het Meet- en Regelprotocol Groningen, NAM, June 2017.
37. Technisch Addendum bij het Meet- en Regelprotocol Groningen, NAM, June 2017.
38. Bommer, J.J., B. Dost, B. Edwards, P.J. Stafford, J. van Elk, D. Doornhof & M. Ntinalexis (2016). Developing an application-specific ground-motion model for induced seismicity. Bulletin of the Seismological Society of America 106(1), 158-173.
39. Bommer, J.J., B. Edwards, P.P. Kruiver, A. Rodriguez-Marek, P.J. Stafford, M. Ntinalexis, E. Ruigrok & B. Dost (2022a). V7 Ground-Motion Model for Induced Seismicity in the Groningen Gas Field. Revision 1, 20 February 2022, 273 pp.
40. Bommer, J.J., P.J. Stafford, B. Edwards, B. Dost, E. van Dedem, A. Rodriguez-Marek, P. Kruiver, J. van Elk, D. Doornhof & M. Ntinalexis (2017). Framework for a ground-motion model for induced seismic hazard and risk analysis in the Groningen gas field, The Netherlands. Earthquake Spectra 33(2), 481-498.
41. Bommer, J.J., B. Edwards, P.P. Kruiver, A. Rodriguez-Marek, P.J. Stafford, B. Dost, M. Ntinalexis, E. Ruigrok & J. Spetzler (2019). V6 Ground-Motion Model for Induced Seismicity in the Groningen Gas Field. Revision 1, 19 December 2019, 196 pp.
42. Bommer, J. J., P. J. Stafford, and M. Ntinalexis (2021b). Empirical Equations for the Prediction of Peak Ground Velocity due to Induced Earthquakes in the Groningen Gas Field, 10 March 2019
43. Bommer, J.J., P.J. Stafford, E. Ruigrok, A. Rodriguez-Marek, M. Ntinalexis, P. P. Kruiver, B. Edwards, B. Dost, and J. van Elk, (2022b). Ground Motion Prediction Models for Induced Earthquakes in the Groningen Gas Field, the Netherlands. Journal of Seismology, under review
44. Dost, B., E. Ruigrok & J. Spetzler (2017). Development of probabilistic seismic hazard assessment for the Groningen gas field. Netherlands Journal of Geoscience 96, s235–s245.
45. Edwards, B. & M. Ntinalexis (2021). Usable bandwidth of weak-motion data: application to induced seismicity in the Groningen Gas Field, the Netherlands. Journal of Seismology, doi: 10.1007/s10950-021-10010-7.

46. Ntinalexis, M., J.J. Bommer, E. Ruigrok, B. Edwards, R. Pinho, B. Dost, A.A. Correia, J. Uilenreef, P.J. Stafford & J. van Elk (2019). Ground-motion networks in the Groningen field: usability and consistency of surface recordings. Journal of Seismology 23(6), 1233-1253.
47. Ntinalexis, M., P.P. Kruiver, J.J. Bommer, E. Ruigrok, A. Rodriguez-Marek, B. Edwards, R. Pinho, J. Spetzler, E. Obando Hernandez, M. Pefkos, M. Bahrampouri, E.P. van Onselen, B. Dost, B., and J. van Elk (2022). A database of ground-motion recordings, site profiles, and amplification factors from the Groningen gas field in the Netherlands. Earthquake Spectra, under review.
48. J. Spetzler, J. & B. Dost (2017). Hypocentre estimation of induced earthquakes in Groningen. Geophysical Journal International 209(1), 453–465.
49. Stafford, P.J., B.D. Zurek, M. Ntinalexis & J.J. Bommer (2019). Extensions to the Groningen ground-motion model for seismic risk calculations: component-to-component variability and spatial correlation. Bulletin of Earthquake Engineering 17, 4417-4439.
50. Empirical Green's Function analysis of some induced earthquake pairs from the Groningen gas field, Steve Oates, Jelena Tomic, Brian Zurek, Tom Piesold and Ewoud van Dedem, Shell/Exxonmobil, Aug 2020.

Appendix A Evaluation of the hypocentre and the source mechanism of the earthquake with a magnitude of 3.1 near Wirdum on 8th October 2022

Event 40 - Wirdum
08 October 2022 02:17:17

10 October 2022

Induced Seismicity Taskforce

Disclaimer

- The results presented in this report have been automatically generated using an unconstrained full waveform, event location and moment tensor inversion workflow, developed by the Induced Seismicity Taskforce at Shell.
- These results have not been previously reviewed.
- For questions related to the results then you should contact:
  - Chris Willacy (Christopher.Willacy@Shell.com) or
  - Jan-Willem Blokland (Jan-Willem.Blokland@Shell.com)

Event summary

The event happened at:

Date	08 October 2022
Time	02:17:17.068413

The event is located at:

Location	Wirdum
Northing (m)	593550
Easting (m)	247250
Depth (m)	2900

The source characteristics are:

	Solution 1	Solution 2
Strike angle (degree)	153.39	307.89
Dip angle (degree)	29.19	55.47
Rake angle (degree)	-69.04	-102.23
Isotropic (percentage)	-28.99	-28.99
CLVD (percentage)	-11.99	-11.99
Magnitude M_{L}	3.10	3.10

Magnitude summary

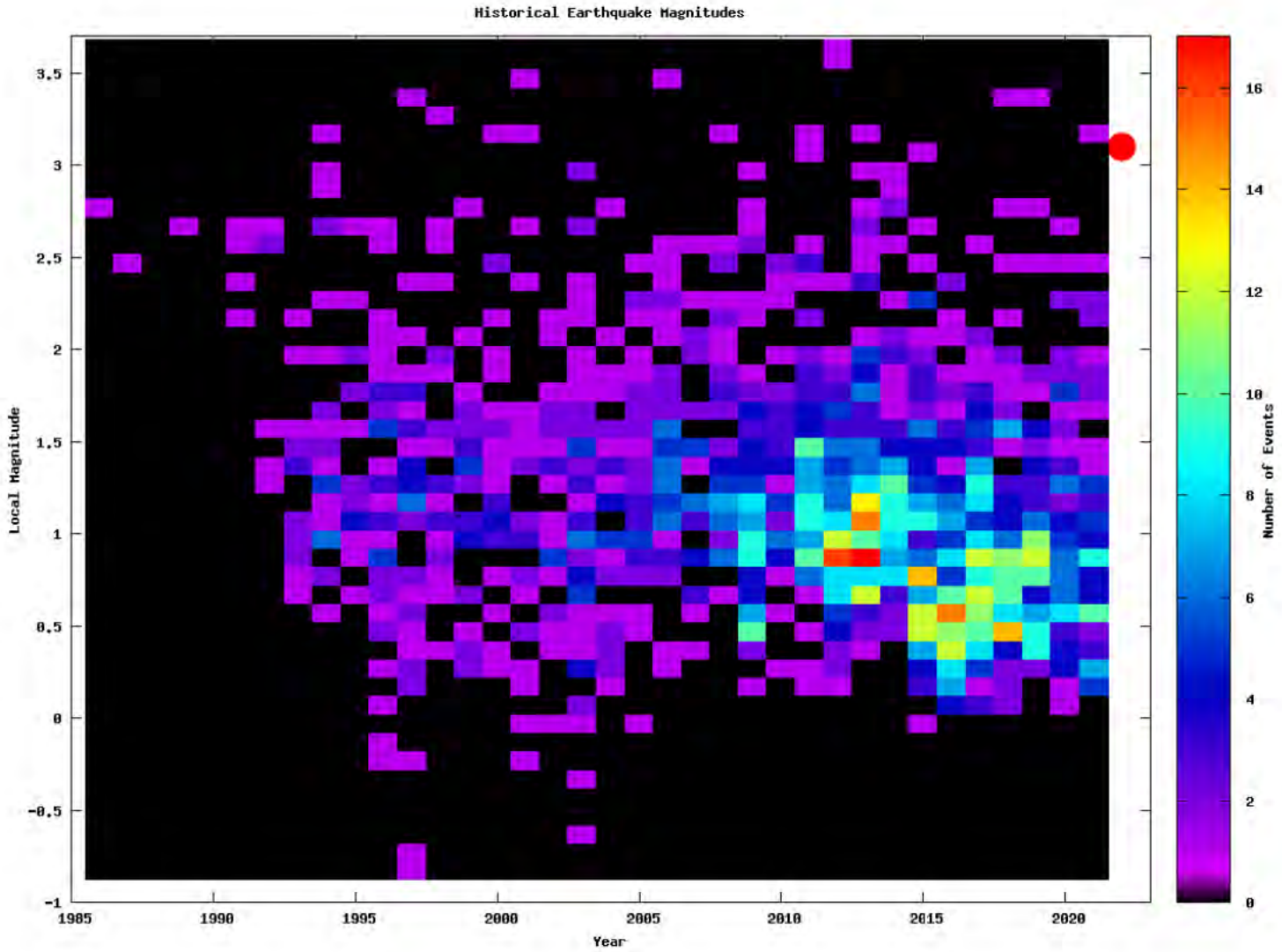

Regional and historical map

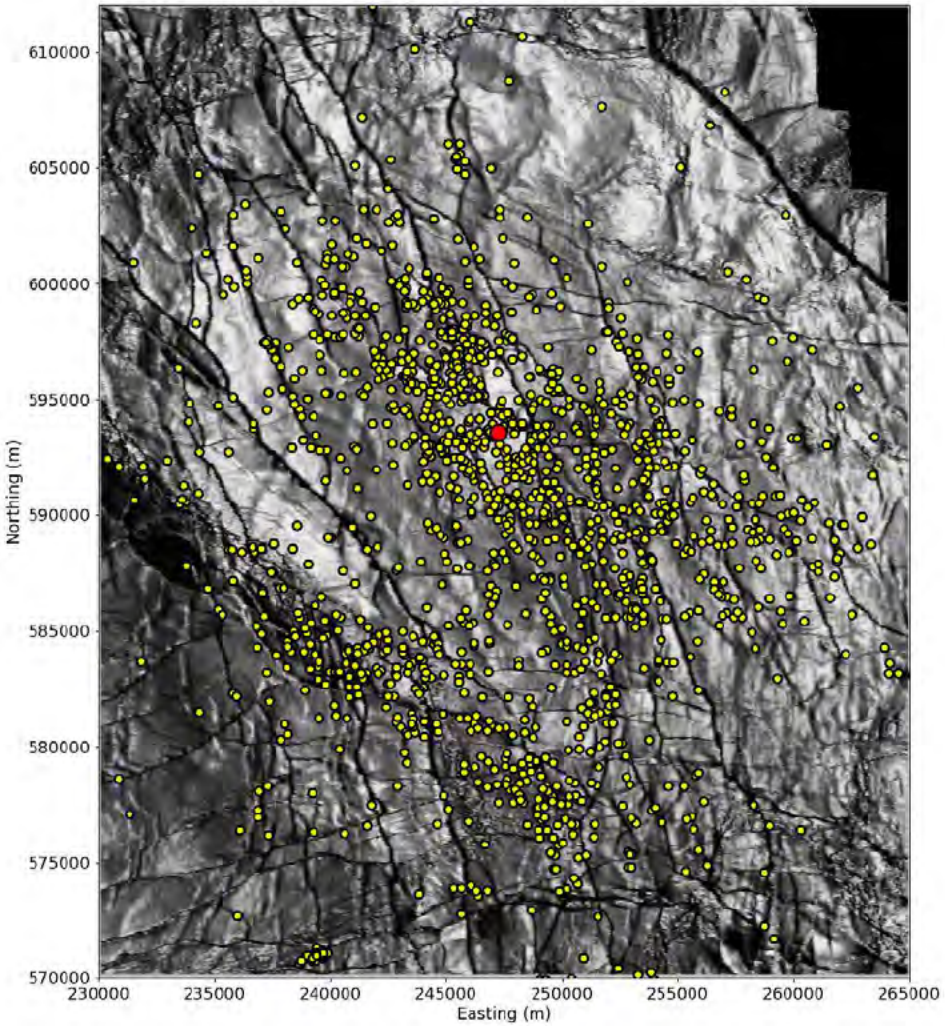

Event depth summary

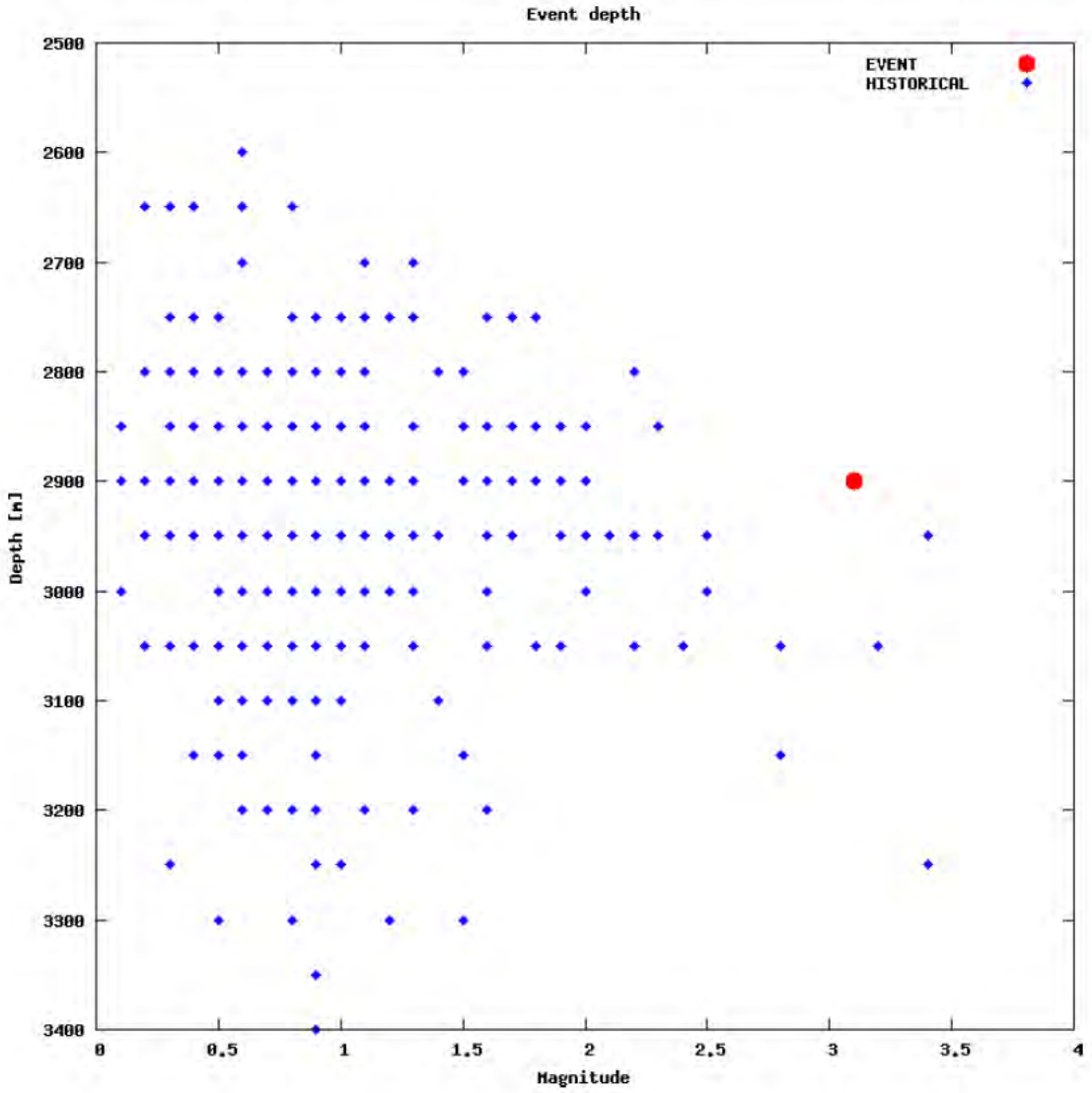

Event location - Map

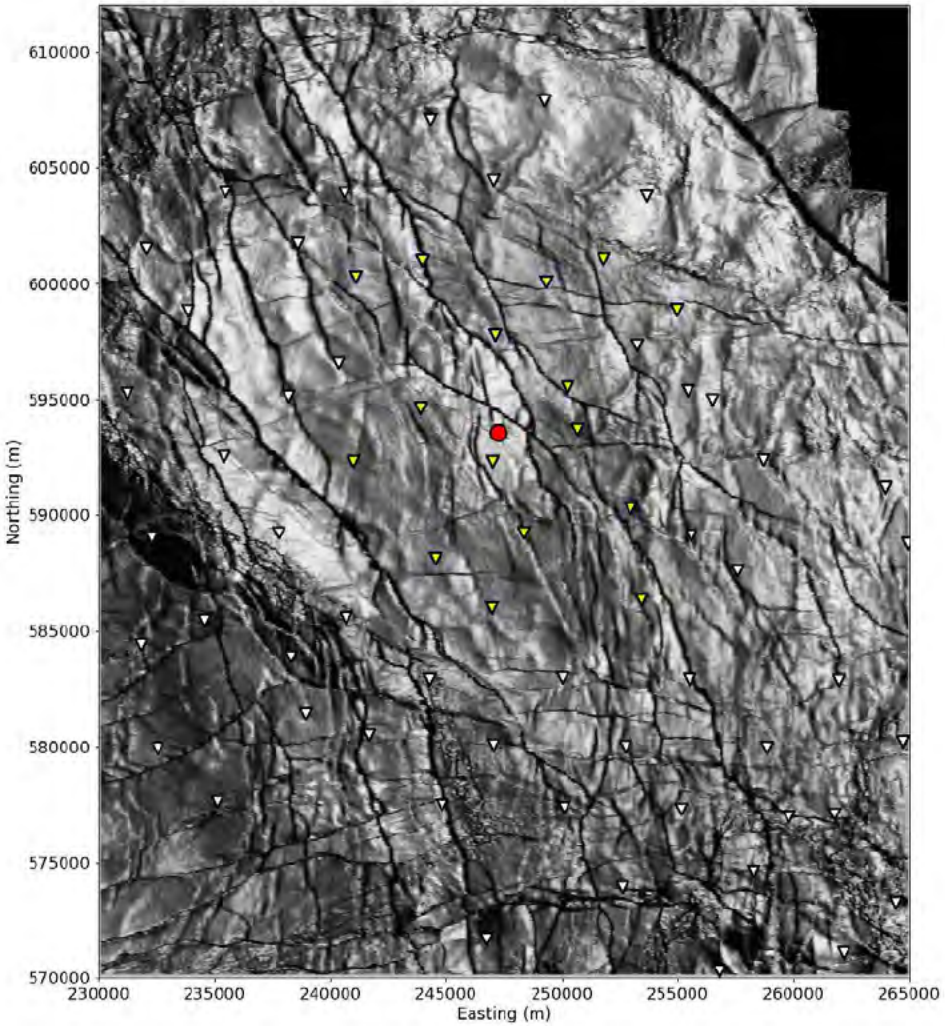

Event location and depth (initial)

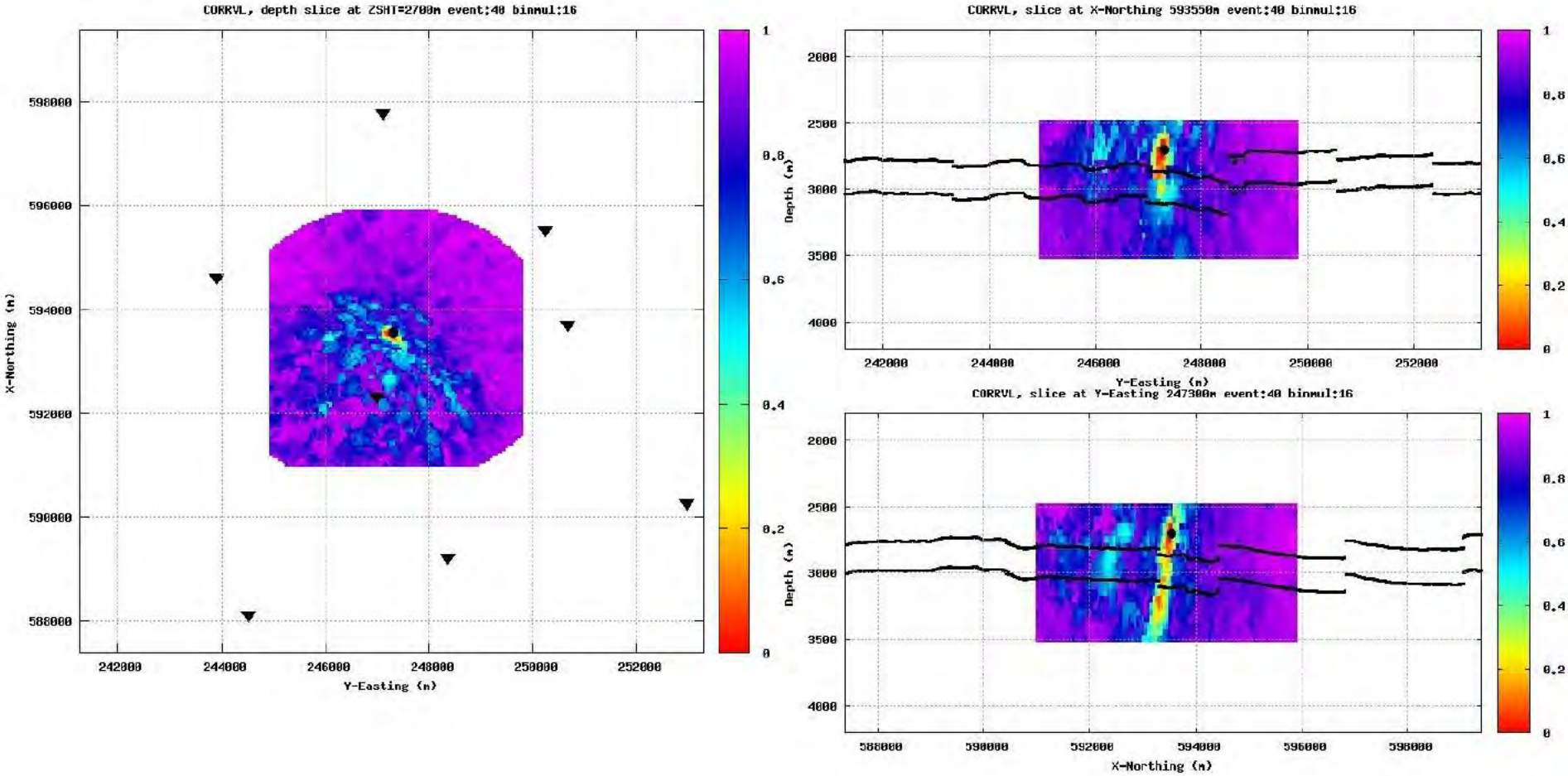

Event location and depth (alternative)

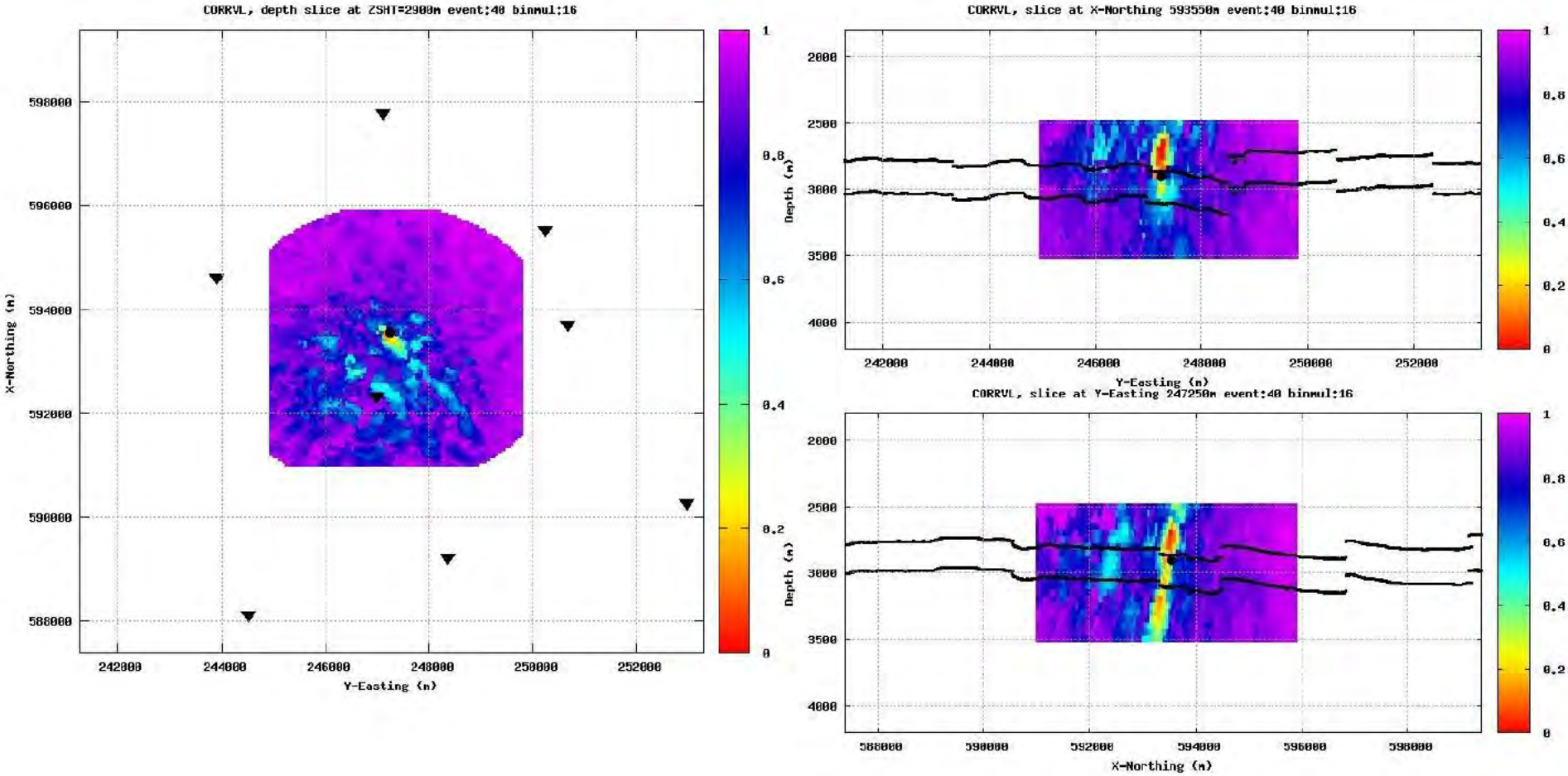

Moment tensor

Double-coupled part

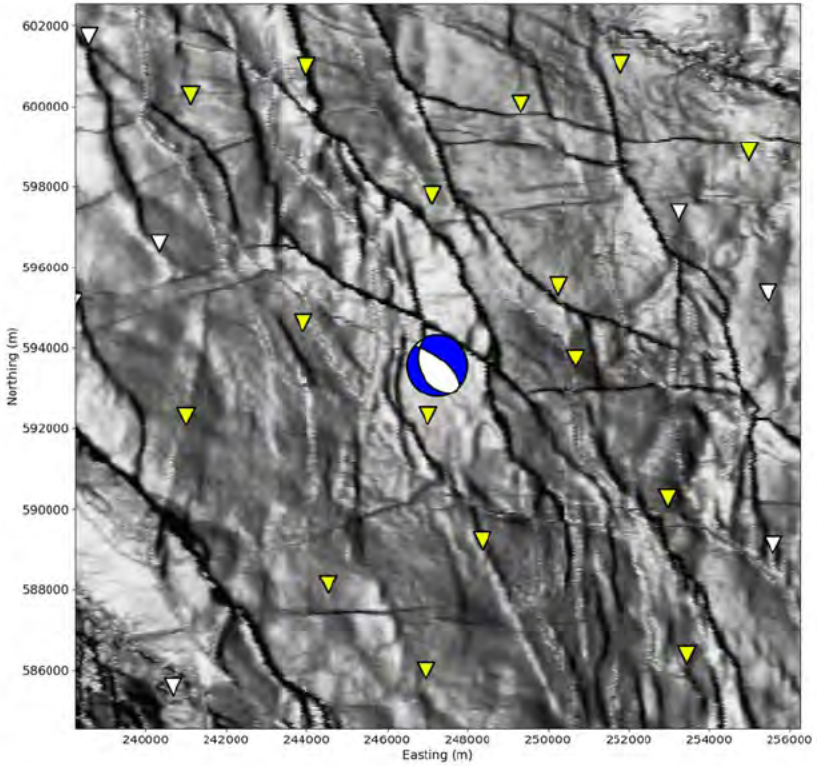

Full

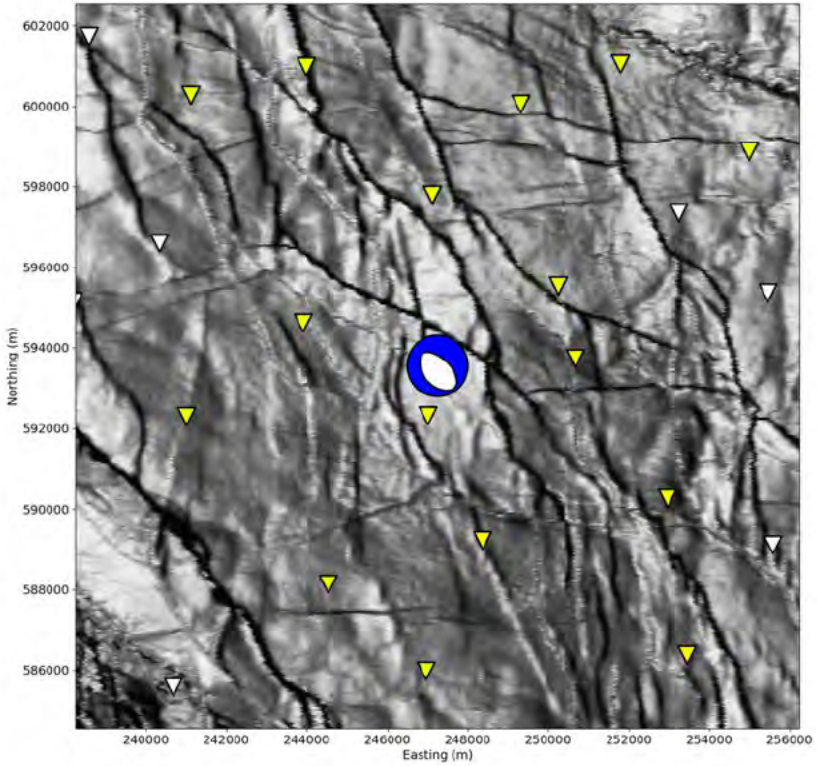

Moment Tensor: Decomposition

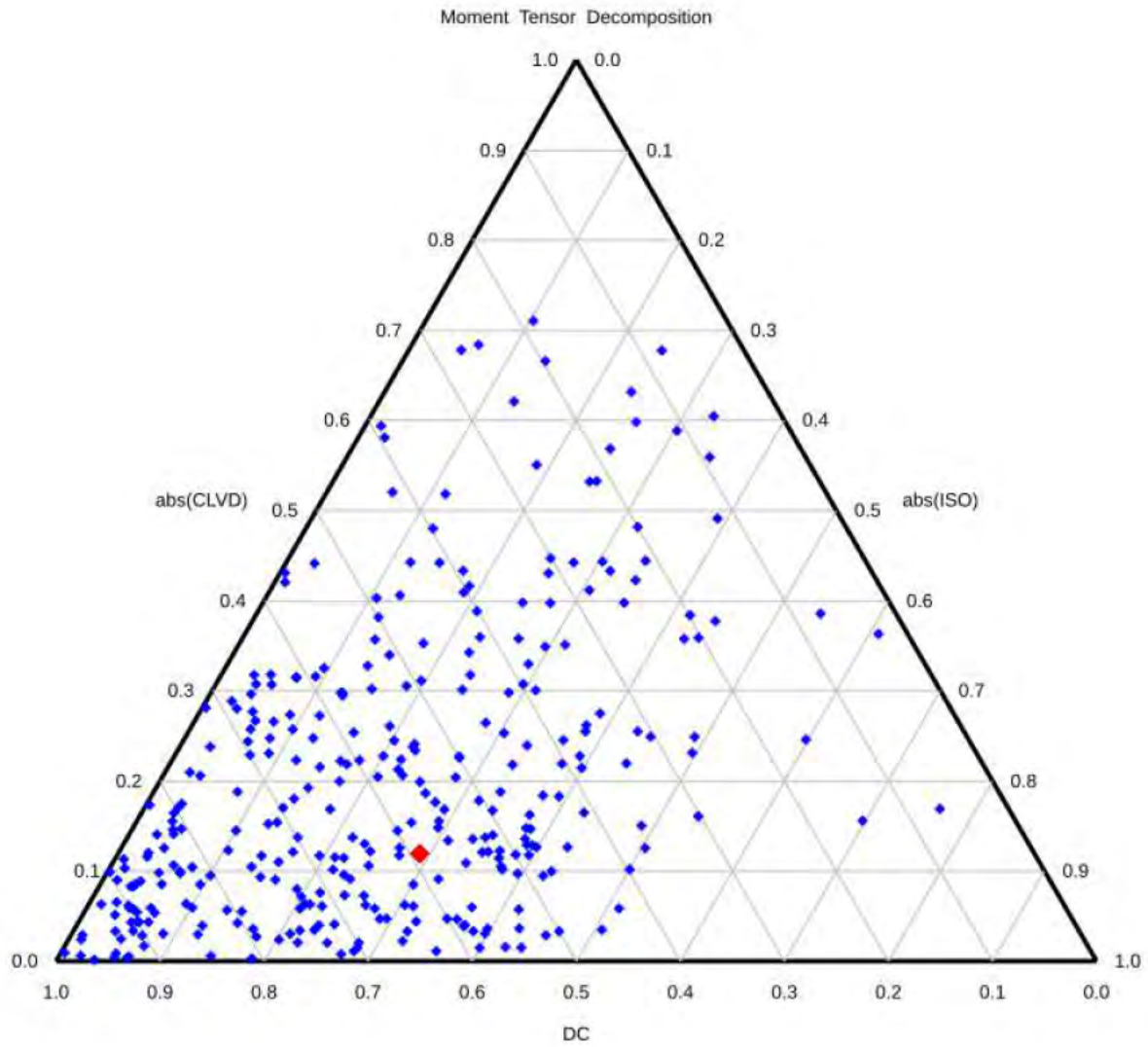

Field data traces

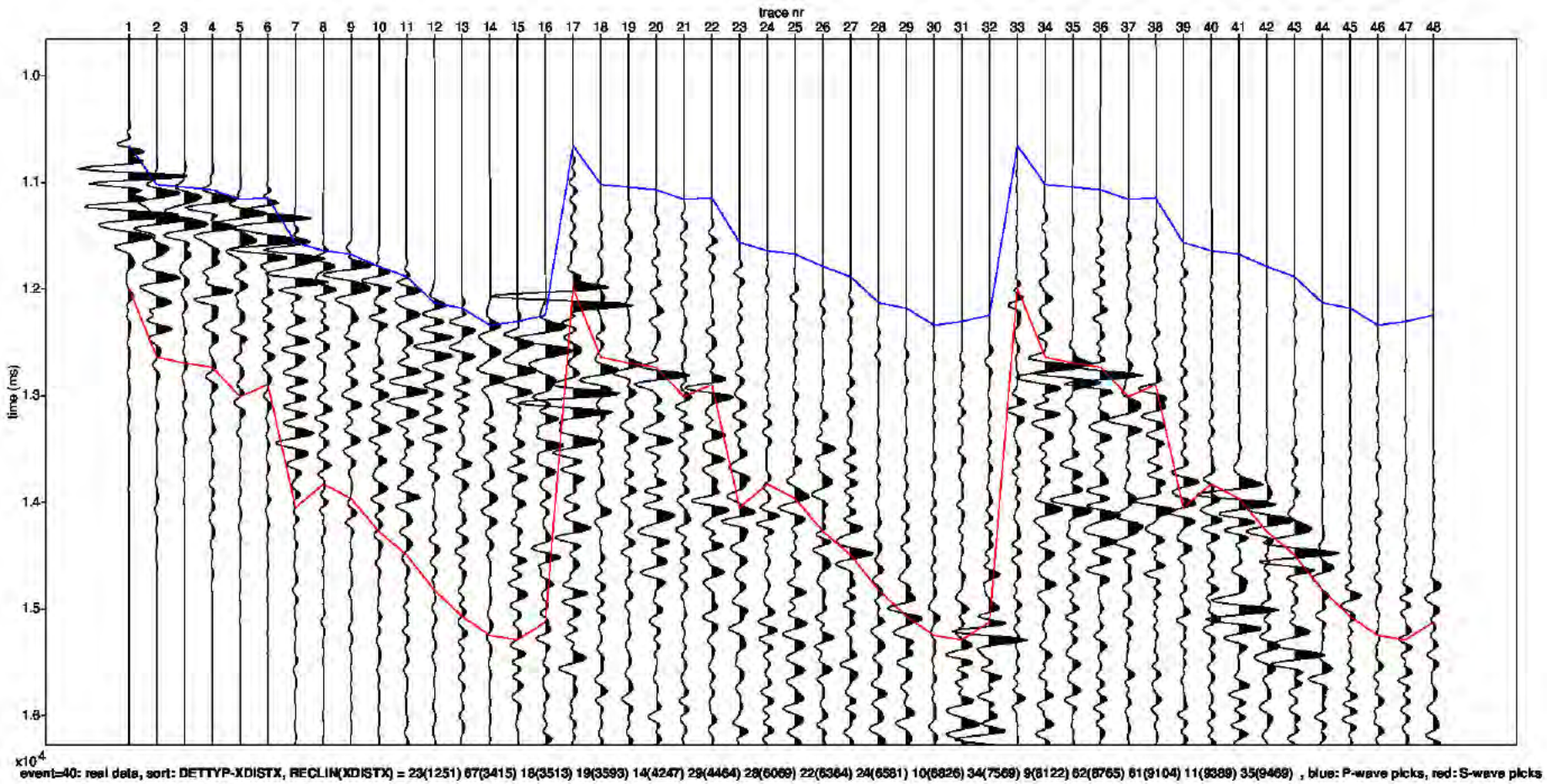

Modelled data traces

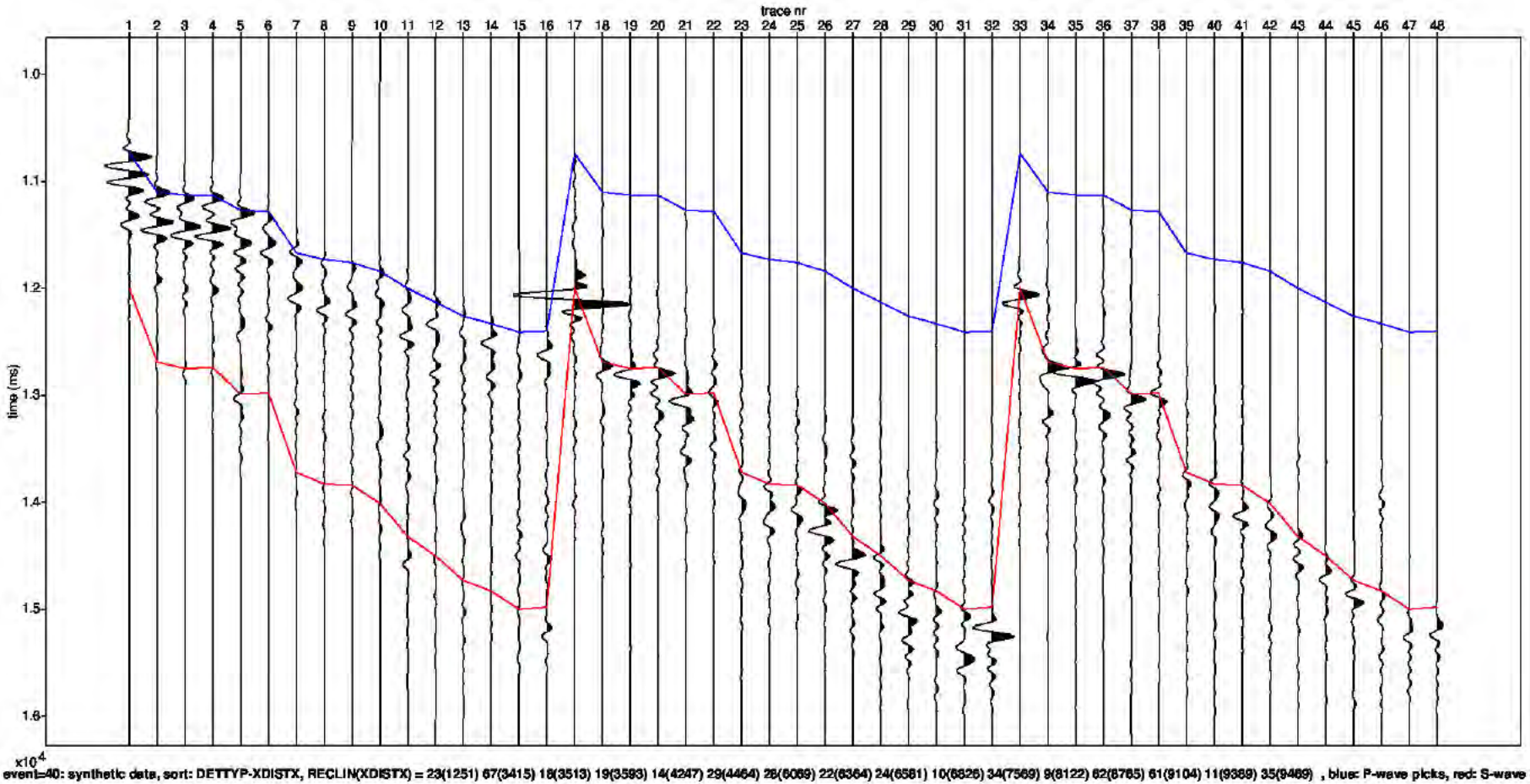

Appendix - Figure Captions

Page

3 Detailed parameter summary for the event. Both primary and secondary focal plane solutions are provided from the moment tensor inversion.

4 Magnitude summary. Prior years are displayed as a “heat map” where the number of events for a given magnitude is displayed per grid cell. The current event is displayed in red.

5 Regional map showing the historical events from KNMI (1986-2019) in blue and the location of the current event in red.

6 Event depth summary. Depths from our automatic workflow (2018-2020) are shown in blue and the current event depth is shown in red. The resolution of the vertical grid is 50m.

7 Event location details for the current event, superimposed on the top Rotliegend depth horizon. Station locations as shown as inverted triangles. Blue triangles are the actual stations used to locate the event whose epicentre is shown by the red dot.

8 QC displays extracted from the objective function for the initial event location. The colour attribute displayed is 1 minus the normalized cross correlation between observed and synthetic waveforms. Station locations are shown as black inverted triangles on the map and the event location is shown by the black dot (left plot). The west to east and north to south vertical profiles are shown on the right. The top and base reservoir are shown for reference as black lines.

Appendix - Figure Captions (continued)

Page

9 QC displays extracted from the objective function for the alternative event location. The colour attribute displayed is 1 minus the normalized cross correlation between observed and synthetic waveforms. Station locations are shown as black inverted triangles on the map and the event location is shown by the black dot (left plot). The west to east and north to south vertical profiles are shown on the right. The top and base reservoir are shown for reference as black lines.

10 Moment tensor inversion results for the event. The double couple portion of the moment tensor is shown on the left and the full moment tensor is displayed on the right. Station locations used in the inversion are shown as inverted triangles.

11 Ternary diagram showing the moment tensor decompositions into relative double-couple(DC), isotropic (ISO) and compensated linear vector dipole (CLVD) contributions. The automatic Shell events (2018-2020) are shown in blue and the current event is highlighted in red.

12 Observed traces for each station and each component. The automatic picks for the P- and S-waves are indicated by the blue and red lines respectively.

13 Modelled waveform data for each station and each component. The automatic picks for the P- and S-waves are indicated by the blue and red lines respectively.

Appendix B Evaluation of the hypocentre and the source mechanism of the earthquake with a magnitude of 1.2 near Garrelsweer on 8th October 2022

Event 41 - Garrelsweer
08 October 2022 05:35:36

10 October 2022

Induced Seismicity Taskforce

Disclaimer

- The results presented in this report have been automatically generated using an unconstrained full waveform, event location and moment tensor inversion workflow, developed by the Induced Seismicity Taskforce at Shell.
- These results have not been previously reviewed.
- For questions related to the results then you should contact:
  - Chris Willacy (Christopher.Willacy@Shell.com) or
  - Jan-Willem Blokland (Jan-Willem.Blokland@Shell.com)

Event summary

The event happened at:

Date	08 October 2022
Time	05:35:36.882520

The event is located at:

Location	Garrelsweer
Northing (m)	593550
Easting (m)	247250
Depth (m)	2900

The source characteristics are:

	Solution 1	Solution 2
Strike angle (degree)	312.24	161.51
Dip angle (degree)	69.15	51.88
Rake angle (degree)	-115.10	-59.75
Isotropic (percentage)	-1.05	-1.05
CLVD (percentage)	48.78	48.78
Magnitude M_{L}	1.20	1.20

Magnitude summary

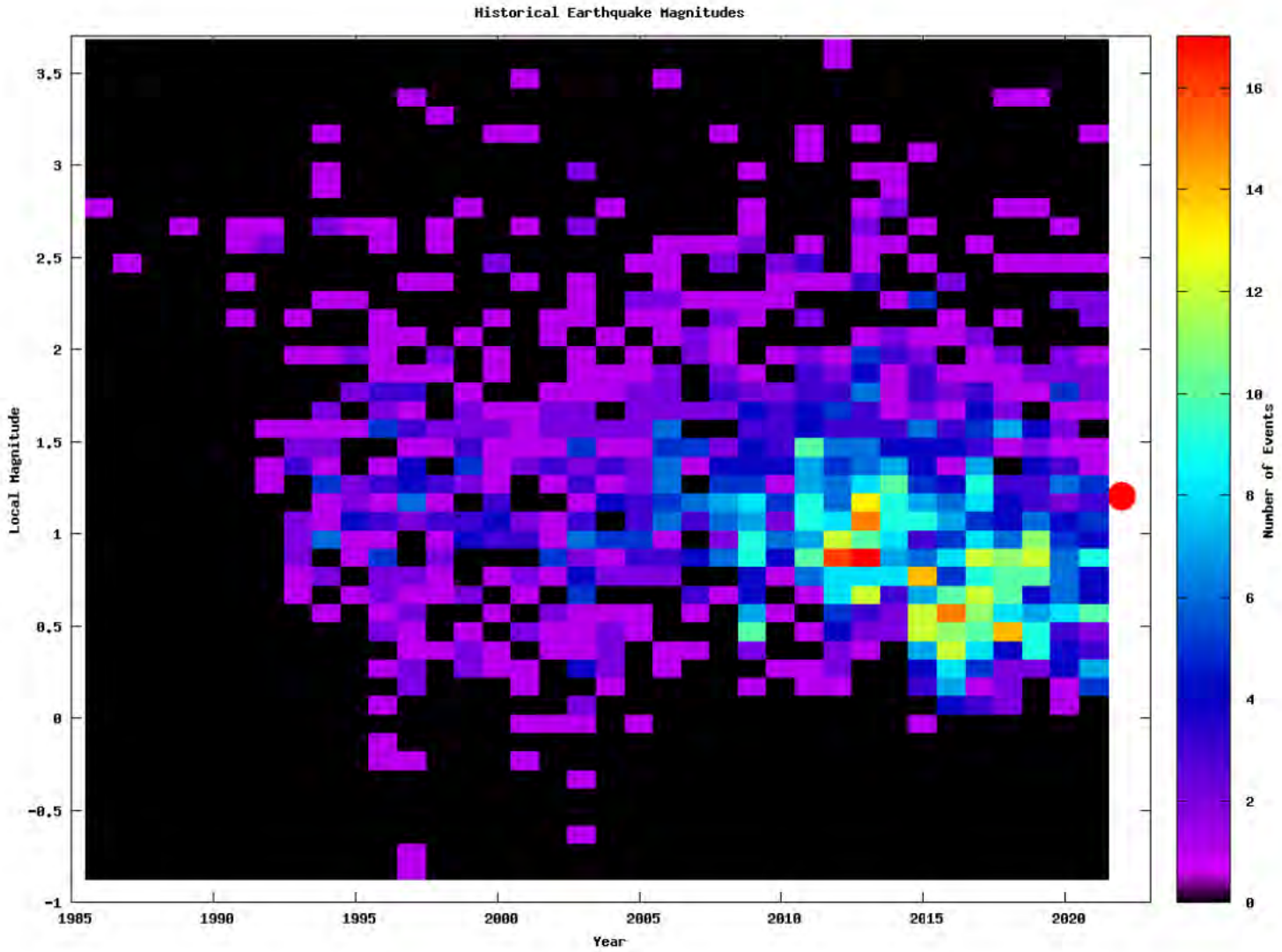

Regional and historical map

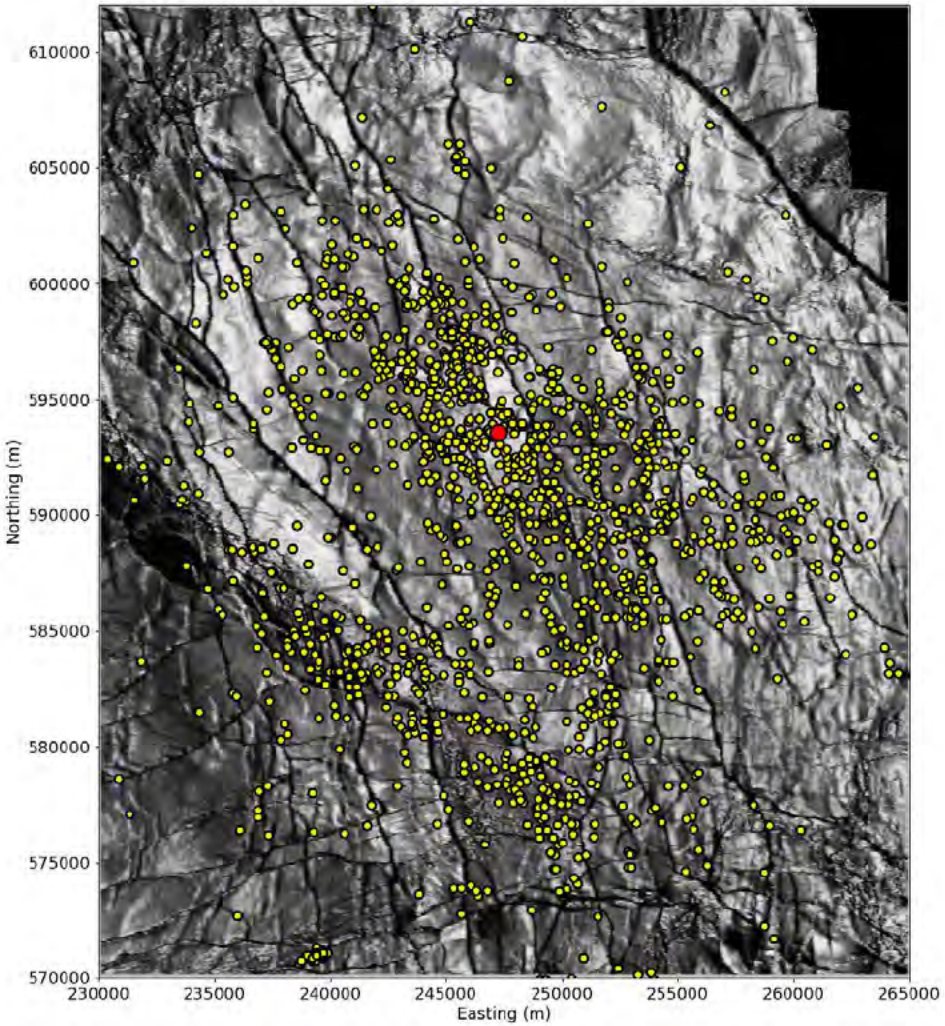

Event depth summary

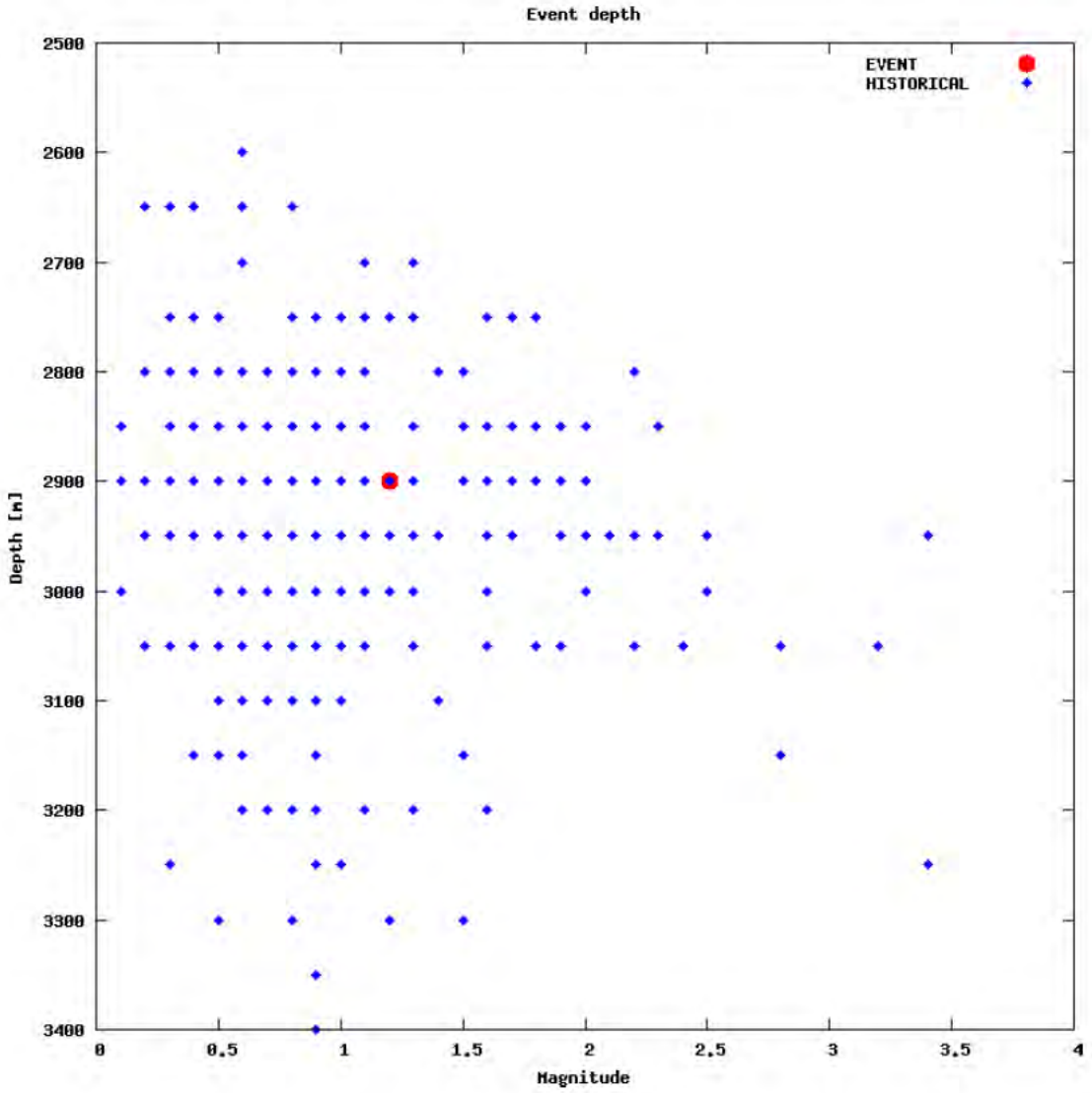

Event location - Map

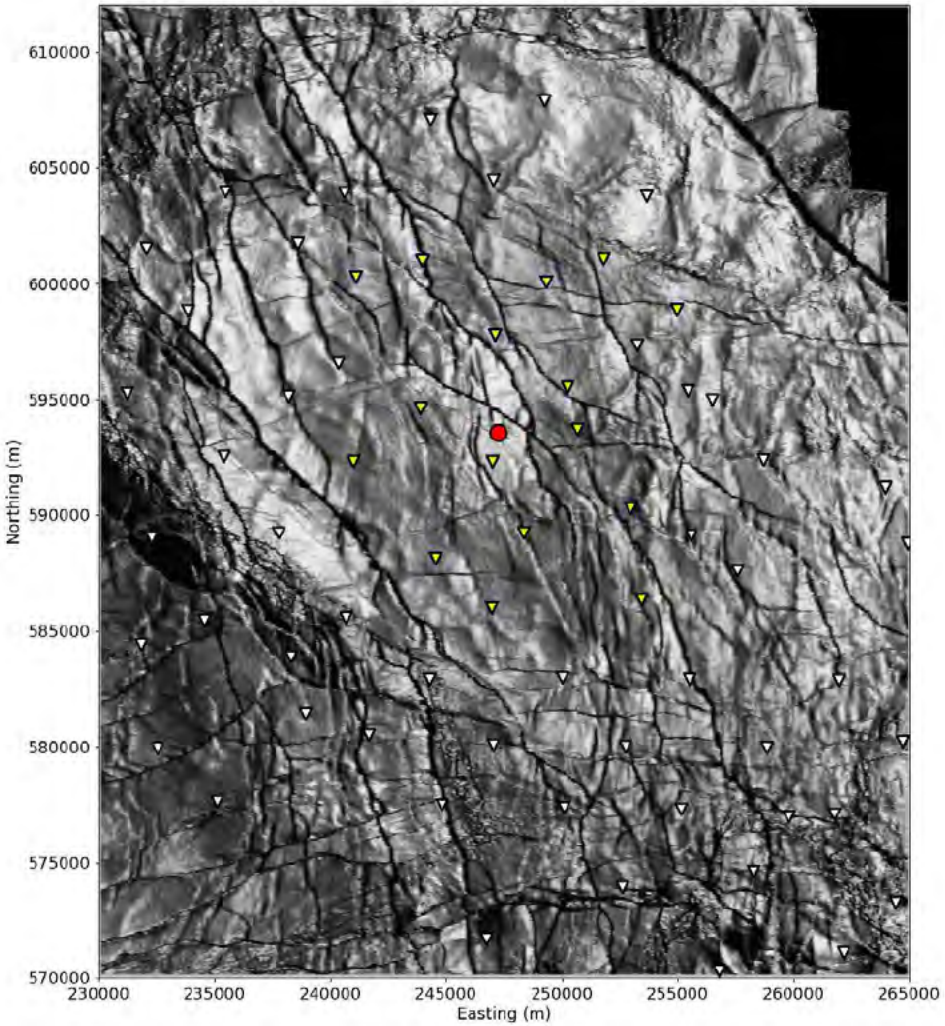

Event location and depth (initial)

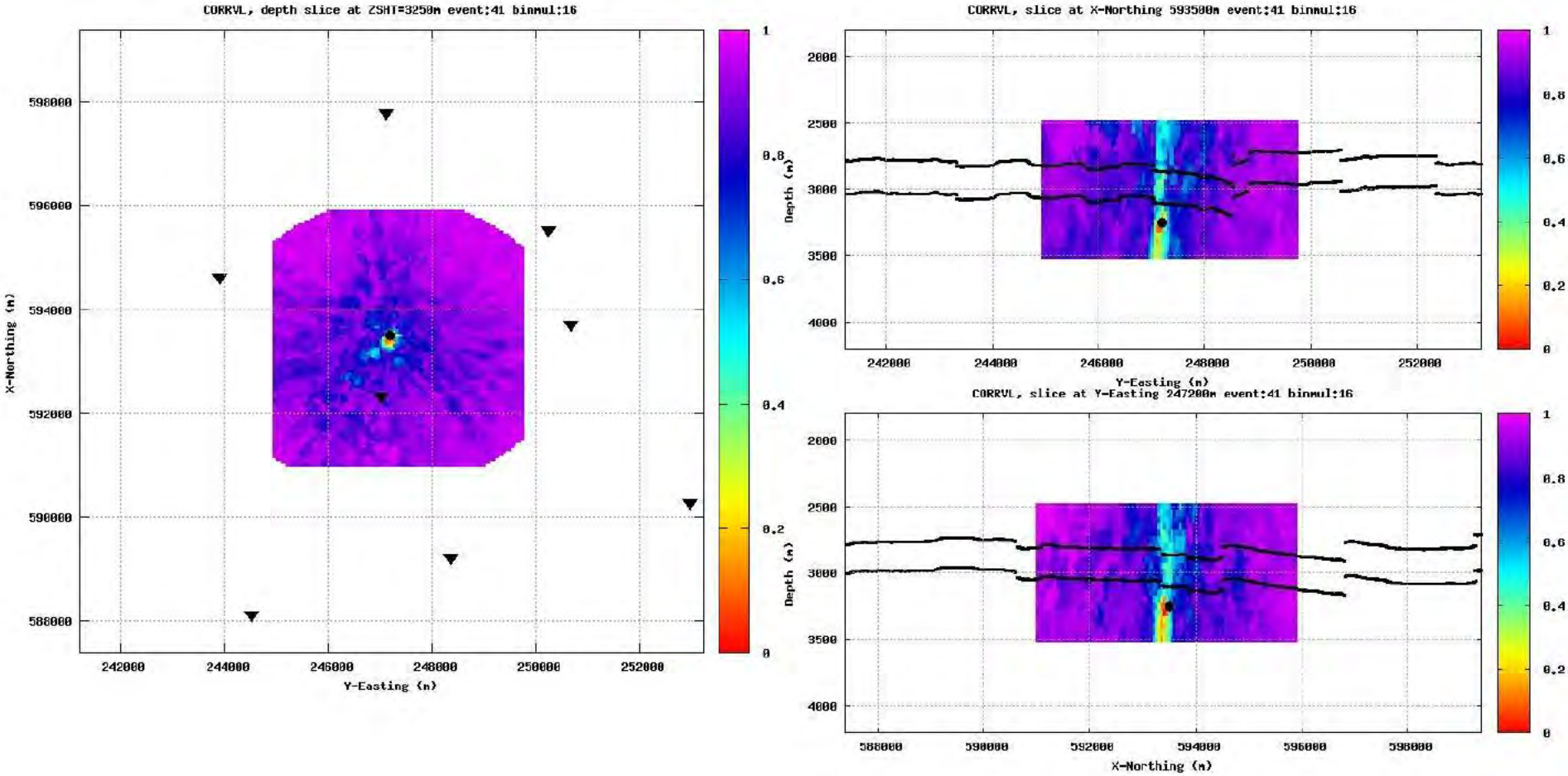

Event location and depth (alternative)

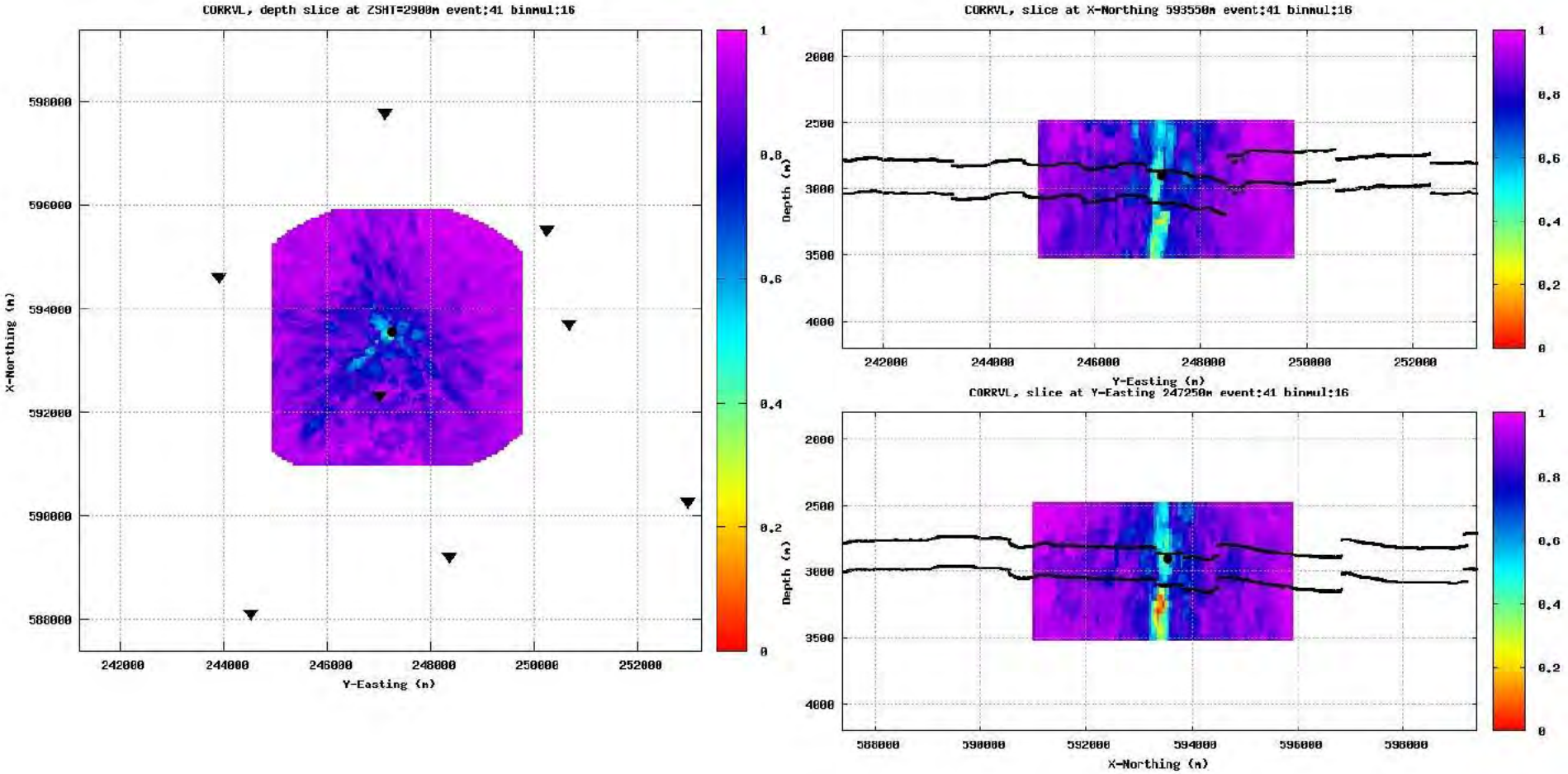

Moment tensor

Double-coupled part

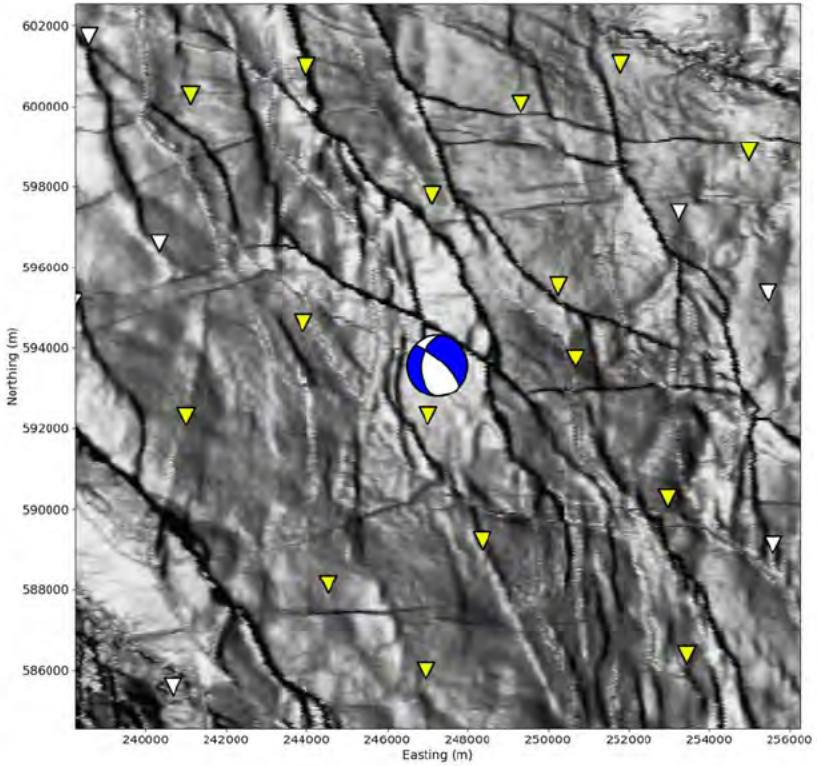

Full

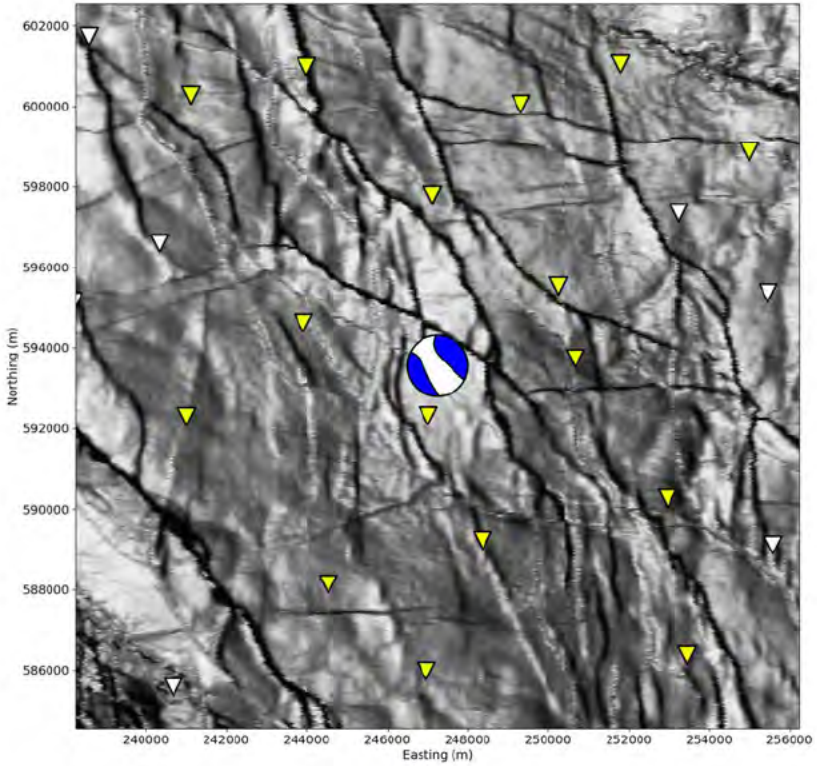

Moment Tensor: Decomposition

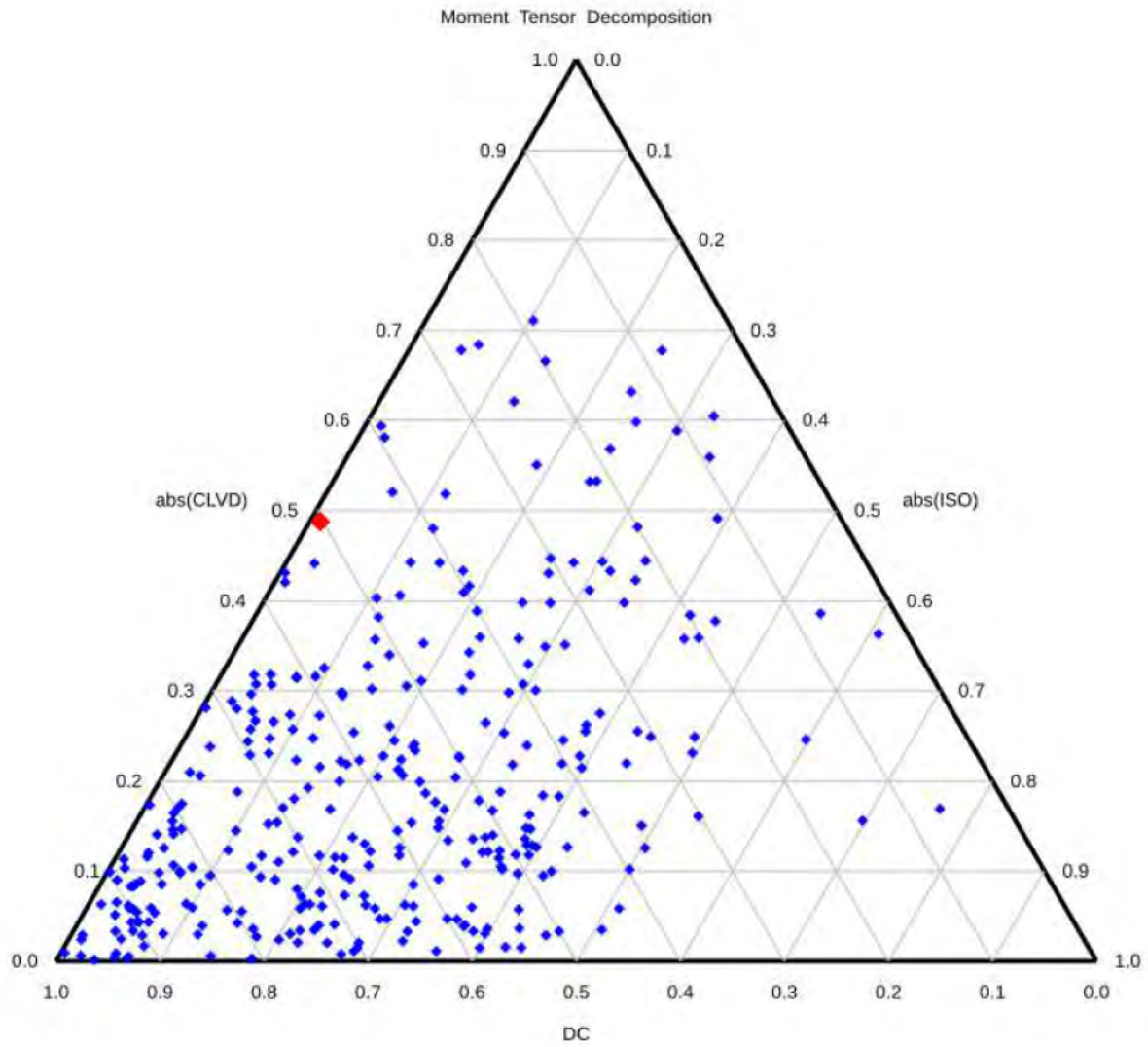

Field data traces

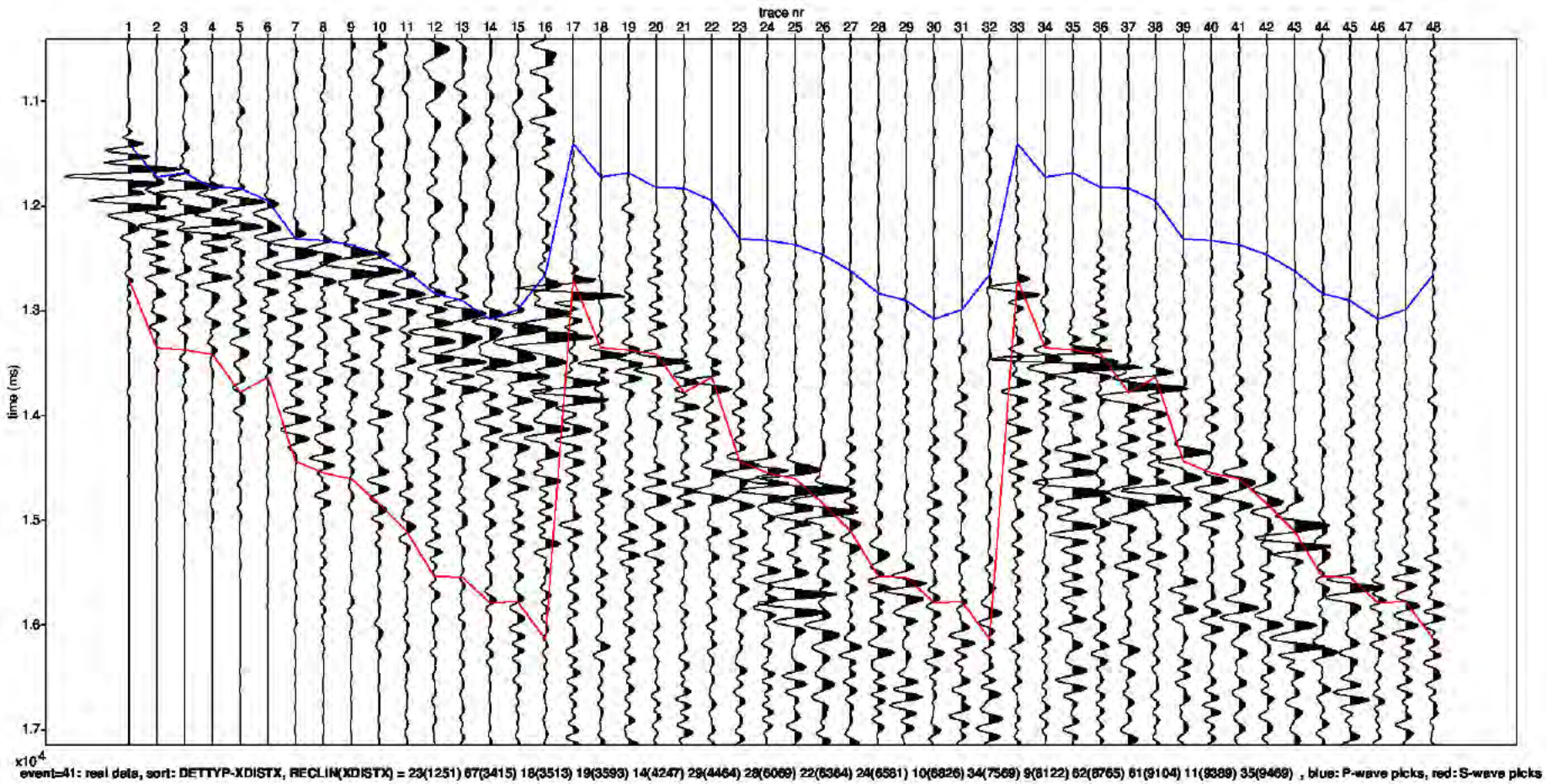

Modelled data traces

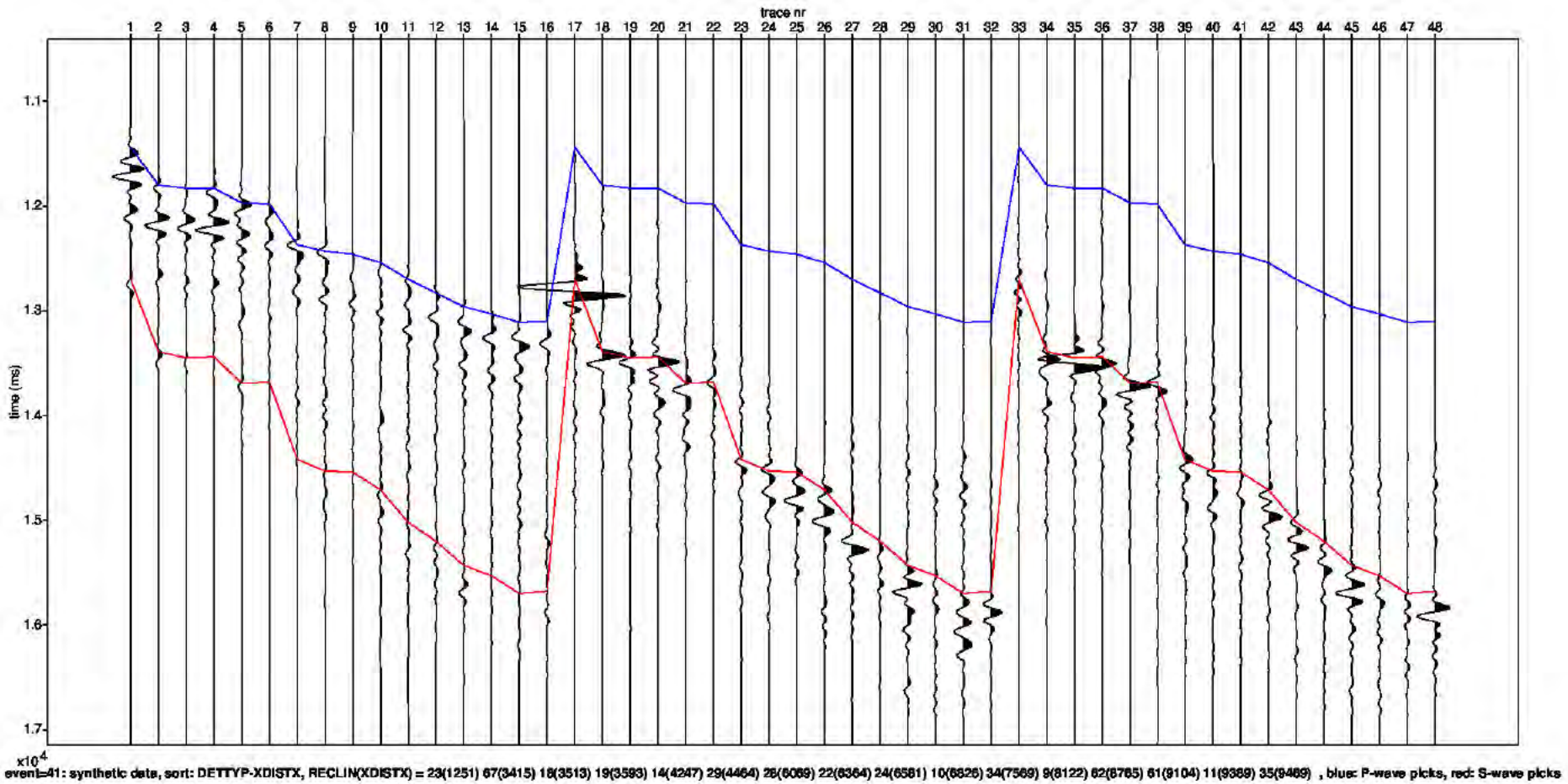

Appendix - Figure Captions

Page

3 Detailed parameter summary for the event. Both primary and secondary focal plane solutions are provided from the moment tensor inversion.

4 Magnitude summary. Prior years are displayed as a “heat map” where the number of events for a given magnitude is displayed per grid cell. The current event is displayed in red.

5 Regional map showing the historical events from KNMI (1986-2019) in blue and the location of the current event in red.

6 Event depth summary. Depths from our automatic workflow (2018-2020) are shown in blue and the current event depth is shown in red. The resolution of the vertical grid is 50m.

7 Event location details for the current event, superimposed on the top Rotliegend depth horizon. Station locations as shown as inverted triangles. Blue triangles are the actual stations used to locate the event whose epicentre is shown by the red dot.

8 QC displays extracted from the objective function for the initial event location. The colour attribute displayed is 1 minus the normalized cross correlation between observed and synthetic waveforms. Station locations are shown as black inverted triangles on the map and the event location is shown by the black dot (left plot). The west to east and north to south vertical profiles are shown on the right. The top and base reservoir are shown for reference as black lines.

Appendix - Figure Captions (continued)

Page

9 QC displays extracted from the objective function for the alternative event location. The colour attribute displayed is 1 minus the normalized cross correlation between observed and synthetic waveforms. Station locations are shown as black inverted triangles on the map and the event location is shown by the black dot (left plot). The west to east and north to south vertical profiles are shown on the right. The top and base reservoir are shown for reference as black lines.

10 Moment tensor inversion results for the event. The double couple portion of the moment tensor is shown on the left and the full moment tensor is displayed on the right. Station locations used in the inversion are shown as inverted triangles.

11 Ternary diagram showing the moment tensor decompositions into relative double-couple(DC), isotropic (ISO) and compensated linear vector dipole (CLVD) contributions. The automatic Shell events (2018-2020) are shown in blue and the current event is highlighted in red.

12 Observed traces for each station and each component. The automatic picks for the P- and S-waves are indicated by the blue and red lines respectively.

13 Modelled waveform data for each station and each component. The automatic picks for the P- and S-waves are indicated by the blue and red lines respectively.

NAM